Short-Packet Communications: Transmission Strategies and Power Control Policies Design

Chunhui Li

November 2021

A Thesis Submitted for the Degree of
Doctor of Philosophy
of The Australian National University

School of Engineering
College of Engineering and Computer Science
The Australian National University

Declaration

The contents of this thesis are the results of original research and have not been submitted for a higher degree to any other university or institution.

Much of the work in this thesis has been published or has been submitted for publication as journal papers or conference proceedings.

The research work presented in this thesis has been performed jointly with Assoc. Prof. Nan Yang (The Australian National University), Dr. Shihao Yan (University of New South Wales), Assoc. Prof. Xiangyun Zhou (The Australian National University), Dr. Changyang She (University of Sydney), Prof. Jinhong Yuan (University of New South Wales) , and Prof. Tony Q. S. Quek (Singapore University of Technology and Design). The substantial majority of this work was my own.

Chunhui Li
School of Engineering,
College of Engineering and Computer Science,
The Australian National University,
Canberra, ACT 2601,
AUSTRALIA

Acknowledgments

I would like to first express my sincere gratitude to my principal supervisor Assoc. Prof. Nan Yang for giving me the opportunity to pursue the doctoral degree under his supervision. I really appreciate his guidance, help, and support in all matters, which always inspires me and keeps me being on the right track during my PhD journey. My special thanks to Assoc. Prof. Xiangyun Zhou, Prof. Parastoo Sadeghi, and Assoc. Prof. Salman Durrani for being part of my supervisory panel. I really appreciate their effort and time for evaluating my annual progress and providing guidance regarding to my PhD study.

I would also like to express my sincere appreciation to Dr. Shihao Yan at the University of New South Wales and Dr. Changyang She at the University of Sydney for their guidance, help, and valuable inputs to our collaborated research works. Many thanks to my collaborators Prof. Jinhong Yuan at the University of New South Wales and Prof. Tony Q. S. Quek at the Singapore University of Technology and Design for their constructive comments and helpful discussions to our research works.

I would like to thank my colleagues from ANU for creating friendly and relaxing study environment. To all the colleagues both in past and present that I met in the office, especially Prof. Thushara D. Abhayapala, Hang Yuan, Dr. Yirui Cong, Dr. Jing Guo, Dr. Wanchun Liu, Dr. Hanchi Chen, Dr. Zhuo Sun, Dr. Khurram Shahzad, Dr. Noman Akbar, Dr. Xiaohui Zhou, Dr. Yanyan Wang, Dr. Xiaofang Sun, Dr. Jianwei Hu, Dr. Zohair Abu-Shaban, Yiran Wang, Zhifeng Tang, Muhammed Akram Mohamed Shafie, Simin Xu, Xinyu Huang, Haoran Jiang, Dr. Xiaolun Jia, Dr. Yucheng Liu, Sahar Idrees, Dr. Yonggang Hu, and Dr. Sheeraz Alvi.

I am grateful to the Australian Government and the Australian National University (ANU) for providing me the PhD scholarship and stipend for my PhD study. Big thanks to the support from the Australian Research Council (ARC) Discovery Project (DP180104062): "Ultra-Reliable and Low-Latency Mission Critical Communications", ANU Professional Development Funding, 2019 ANU CECS Dean's Travel Grant, 2020 Vice-Chancellor's HDR Travel Grant for my PhD study in ANU, conference attendance, and overseas academic visits.

I would like to express my deepest gratitude and love to my parents Jianming Lu and Jun Li, my grandparents Wenyun Li and Yiying Zhang, my parents-in-law Wanping Wei and Shen Dou, and my wife Ran Wei for their unconditional love, unlimited support, and continuing encouragement. I am sincerely grateful to my wife for supporting and accompanying me during the ups and downs moments along these years. This thesis is dedicated to my family, especially to my wife.

Abstract

Ultra-reliable and low-latency communications (URLLC) has been envisaged as the enabling paradigm to support real-time communications with stringent requirements on latency and reliability. The realization of URLLC will bring life-changing applications, e.g., smart manufacturing for Industrial 4.0, autonomous networked vehicles, and remote surgery, to human society. Notably, these applications typically require a target decoding error probability to be less than 10^{-7} within a latency being lower than 1 ms. Such strictly low latency imposes an unprecedented restriction on the size of packets. As such, short-packet communications (SPC) has been proposed as the fundamental method to reduce the latency for URLLC.

This thesis aims to gain a comprehensive understanding of SPC for URLLC. Specifically, this thesis investigates and addresses the following issues: 1) how to design SPC with limited channel estimation overhead in SPC (Chapters 2 and 3), 2) how to improve the design of SPC to reduce the communication latency for URLLC (Chapter 4), and 3) how to design secure SPC for URLLC under statistical quality-of-service (QoS) constraints (Chapter 5). The contributions made in this thesis are summarized as follows:

First, we investigate two different channel training strategies for SPC in Chapter 2. We study the requirement on channel reciprocity to activate uplink channel training, instead of downlink channel training, to achieve a higher data rate for the downlink transmission from a multi-antenna base station to a single-antenna user. We show the necessity and benefits of activating uplink channel training for SPC with multiple transmit antennas. Then, we further study the optimal SPC strategy in a multiple-input single-output system in Chapter 3. To maximize the average achievable data rate, we determine the optimal allocation of the finite resource (e.g., the total transmit power and a finite number of symbol periods) for downlink training, uplink feedback, and data transmission.

Second, to reduce communication latency, in Chapter 4, we propose to use channel inversion power control (CIPC) with channel reciprocity to eliminate the overhead of channel state information (CSI) feedback, as well as achieve one-way URLLC where only the transmission in one direction requires ultra reliability and low latency. Based on channel reciprocity, the proposed CIPC schemes guarantee that the power of the received signal used to decode the information is a constant value Q, by varying the transmit signal and power, which relaxes the assumption of knowing CSI at the user. We derive new analytical expressions for the packet loss probability of the proposed CIPC schemes, based on which we determine a closed interval and a convex set for optimizing Q in CIPC with imperfect and perfect channel reciprocities, respectively.

Finally, we study how to realize secure SPC subject to a statistical QoS requirement and an average power constraint in Chapter 5. We compare the secure transmission rates of short packets in different scenarios (i.e., with/without eavesdropper's instantaneous CSI and with/without channel estimation errors). To find the optimal power control policy that maximizes the effective secrecy throughout under QoS and power constraints, we apply an unsupervised deep learning method with low complexity to address constrained functional optimization problems, which do not have a closed-form solution in general. To provide more insights and demonstrate the effectiveness of unsupervised deep learning, we derive the closed-form expression for the optimal policy in a special case.

This thesis advances our understanding of the fundamental performance of SPC for URLLC. It also provides guidelines to assist URLLC designers to solve important problems on how to fully explore the advantages of SPC in practical wireless URLLC systems.

List of Publications

Journal Articles

J1. **C. Li**, N. Yang, and S. Yan, "Optimal transmission of short-packet communications in multiple-input single-output systems," *IEEE Trans. Veh. Technol.*, vol. 68, no. 7, pp. 7199–7203, Jul. 2019. (Chapter 3)

J2. R. Chen, **C. Li**, S. Yan, R. Malaney, and J. Yuan, "Physical layer security for ultra-reliable and low-latency communications," *IEEE Wireless Commun.*, vol. 26, no. 5, pp. 6-11, Oct. 2019. (not included in this thesis)

J3. **C. Li**, S. Yan, N. Yang, and X. Zhou, "Truncated channel inversion power control to enable one-way URLLC with imperfect channel reciprocity," submitted to *IEEE Trans. Wireless Commun.*. (Chapter 4)

J4. **C. Li**, C. She, N. Yang and T. Q. S. Quek, "Secure transmission rate of short packets with queueing delay requirement," *IEEE Trans. Wireless Commun*, accepted on 30 June 2021, Early Access. (Chapter 5)

J5. Z. Sun, N. Yang, **C. Li**, J. Yuan, and T. Q. S. Quek, "Deep learning based transmit power control for device activity detection and channel estimation in massive access," *IEEE Wireless Commun. Lett.*, accepted on 16 October 2021, Early Access. (not included in this thesis)

Conference Papers

C1. **C. Li**, S. Yan, and N. Yang, "On channel reciprocity to activate uplink channel training for downlink wireless transmission in Tactile Internet applications," in *Proc. IEEE Int. Conf. Commun. (ICC) Workshop*, Kansas City, MO, May 2018, pp. 1-6. (Chapter 2)

C2. **C. Li**, S. Yan, N. Yang, X. Zhou, and R. Chen, "One-way URLLC with truncated channel inversion power control," in *Proc. IEEE Global Commun. Conf. (Globecom) Workshop*, Waikoloa, HI, Dec. 2019, pp. 1-6. (Chapter 4)

C3. Z. Tang, Z. Sun, **C. Li** and N. Yang, "Reliability performance of transmitter selection in wireless vehicular networks," in *Proc. IEEE/CIC Int. Conf. Commun. in China (ICCC)*, Chongqing, China, Aug. 2020, pp. 1-6. (not included in the thesis)

C4. **C. Li**, C. She, and N. Yang, "Unsupervised learning for secure transmissions of short packets under statistical QoS constraints," in *Proc. IEEE Global Commun. Conf. (Globecom) Workshop*, Taipei, Taiwan (ROC), Dec. 2020, pp. 1-6. (Chapter 5)

Acronyms

3GPP	3rd Generation Partnership Project
ITU	International Telecommunication Union
NR	New Radio
5G	fifth generation
LTE	Long Term Evolution
URLLC	Ultra-Reliable and Low Latency Communications
eMBB	enhanced Mobile Broadband
mMTC	massive Machine-Type Communications
TDD	time division duplex
TTI	transmission time interval
RAN	radio access network
MAC	media access control
PLS	physical layer security
SNR	signal-to-noise ratio
SINR	signal-to-interference-plus-noise ratio
MMSE	minimum mean square error
MISO	multiple-input single-output
MIMO	multiple-input multiple-output
BS	base station
AP	access point
CDI	channel direction information
CSI	channel state information

AWGN	additive white Gaussian noise
PDF	probability density function
CDF	cumulative distribution function
SGD	stochastic gradient descent
IoT	Internet of Things
IoE	Internet of Everything
CIPC	channel inversion power control
WST	weighted sum throughput
TTP	total transmit power
DNN	deep neural network
GNN	graph neural network
i.i.d.	independent and identically distributed
w.r.t.	with respect to

Notations

$\mathbb{E}[\cdot]$	the expectation operator
$\mathbb{E}_x[\cdot]$	the expectation operator with respect to x
$\Pr(\cdot)$	probability
$\Pr(\cdot\|\cdot)$	conditional probability
$\|\cdot\|$	the Euclidean norm or $\mathcal{L}^2$-norm
$\|\cdot\|$	the modulus
$\log_2(\cdot)$	logarithm to base 2
$\log_{10}(\cdot)$	logarithm to base 10
$\ln(\cdot)$	natural logarithm
$(\cdot)^{\mathrm{T}}$	the transpose operator
$(\cdot)^*$	the conjugate operator
$\mathcal{O}(\cdot)$	$f(x) = \mathcal{O}(g(x))$ if and only if $\lim_{x\to\infty} f(x)/g(x) = \text{constant}$
$\mathbf{I}_A$	$A \times A$ identity matrix
$\mathcal{CN}(\mu, \nu)$	circularly symmetric complex Gaussian distribution with the mean of μ and the variance of ν

Contents

Declaration iii

Acknowledgments v

Abstract vii

List of Publications ix

Acronyms xi

Notations xiii

1 Introduction 1

1.1 Motivation . . . 1

1.1.1 Research Challenges . . . 4

1.1.1.1 Signalling Overhead in Short-Packet Communications . . . 4

1.1.1.2 Secrecy in Short-Packet Communications . . . 4

1.1.1.3 Non-Convex Optimization in Short-Packet Communications . 5

1.1.2 Background . . . 5

1.1.2.1 Review of Traditional Performance Metrics in Infinite Blocklength Regime . . . 6

1.1.2.2 Performance Metrics in Finite Blocklength Regime . . . 6

1.2 Literature Review . . . 7

1.2.1 Transmission Design of Short-Packet Communications . . . 8

1.2.2 Channel Inversion Power Control in SPC for One-Way URLLC . . . 10

1.2.3 Physical Layer Security in Short-Packet Communications . . . 10

1.3 Thesis Outline and Contributions . . . 12

2 Channel Training Strategies for SPC 17

2.1 Introduction . . . 17

2.2 System Model . . . 17

2.2.1 Channel Training . . . 18

2.2.2 Data Transmission . . . 19

2.2.3 Data Rate with Finite Blocklength . . . 19

2.3 Achievable Data Rates of Uplink and Downlink Channel Training Strategies . . 20
2.3.1 Achievable Data Rate of Uplink Channel Training 20
2.3.2 Achievable Data Rate of Downlink Channel Training 21
2.4 Determination of Channel Reciprocity for Uplink Channel Training Outperforming Downlink Channel Training 23
2.5 Numerical Results 23
2.6 Summary 25

3 Optimal Resource Allocation for SPC 27
3.1 Introduction 27
3.2 System Model 27
3.2.1 Downlink Training 28
3.2.2 Uplink Feedback 29
3.3 Performance Optimization 29
3.3.1 Lower Bound on Average Data Rate 30
3.3.2 Formulating and Solving Optimization Problem 31
3.4 Numerical Results 32
3.5 Summary 35

4 Channel Inversion Power Control for One-Way URLLC 37
4.1 Introduction 37
4.2 System Model 37
4.2.1 Channel Inversion Power Control 39
4.2.2 Fixed-Rate Transmission and Packet Loss Probability 41
4.3 Truncated and Conventional CIPC with Imperfect Channel Reciprocity 43
4.3.1 Packet Loss Probability of Truncated CIPC Scheme 43
4.3.2 Optimization of Q for Truncated CIPC Scheme 45
4.3.3 Packet Loss Probability of Conventional CIPC Scheme 47
4.4 Truncated CIPC with Perfect Channel Reciprocity 48
4.4.1 Packet Loss Probability of Truncated CIPC Scheme 48
4.4.2 Optimization of Q for Truncated CIPC Scheme 49
4.5 Numerical Results 50
4.6 Summary 55

5 Secure Transmission Rate of Short Packets 57
5.1 Introduction 57
5.2 System Model and Performance Metrics 58
5.2.1 System Model 58
5.2.2 Performance Metrics 58

5.3 Problem Formulation . . . 61
5.3.1 Problem Formulation in Full CSI Scenario . . . 61
5.3.2 Problem Formulation in Partial CSI Scenario . . . 62
5.4 Closed-form Solution in Special Case . . . 64
5.4.1 Special Case in Full CSI Scenario . . . 64
5.4.2 Special Case in Partial CSI Scenario . . . 66
5.5 An Unsupervised Learning-Based Solution in General Cases . . . 68
5.5.1 General Case in Full CSI Scenario . . . 68
5.5.2 General Case in Partial CSI Scenario . . . 70
5.6 Power Control Policy with Imperfect CSI . . . 71
5.6.1 Channel Estimation Error Model . . . 72
5.6.2 Full CSI Scenario . . . 73
5.6.2.1 Closed-form Solution in Special Case . . . 74
5.6.2.2 Unsupervised Learning for Power Control in General Case . 74
5.6.3 Partial CSI Scenario . . . 76
5.6.3.1 Closed-form Solution in Special Case . . . 77
5.6.3.2 Unsupervised Learning for Power Control in General Case . 77
5.7 Numerical Results . . . 78
5.7.1 System Parameters . . . 79
5.7.2 Performance Evaluation . . . 80
5.8 Summary . . . 83

6 Conclusions **85**
6.1 Thesis Conclusions . . . 85
6.2 Future Research Directions . . . 87

A Appendix A **91**
A.1 Proof of Theorem 2.1 . . . 91
A.2 Proof of Proposition 2.1 . . . 92

B Appendix B **95**
B.1 Proof of Theorem 3.1 . . . 95
B.2 Proof of Theorem 3.2 . . . 95

C Appendix C **97**
C.1 Proof of Lemma 4.1 . . . 97
C.2 Proof of Corollary 4.1 . . . 98
C.3 Proof of Proposition 4.1 . . . 98

Bibliography **103**

List of Figures

2.1 The lower bound on the data rate achieved by the uplink channel training versus the average SNR ρ_{b} for different values of ϕ with $N_{\mathrm{B}} = 5$, $\varepsilon = 10^{-9}$, and $T = 200$. 24

2.2 The lower bounds on the data rates achieved by the uplink and downlink channel training strategies versus the channel reciprocity coefficient ϕ for different value of N_{B} with $\rho_{\mathrm{b}} = 10$ dB, $\varepsilon = 10^{-9}$, and $T = 200$. 24

2.3 The minimum channel reciprocity coefficient ϕ^* versus the blocklength T for different values of ρ_{b} with $N_{\mathrm{B}} = 10$ and $\varepsilon = 10^{-5}$. 25

3.1 The average data rate R versus transmit SNR for different feedback symbol period T_f with $T = 200$, $N_A = 4$ and $\varepsilon = 10^{-6}$. 33

3.2 The optimal feedback symbol period T_f^* and the optimal power allocation coefficient η^* versus T with $\rho = 10$ dB and $\varepsilon = 10^{-9}$. 34

3.3 The transmit SNR for downlink training and data transmission versus T for different N_A with $\rho = 10$ dB and $\varepsilon = 10^{-9}$. 34

3.4 The average data rate R versus transmit SNR for different values of ε and T with optimal η^* and $N_A = 4$. 35

4.1 Illustration of the considered one-way URLLC scenario. 38

4.2 The packet loss probability $P_\varepsilon(Q)$ versus the power of received signals Q in the truncated CIPC scheme with $R = 0.8$, $\phi = 0.9$, $T = 100$, $N_{\mathrm{t}} = 4$, and $P_{\max} = 23$ dBm. 50

4.3 The packet loss probability $P_\varepsilon(Q)$ versus the power of received signal Q in the truncated CIPC scheme for different value of N_{t} with $R = 0.3$, $T = 150$, $\phi = 0.9$, and $P_{\max} = 10$ dBm. 52

4.4 The achievable minimum $P_\varepsilon(Q)$ versus the channel reciprocity coefficient ϕ for different number of transmit antennas N_{t} with $R = 0.5$, $T = 150$, and $P_{\max} = 23$ dBm. 53

4.5 The packet loss probability with perfect channel reciprocity, $P_\varepsilon^{\phi=1}(Q)$, versus the power of receive signal Q in the truncated CIPC scheme with $R = 0.5$, $T = 150$, $\phi = 0.8$, $N_{\mathrm{t}} = 4$, and $P_{\max} = 10$ dBm. 54

4.6 The maximum rate R versus the power of received signal Q in the truncated CIPC scheme with perfect channel reciprocity, i.e., $\phi = 1$, for different packet loss probabilities $P_{\varepsilon}^{\phi=1}(Q)$ with $T = 150$, $N_{\mathrm{t}} = 4$, and $P_{\max} = 23$ dBm. 54
4.7 The minimum packet loss probability $P_{\varepsilon}^{*,\phi=1}(Q)$ versus the maximum transmit power $P_{\max}$ for different values of R with $N_{\mathrm{t}} = 5$ and $T = 150$. 55

5.1 Queueing model. 59
5.2 Illustration of our DNN model with one input layer, four hidden layers, and one output layer. 79
5.3 Convergence of the proposed unsupervised learning method in full CSI scenario in terms of (a) the normalized effective secrecy throughput and (b) the normalized average power constraint versus the iteration number for different value of d, where $\bar{P} = 20$ dBm, $\varphi_b = \varphi_e$, $\theta = 10^{-3}$, $\beta = 1$, $\varepsilon_c = 10^{-5}$, and $\delta = 10^{-2}$. 81
5.4 Performance comparison of unsupervised learning in full CSI scenario with different power control policies for different value of d, where $\bar{P} = 20$ dBm, $\varphi_b = \varphi_e$, $\theta = 10^{-3}$, $B = 1$ MHz, $\beta = \frac{\theta T_c B}{\ln 2} \neq 1$, $\varepsilon_c = 10^{-5}$, and $\delta = 10^{-2}$. . . . 82
5.5 Normalized effective secrecy throughput versus the average SNR at the intended user with different QoS requirements, where $V_b = V_e = 1$, $\beta = 1$, $\varphi_b = \varphi_e$, $\varepsilon_c = 10^{-5}$, $\delta = 10^{-2}$, and $d = 300$ m. 82
5.6 Normalized effective secrecy throughput and normalized average power constraint in full CSI scenario versus the variance of channel estimation errors, where $\bar{P} = 20$ dBm, $\theta = 10^{-3}$, $\beta = 1$, $\varphi_b = \varphi_e$, $\varepsilon_c = 10^{-5}$, $\delta = 10^{-2}$, and $d = 200$ m. 83

List of Tables

1.1 Use cases of real-time interactive applications [1] 2
1.2 Relationships of performance metrics in finite and infinite regimes 7

5.1 Simulation Parameters and Hyper-Parameters 79

Chapter 1

Introduction

1.1 Motivation

The fifth generation (5G) and beyond wireless communications aim to connect everything that may benefit from being connected [2, 3], i.e., the Internet of Everything (IoE)[1]. The connected "Everything" includes human, process, data, and things [3], where "things" can be autonomous machines and devices, e.g., smart phones, sensors, actuators, cameras, vehicles [2] with different levels of energy consumption, computation capability, transmit power, and latency requirement. This calls for a fundamental shift from current networks originally designed for human-centric communications (i.e., high data rate) to machine-centric communications, which is envisioned for addressing the specific needs of "things" by enabling new applications with stringent requirements on latency[2] and reliability[3]. The envisioned services in 5G and beyond can be grouped into three main scenarios [2, 7, 8], as follows:

- **enhanced Mobile Broadband (eMBB)**: This scenario provides enhanced access to multi-media content, services and data with improved performance and increasingly seamless user experience.
- **Ultra-Reliable and Low Latency Communications (URLLC)**: This scenario enables the real-time communications with stringent requirements on latency and reliability.
- **massive Machine-Type Communications (mMTC)**: This scenario supports ubiquitous connectivity for an enormous amount of low-cost devices in energy-efficient way.

The arrival of 5G and beyond will open up lucrative new business opportunities for many industrial sectors. One of the main challenges in 5G and beyond is the inclusion of support for real-time interactive applications such as remote driving, intelligent transport systems, next-generation factory automation, tele-surgery and Tactile Internet [2, 7, 8]. Such communication

[1] Cisco defines the IoE as the networked connection of people, process, data, and things.

[2] International Telecommunication Union (ITU) defines the latency as the time for a packet delivery from the source to the destination in radio access network while satisfying being on the order of millisecond [2, Page 13].

[3] Reliability refers to the success probability of data transmission within a defined latency bound in channel quality of coverage edge [4, 5, 6].

aims to enable the wireless exchange of small packets with ultra-high reliability (error probability is on the order of 10^{-5}) and ultra-low latency (user plane latency is on the order of 1 ms) [9]. For example, different real-time interactive applications require diverse requirements on latency and reliability. A brief summary of use cases is listed in Table 1.1 [1].

As can be seen from Table 1.1, the ultimate goal is to deliver small packets with high reliability in a real-time manner. In Table 1.1, there are two key parameters related to latency,

Table 1.1: Use cases of real-time interactive applications [1]

Use Case	Latency	Reliability (%)	Packet Size	Traffic Model
Power distribution (Outage management)	5 ms end-to-end latency, 3 ms air interface latency	99.9999	100 bytes	aperiodic
Power distribution (Protection)	15 ms end-to-end latency, 7 ms air interface latency	99.999	250 bytes	periodic
Augmented reality/ Virtual reality	1 ms air interface latency/ 4 ms air interface latency	99.999	32 bytes/ 200 bytes	aperiodic
Factory automation (Motion control)	2 ms end-to-end latency, 1 ms air interface latency	99.9999	32 bytes	periodic
Intelligent transport system	10 ms end-to-end latency, 7 ms air interface latency	99.999	1370 bytes	periodic

including (1) user plane latency (air interface latency), and (2) end-to-end latency. Specifically, according to ITU, the minimum requirement for user plane latency[4] in URLLC should not exceed 1 ms [2, 5]. Similarly, the reliability requirement for URLLC defined in 3GPP Release 16 [8, Page 25] requires that a single transmission of a small packet (i.e., 32 bytes) should satisfy a reliability of $1-10^{-5}$ (i.e., 99.999%) with a user plane latency of 1 ms. It is noted that the definitions of latency and user plane latency are the same. Therefore, in this thesis, these two terms are used interchangeably.

Besides, the overall end-to-end latency in cellular networks is determined by the delays in radio access network (RAN), backhaul, core network, data center/cloud, and Internet server [10, 11, 12, 13]. It increases significantly with the network load and the transmission distance between the transmitter and the receiver and [12]. It is worthwhile to mention that communicating with the gateway of the core network toward the Internet takes a minimum of 39 ms in Long Term Evolution (LTE) networks [11], where the latency in RAN contributes to a large proportion of the end-to-end latency (i.e., $10-20$ ms [14]). We also find that the assumption

[4]ITU defines the user plane latency as "the contribution of the radio network to the time from when the source sends a packet to when the destination receives it (in ms)" [5, Page 7].

adopted commonly in 3GPP for a core/Internet latency component in LTE varies from 1 to 20 ms [10, Page 10]. Although the core network can be located close to the RAN to reduce the latency [15], the latency of 1 ms cannot be achieved when considering the core network. For URLLC applications, the end-to-end latency mainly focuses on the latency in RAN. From the radio communication perspective, the latency in RAN is mainly contributed by the physical layer and media access control (MAC) layer [11, 13, 16].

To achieve 1 ms latency in RAN, a short frame structure in 5G New Radio (NR) [17, 18, 19] is proposed for short transmission time interval (TTI) by using mini-slots (durations of $1 \sim 13$ OFDM symbols) instead of a fixed slot duration in LTE (durations of 14 OFDM symbols) [20]. There are two main reasons for a short frame structure in 5G NR. Firstly, the TTI is set to the same as the duration of one subframe (i.e., 1 ms) in LTE, which leads to the current latency in LTE varying from several tens to hundreds of ms. Thus, the subframe length in 5G NR should be much shorter than 1 ms to meet the latency requirement. For example, the new subframe needs to take less than 1 ms to complete a single transmission which includes the process of scheduling request, grant, data transmission, and acknowledgment. Secondly, in current LTE networks, the subcarrier spacing is 15 kHz, and the operating frequency is below 6 GHz. It is noted that frequency drift will occur due to poor local oscillator, which is in proportion to the operating frequency. For example, 5G networks are expected to use mmWave in high frequency, e.g., 26 GHz; therefore, a small fraction of frequency drift will make doppler shift to be over several tens of kHz. Against this background, wider subcarrier spacing is expected to be used in 5G NR. It will lead to shorter symbol length. Hence, the subframe will become shorter when the same number of symbols are required in a subframe with shorter symbol length.

The strictly low latency in URLLC imposes an unprecedented restriction on the size of packets. Indeed, short packets have been recognized as the typical forms of the traffic generated by sensors and small mobile devices involved in mMTC and URLLC [21]. For example, in industrial manufacturing and control systems, measurements and control commands are of small size (e.g., 10 to 32 bytes) [19, 22, 23] and need to be communicated in real-time with ultra-high reliability. The proposed short frame structure in 5G NR is beneficial to transmit short packets for URLLC to reduce the latency up to 0.25 ms by dynamically adjusting the size of TTI [24]. The short TTI includes the phases for control signaling, uplink and downlink data transmissions, where control information contains scheduling requests/grants, transmission format information, and acknowledgments [18, 20].

Against this background, this thesis is motivated to investigate the fundamental problem of how to design short-packet communications (SPC) to achieve URLLC by optimizing radio resource management in such short TTI while satisfying the stringent requirements on latency and reliability.

1.1.1 Research Challenges

1.1.1.1 Signalling Overhead in Short-Packet Communications

The 5G and beyond networks are envisioned to support SPC for mission-critical applications [21, 25], e.g., industrial automation and distributed smart grid, in which short packets (measurements, control commands, and status updates are of small size 10-32 bytes) are expected to exchange wirelessly with ultra-low latency and ultra-high reliability. However, the frameworks in current wireless networks cannot be directly adopted to examine SPC. It is due to the fact that current wireless networks are originally designed to transmit long packets for humman-centric communications rather than short packets for mMTC/URLLC. It is worthwhile to mention that the difference between long and short packets is characterized by the ratio of the size of control information to the size of data information/the overall packet, where the packet size (blocklength) is described by the number of degrees of freedom (channel uses or symbols) that are needed to transmit the packet. Indeed, the control information in SPC is as important as data information, while being negligible in current networks that use long-packets for packets transmission.

SPC takes the effect of finite blocklength into account, which is different from the traditional long-packet communications (i.e., blocklength is sufficiently long to obtain an arbitrarily low error probability [26]). As a consequence, the error probability in SPC is non-negligible [21, 25, 27]. Against this background, the overhead in SPC has to be carefully designed to achieve the stringent requirement on latency and reliability, since this overhead is not negligible and may become the dominating factor when the blocklength is finite and short. Within the overhead, the part used for channel training which enables transceivers to learn the channel state information (CSI) is unavoidable and could dominate the total overhead. Therefore, it is necessary to investigate how to reduce the signalling overhead within limited resource (i.e., the blocklength is finite and short) while satisfying the strict reliability requirement in SPC.

1.1.1.2 Secrecy in Short-Packet Communications

Due to the broadcast nature of the wireless medium, wireless transmissions are vulnerable to security attacks [9, 28, 29, 30]. Existing cryptographic techniques are used at the upper layers of the Open Systems Interconnection protocol architecture to prevent the illegitimate user from accessing confidential information [28, 29]. Considering the strict delay budget in URLLC, the latency caused by cryptography for encryption and decryption will become the bottleneck for URLLC. Comparing to the traditional cryptographic approach, physical layer security (PLS) has shown great potentials in 5G and beyond networks [31, 32, 33]. The key idea of PLS is to realize wireless security at the physical layer by exploiting the intrinsic randomness of the wireless medium. The advantages of PLS are mainly three folds [29, 31, 32, 34]: (1) security level guarantee at the physical layer, (2) applicable to low-latency communications, (3) low im-

plementation overheads for diverse/dynamic traffic in 5G and beyond networks. Specifically, the security level achieved via PLS does not rely on the computational ability of illegitimate users. Even if illegitimate users have powerful computational abilities to solve complicated mathematical problems for deciphering, the security requirement can still be satisfied due to the uncertainty in wireless channels [31, 32].

Apart from the aforementioned intrinsic benefits of PLS, the latency caused by secret key exchange and encryption/decryption procedure is also a vital problem for URLLC. Since PLS does not need additional time (or channel uses) for secret key exchange and management or encryption/decryption as in the cryptographic method [34], it is suitable to transmit short packets in URLLC. Furthermore, 5G and beyond networks need to support diverse/dynamic traffic and the overheads for secret key distribution, key management, and upper-layer cryptographic approaches will be high, especially for hierarchical or decentralized architectures. To handle this issue, PLS techniques can be used directly without complicated cryptographic approaches at the upper layers, which significantly reduces implementation overheads. Therefore, PLS is a promising approach to meeting the requirements on latency, reliability, and security. Despite so, how to employ PLS techniques in SPC to achieve security under stringent requirements on latency and reliability for URLLC applications is still unclear, which needs to be comprehensively investigated.

1.1.1.3 Non-Convex Optimization in Short-Packet Communications

Shannon's capacity has been widely used to characterize the maximal achievable rate in the infinite blocklength regime, which is jointly convex in bandwidth and transmit power. However, considering finite blocklength in SPC, the maximal achievable rate is neither convex nor concave with respect to (w.r.t.) radio resources (i.e., bandwidth and transmit power) [35, 36], which leads to non-convex Quality of Services (QoS) constraints in optimizing resource allocation for URLLC. In other words, radio resource management in SPC is very challenging. Besides, the maximal achievable rate in the finite blocklength regime is lower than Shannon's capacity, which leads to the fact that the latency and reliability will be underestimated if Shannon's capacity is used in optimizing resource allocation for URLLC [37]. Therefore, it is desirable to propose a novel framework in dealing with non-convex optimization problems in SPC.

1.1.2 Background

In this subsection, we provide the background information of performance metrics (e.g., maximal achievable rate and decoding error probability) used in this thesis for evaluating SPC, which largely makes the thesis self-contained.

1.1.2.1 Review of Traditional Performance Metrics in Infinite Blocklength Regime

The current wireless communication systems are actually assumed to work in the asymptotic scenario where the blocklength is infinite. In such systems, the channel capacity C [26, 38] and the outage capacity C_ε [38, 39] are used as main performance metrics. Specifically, the channel capacity C is the maximal achievable rate at which the message can be transmitted with an arbitrarily low error probability by choosing sufficiently large blocklength. The outage capacity C_ε is the maximal achievable rate at which the message can be transmitted with the error probability being less than ε ($\varepsilon > 0$) by choosing sufficiently large blocklength.

According to the definition of C and C_ε, we note that there are no restrictions on the blocklength and C can be obtained from C_ε by letting ε tend to 0, given by

$$C = \lim_{\varepsilon \to 0} C_\varepsilon. \tag{1.1}$$

1.1.2.2 Performance Metrics in Finite Blocklength Regime

Maximal Achievable Rate: It has been shown that the traditional performance metrics (C and C_ε) provide inaccurate estimates on the maximum achievable rate in the context of SPC [21, 25]. Specifically, they are both asymptotic quantities by adopting the assumption of infinite blocklength. Besides, the outage capacity fails to capture the rate penalty due to the channel-estimation overhead while the channel capacity is independent on the packet reliability. However, the blocklength, channel-estimation overhead, and reliability need to be taken into account simultaneously for addressing the feasibility of SPC.

Against this background, a natural question to ask is *"What are the performance metrics for SPC?"*. Fortunately, pioneering work on finite blocklength [27] provided the theoretical principles that quantify the maximum coding rate for finite and short blocklength. In the finite blocklength, the maximum achievable rate, denoted as $R(T,\varepsilon)$ [27], is given by

$$R(T,\varepsilon) \approx C(\gamma) - \sqrt{\frac{V(\gamma)}{T}} f_Q^{-1}(\varepsilon) + \mathcal{O}\left(\frac{\log_2 T}{T}\right) \tag{1.2}$$

$$\approx C(\gamma) - \sqrt{\frac{V(\gamma)}{T}} f_Q^{-1}(\varepsilon), \tag{1.3}$$

where T is the blocklength (i.e., the number of channel uses), ε is the decoding error probability, $C(\gamma) = \log_2(1+\gamma)$ is the channel capacity, $V = (\log_2 e)^2 \left[1 - 1/(1+\gamma)^2\right]$ is the channel dispersion [27], $\mathcal{O}(\frac{\log_2 n}{n})$ comprises remainder terms of order $\frac{\log_2 n}{n}$, and $f_Q^{-1}(\cdot)$ denotes the inverse of the Gaussian Q-function given by

$$f_Q(x) \triangleq \int_x^\infty \frac{1}{\sqrt{2\pi}} e^{-\frac{t^2}{2}} dt. \tag{1.4}$$

The approximation in (1.3) is referred as the *normal approximation* [27] by ignoring the term of $\mathcal{O}(\frac{\log_2 n}{n})$. It has been shown that the approximation of $R(T,\varepsilon)$ is accurate for even very short blocklength (e.g. $T = 100$) [25, 27].

Notably, the expression for $R(T,\varepsilon)$ can be regarded as a general expression for traditional performance metrics of C and C_ε, which can be directly obtained from $R(T,\varepsilon)$ by taking appropriate limits. The corresponding relationships are summarized in Table 1.2.

Table 1.2: Relationships of performance metrics in finite and infinite regimes

Performance Metrics	Relationships to $R(T,\varepsilon)$	Blocklength
C	$C = \lim_{\varepsilon\to 0} C_\varepsilon = \lim_{\varepsilon\to 0}\lim_{n\to\infty} R(T,\varepsilon)$	Infinite
C_ε	$C_\varepsilon = \lim_{n\to\infty} R(T,\varepsilon)$	Infinite

Decoding Error Probability: It is noted that in the infinite regime for a given $\varepsilon > 0$, the outage capacity C_ε [38, 39] is the supremum of all rates R satisfying the outage probability is lower than ε, i.e., $P_{\text{out}}(R) \leq \varepsilon$, namely

$$C_\varepsilon = \sup\{R : P_{\text{out}}(R) \leq \varepsilon\}, \tag{1.5}$$

where the outage probability $P_{\text{out}}(R)$ is defined as a function of the rate R, given by

$$P_{\text{out}}(R) = \Pr\left[\log_2(1+\gamma) < R\right] = \Pr\left[\gamma < 2^R - 1\right] = F_\gamma(2^R-1) = \int_0^{2^R-1} f_\gamma(\gamma)d\gamma, \tag{1.6}$$

where γ is the instantaneous SNR, $f_\gamma(\gamma)$ is the probability density function (PDF) of γ, and $F_\gamma(\gamma)$ is the cumulative distribution function (CDF) of γ.

However, for a given maximal achievable rate R, the decoding error probability ε in the finite blocklength regime, can be obtained as

$$\varepsilon = \mathbb{E}\left[f_Q\left(\frac{C(\gamma)-R}{\sqrt{V(\gamma)/T}}\right)\right] = \int_0^\infty f_Q\left(\frac{C(\gamma)-R}{\sqrt{V(\gamma)/T}}\right) f_\gamma(\gamma)d\gamma. \tag{1.7}$$

The difference between the outage probability in (1.6) and the decoding error probability in (1.7) is that the former is the integration of a PDF weighted by an indicator function while the latter is the integration of a PDF weighted by a Gaussian Q-function which is never zero.

1.2 Literature Review

A number of performance limiting factors need to be addressed in order to unlock the full potential of SPC for URLLC scenarios. In this thesis, we mainly focus on the following three

important problems of SPC:

- How to design SPC with limited channel estimation overhead in the finite blocklength regime?
- How to use channel inversion power control with channel reciprocity to improve the design of SPC for signalling overhead reduction?
- How to employ PLS techniques in SPC to achieve security under stringent requirements on latency and reliability for URLLC applications?

The related prior work is described in this section. The limitations of the existing work are also discussed.

1.2.1 Transmission Design of Short-Packet Communications

Very recently, the benefits of SPC have been examined for emerging wireless mechanisms, such as mobile edge computing [40], non-orthogonal multiple access[41, 42], physical layer security [43, 44], cooperative relaying [45, 46, 47, 48], cooperative Internet of Things (IoT) networks [49], factory automation [50], UAV communication systems [51, 52], wireless energy transfer [48, 53], and radio resource management [16, 54, 55]. Recently, a novel architecture that applies deep learning with wireless edge intelligence for SPC was proposed in [56, 57, 58], which aims to provide practical guidelines into latency reduction in SPC for URLLC applications. In practical communication systems, the wise resource allocation for channel estimation overhead plays a significant role in determining the transmission performance. Traditionally, the impact of channel estimation overhead has been studied in the asymptotic scenario with infinite blocklength (e.g., see [59, 60]). However, there have been only a few studies (e.g., [21, 25, 55]) that investigated the impact of channel estimation overhead when the blocklength is finite and short. While [16, 25, 40, 42, 46, 53, 54, 59, 60] stand on their own merits, the design of SPC with limited channel estimation overhead is still recognized as an open research issue.

Channel Training Strategy: In order to satisfy the reliability requirement for URLLC, the overhead in SPC has to be redesigned, since this overhead is not negligible compared to the packet length. Within the overhead, the part used for channel estimation is unavoidable and could dominate the total overhead when the requirement of URLLC is very stringent. For the time division duplex (TDD) wireless communications from a base station (BS) to a user, there are two channel training strategies before data transmission, including downlink channel training and uplink channel training. For downlink channel training, the BS transmits pilot signals to enable the user for estimating the downlink CSI from the BS to the user and then the user feeds back the estimation to the BS. For uplink channel training, the user transmits pilot signals to enable the BS for estimating the uplink CSI from the user to the BS and then

the BS learns the downlink CSI based on the channel reciprocity between the uplink and the downlink. Although uplink and downlink channel training are widely adopted in wireless communications, their performance has never been examined in the context of SPC. The most pressing challenge here is that the impact of the finite blocklength needs to be considered, where the achievable data rates have never been derived by considering the cost of different channel training strategies and the effect of the channel dispersion.

Channel Reciprocity: It is well known that the benefits of utilizing channel reciprocity to enable uplink channel training in multiple-input multiple-output (MIMO) systems scale linearly with the number of transmit antennas at the BS [61, 62]. This is due to the fact that the resources (e.g., time slots) used in the downlink channel training are linear functions of the number of transmit antennas [61], while the ones used in the uplink channel training are independent of this number [62]. However, achieving channel reciprocity in practical scenarios requires appropriate hardware calibrations to compensate for the unknown amplitude scaling and phase shift between the downlink and uplink channels [63]. Meanwhile, we note that the performance of uplink channel training highly depends on the amount of the achieved channel reciprocity. Against this background, a never-before-answered question is *"How much channel reciprocity is required to guarantee the uplink channel training to outperform the downlink channel training?"*. The answer to this question is pivotal for reducing the wireless transmission latency in SPC for URLLC applications.

Channel Estimation Overhead: Considering the low-latency constraint, the coding blocklength (i.e., channel uses or packet size) is required to be as short as possible in URLLC applications [22, 23]. We note that it is a huge challenge to satisfy the reliability and latency requirements of URLLC when the coding blocklength becomes short and limited in practice. Specifically, the decoding error probability is no longer arbitrarily small for finite blocklength and accurate CSI is hard to be achieved in wireless networks within a short time period. Existing studies, aiming at ensuring the requirements of URLLC in the finite blocklength regime, mainly assumed that the CSI is available or can be accurately estimated by using negligible channel uses. For instance, radio resource management in the finite blocklength regime was investigated to satisfy QoS requirements with signaling overhead for downlink transmission via cross-layer resource allocation in [54], and for short packet delivery via joint uplink and downlink optimization in [64]. In [65], the optimal power allocation was studied for QoS-constrained downlink multi-user networks with different types of data arrival. In the aforementioned studies, the cost of channel estimation to satisfy QoS requirements was ignored by adopting the assumption that CSI is *a prior* available or estimated by using negligible resources. Meanwhile, the impact of channel estimation cost on transmitting short packets in the finite blocklength regime was examined in the literature (e.g., [25, 66]), which revealed that such cost can be dominant and significantly affects the achievable reliability, especially when the low-latency requirement is very stringent. Therefore, how to significantly reduce or avoid

the channel estimation overhead becomes an urgent and challenging research problem in SPC.

1.2.2 Channel Inversion Power Control in SPC for One-Way URLLC

Following the aforementioned discussions, we note that traditional channel estimation with feedback may cost extra signalling overhead, which results in non-negligible transmission and processing delay. As such, the traditional channel estimation may not work properly in some URLLC services. Against this background, traditional channel estimation needs to be revisited or modified with novel design in order to fulfill the strict requirements of URLLC. When channel reciprocity holds, channel inversion power control (CIPC) can be used for wireless communications, while eliminating the conventional requirement that a user needs to know the CSI for decoding information [67, 68]. This is due to the fact that a BS can use CIPC to adjust the magnitude and phase of the channel by varying the transmit power with a proper precoding signal. As a consequence, the effective channel is a constant value, which is *a prior* agreed between the BS and the user. This property leads to that CIPC may serve as a key enabler of one-way URLLC in future wireless networks. Notably, one-way URLLC has a wide range of applications. For example, in vehicular wireless networks the communication from a BS to a vehicle that delivers an urgent message triggered by the reception and processing of the uplink information requires one-way URLLC, while the communication on the other way (mainly delivering periodically measurements or updates) may not require URLLC. Similar application scenarios can also be found in digital medical systems and industrial IoT systems.

Although CIPC has been studied in different communication scenarios (e.g., [67, 68, 69]), its performance and the associated optimization of the agreed constant power have never been investigated in the context of SPC. It is worthwhile to mention that the optimization problem in SPC is non-convex in general due to the consideration of maximal achievable rate in finite blocklength regime. Besides, we note that channel reciprocity may not be perfect in practice due to the challenging channel hardening issues [70, 71, 72]. As such, the impact of the imperfectness on the performance of CIPC in one-way URLLC should be examined. In CIPC, the power at the BS needs to approach infinity to ensure a constant power of the received signal that is used to decode the useful information for some low-quality channel realizations. As such, another key factor that limits the performance of CIPC is the maximum transmit power constraint, which determines when the BS has to suspend its transmission. These issues motivate us to tackle the feasibility and the optimal design of using CIPC in SPC to achieve the one-way URLLC and establish the fundamental limit of one-way URLLC achieved by CIPC.

1.2.3 Physical Layer Security in Short-Packet Communications

PLS has been well investigated in the existing literature [29, 32, 73, 74], where the blocklength of channel codes is assumed to be long enough for achieving the secrecy capacity.

However, to meet the latency and reliability requirements in URLLC applications, the blocklength of channel codes is short and the decoding error probability should be considered [75]. Given this necessity, [76] derived a lower bound on the maximal achievable secrecy rate in the finite blocklength regime. Based on this result, secure short-packet transmissions were further studied in [34, 44, 77]. In [44], the secrecy throughput in the finite blocklength regime was studied, where the optimal blocklength was found under the secrecy constraint for the single-antenna case and an artificial-noise-aided transmission scheme was investigated for the multiple-antenna case. [34] studied the resource allocation for a secure multi-user downlink short-packet transmission system, where the weighted sum throughput (WST) maximization and total transmit power (TTP) minimization problems were addressed by jointly optimizing bandwidth and power allocation. More recently, the total transmit power minimization problem in URLLC was studied in [77], where artificial noise is used to enhance the secrecy by degrading the eavesdropper's channel.

In addition to the transmission delay at the physical layer, the queueing delay at the link layer is a significant component of the end-to-end latency. The existing studies on the secure transmission under statistical quality-of-service (QoS) constraints (i.e., a queueing delay bound and a delay bound violation probability) mainly focused on the scenarios with long coding blocklength. Specifically, [78] optimized the power control policy to maximize the secrecy data rate under statistical QoS constraints. The throughput and energy efficiency of secure transmission of delay-sensitive data was studied in [79]. In [80], joint link selection and power control policies were proposed to improve the secrecy throughput of a buffer-aided two-hop communication link. Recently, how to achieve security and statistical QoS constraints in non-orthogonal multiple access and cognitive radio networks were studied in [81] and [82], respectively. Despite that these papers stand on their own merits, the impact of short coding blocklength on secure transmission under statistical QoS constraints has not been investigated.

It is worth noting that the effect of channel estimation errors has not been taken into account in the previous studies. For example, in [44], the transmitter was assumed to have perfect CSI of the intended user and only the statistical CSI of the eavesdropper. In [34, 77, 80, 81], the perfect CSI of both the intended user and the eavesdropper was assumed to be available at the transmitter. Such an assumption is over-optimistic and impractical in real wireless systems. Therefore, how to improve the achievable secrecy rate in the short blocklength regime with channel estimation errors remains an open problem. It is further noted that the solutions to WST maximization and TTP minimization problems in [34, 77] are suboptimal since the successive convex approximation is used to convert non-convex problems to convex ones. Although their results provide useful insights, the suboptimal solutions not only result in non-negligible performance loss but also require iterative search with relatively high computational complexity.

Recent breakthroughs in deep learning show that the deep neural network (DNN) is one

of the most promising tools for functional approximation in wireless communication systems [75]. If we can find the optimal solutions by using optimization algorithms, such as the algorithm in [65], we can train a DNN by using the optimal solutions as labeled training samples. Alternatively, one can use the objective function of the optimization problem as the loss function to train a DNN [83]. After offline training, the output of DNN (a near-optimal solution) can be obtained by using the forward-propagation algorithm, which has low computational complexity [56]. When using deep learning to optimize wireless networks, there are two major issues: 1) lack of labeled training samples if the optimal solutions cannot be obtained and 2) no QoS guarantee or power constraint if the objective function is used as the loss function. To handle these issues, unsupervised deep learning has been proposed to solve constrained optimization problems in [84, 85].

1.3 Thesis Outline and Contributions

This thesis mainly focuses on the transmission strategies and power control policies design of SPC for URLLC applications. To reach these research goals, we consider different channel training strategies, optimal resource allocation, and channel inversion power control with channel reciprocity to reduce the signalling overhead in SPC. We also establish a framework for optimizing the power control policy to realize the secure transmission rate of short packets while satisfying the URLLC requirement. The specific contributions of each chapter are detailed below:

Chapter 2 – Channel Training Strategies for SPC

In Chapter 2, we study the dowlink and uplink channel training strategies in SPC. Our results show the necessity and benefits of activating the uplink channel training for SPC with multiple transmit antennas. The main contributions of this chapter are summarized as follows:

- We examine the performance of the downlink and uplink channel training strategies in SPC. Specifically, we derive closed-form expressions for the lower bounds on the data rates achieved by these two strategies. These expressions allow us to determine the minimum channel reciprocity that is required to ensure a higher data rate achieved by the uplink channel training relative to the downlink channel training. We then determine an analytical expression to approximate this minimum channel reciprocity to draw useful insights into the affecting parameters.

- Our examination indicates that the minimum channel reciprocity decreases as the total blocklength decreases, which demonstrates the superiority of the uplink channel training in the context of SPC. As expected, our results show that this minimum channel

reciprocity also decreases as the number of transmit antennas at the BS increases. This indicates that the uplink channel training becomes more desirable and easier to achieve when a large number of transmit antennas are deployed at the BS. The derived minimum channel reciprocity provides practical guidelines on choosing channel training strategies and channel reciprocity calibrations.

The results in this chapter have been presented in [86], which is listed again for ease of reference:
[86] **C. Li**, S. Yan, and N. Yang, "On channel reciprocity to activate uplink channel training for downlink wireless transmission in Tactile Internet applications," in *Proc. IEEE Int. Conf. Commun. (ICC) Workshop*, Kansas City, MO, May 2018, pp. 1-6.

Chapter 3 – Optimal Resource Allocation for SPC

In Chapter 3, we study the optimal resource allocation (e.g., the total transmit power and a finite number of symbol periods) for downlink training, uplink feedback, and data transmission to maximize the average data rate in a multiple-input single-output (MISO) system which adopts SPC. The main contributions of this chapter are summarized as follows:

- We design the optimal power and symbol period allocation to maximize the average data rate of the downlink in a MISO system which uses SPC. In the system with finite blocklength T, the N_A-antenna access point (AP) estimates the downlink channel with the aid of downlink training and uplink feedback, and then performs data transmission.
- We derive an approximate closed-form expression for the lower bound on the average data rate taking into account T, based on which we determine the optimal symbol periods allocated to downlink training, uplink feedback, and data transmission, as well as the optimal power allocation between downlink training and data transmission. Aided by numerical results, we examine the impact of system parameters on the optimal power and symbol period allocation.

The results in this chapter have been presented in [66], which is listed again for ease of reference:
[66] **C. Li**, N. Yang, and S. Yan, "Optimal transmission of short-packet communications in multiple-input single-output systems," *IEEE Trans. Veh. Technol.*, vol. 68, no. 7, pp. 7199–7203, Jul. 2019.

Chapter 4 – Channel Inversion Power Control for One-Way URLLC

In Chapter 4, we study the feasibility and optimal design of using CIPC to reduce the channel estimation overhead for achieving one-way URLLC and establish the fundamental limit of

one-way URLLC achieved by CIPC. The main contributions of this chapter are summarized as follows:

- We develop a fundamental framework for using the truncated CIPC scheme to achieve one-way URLLC. To this end, we first derive a new expression for the packet loss probability P_ε of this scheme, which is determined by both the decoding error probability caused by the finite blocklength T and the transmission probability enforced by the maximum transmit power $P_{\max}$. We then derive an approximated but easy-to-calculate expression for P_ε as a function of the channel reciprocity characterised by the parameter ϕ, based on which we explicitly determine a closed interval for the optimal constant value Q to minimize P_ε, where Q is the received signal power *a priori* agreed between the BS and the user.

- We analyze the performance of the conventional CIPC scheme in the context of one-way URLLC, which is the special case of the truncated CIPC scheme with $P_{\max} \to \infty$. The packet loss probability P_ε of the conventional CIPC scheme converts into the decoding error probability caused by the finite blocklength T, which enables us to derive a closed-form expression (as an explicit expression of the blocklength T and the channel reciprocity parameter ϕ) to approximate P_ε. The packet loss probability of the conventional CIPC scheme offers an upper bound on the performance of the truncated CIPC scheme. Thus, the closed-form expression significantly facilitates us to examine the performance limit of one-way URLLC achieved by CIPC with imperfect channel reciprocity (i.e., $0 < \phi < 1$).

- We derive the packet loss probability for the truncated CIPC scheme with perfect channel reciprocity (i.e., $\phi = 1$), denoted as $P_\varepsilon^{\phi=1}$, which is not a special case of that for the truncated CIPC scheme with imperfect channel reciprocity. We analyze the convexity of P_ε w.r.t. Q and establish a convex set for optimizing the value of Q in the truncated CIPC scheme with perfect channel reciprocity. Our examination draws novel design guidelines for achieving one-way URLLC with CIPC schemes. For instance, the maximum transmit power or number of transmit antennas can be explicitly determined using our analysis to perform a fixed-rate transmission with specific requirements on reliability and latency.

The results in this chapter have been presented in [87, 88], which are listed again for ease of reference:

[87] **C. Li**, S. Yan, N. Yang, X. Zhou, and R. Chen, "One-way URLLC with truncated channel inversion power control," in *Proc. IEEE Global Commun. Conf. (Globecom) Workshop*, Waikoloa, HI, Dec. 2019, pp. 1-6.

[88] **C. Li**, S. Yan, N. Yang, and X. Zhou, "Truncated channel inversion power control to enable one-way URLLC with imperfect channel reciprocity," submitted to *IEEE Trans. Commun*.

Chapter 5 – Secure Transmission Rate of Short Packets

In Chapter 5, a comprehensive study of secure SPC with different assumptions on the CSI is carried out. We investigate how much CSI is needed to realize secure SPC under the average power constraint and queueing delay requirement. The main contributions of this chapter are summarized as follows:

- We establish a framework for optimizing the power control policy under average transmit power constraints. Based on the performance metric in [78], we formulate the objective function as the effective secrecy throughput, which is the maximum achievable secrecy rate in the finite blocklength regime with the statistical QoS requirement. The framework is applied in four different scenarios, i.e., 1) the full CSI scenario (i.e., perfect CSI of both the intended user and eavesdropper are available at the transmitter), 2) the partial CSI scenario (i.e., perfect CSI of the intended user and statistical CSI of the eavesdropper are available at the transmitter), 3) the full CSI scenario with channel estimation errors, and 4) the partial CSI scenario with channel estimation errors.

- To provide useful insights, we derive the closed-form expressions for the optimal power control policies in a special case. By comparing the solutions in the full CSI scenario and the partial CSI scenario, we find that when the average signal-to-noise ratio (SNR) is high, the knowledge of the perfect CSI of the eavesdropper only provides marginal performance gain in terms of the effective secrecy throughput.

- To find numerical solutions with low-computational complexity in general cases, we apply an unsupervised learning approach to find the optimal power control policy numerically. The underlying idea is to use a DNN to approximate the normalized power control policy and apply the primal-dual method to optimize the parameters of the DNN and the Lagrangian multiplier. We validate the convergence behaviors, effectiveness and accuracy of the proposed unsupervised learning method in both the special and general cases. Numerical results show that the learning-based power control policy approaches the closed-form optimal policy as the number of iterations increases in the special cases, and achieves higher secure effective throughput than two existing power control policies in general cases, namely, the “water-filling" policy in [38] and the constant power control policy.

- We further investigate the impacts of channel estimation errors on the normalized power control policies in the full and partial CSI scenarios, where we consider imperfect channel estimation at the receiver and assume perfect feedback from the receiver to the AP. Numerical results show that in the presence of channel estimation errors, the learning-based power control policy can guarantee the average power constraint, while the closed-form optimal power control policy cannot.

The results in this chapter have been presented in [89, 90], which are listed again for ease of reference:

[89] **C. Li**, C. She, and N. Yang, "Unsupervised learning for secure transmissions of short packets under statistical QoS constraints," in *Proc. IEEE Global Commun. Conf. (Globecom) Workshop*, Taipei, Taiwan (ROC), Dec. 2020, pp. 1-6.

[90] **C. Li**, C. She, N. Yang and T. Q. S. Quek, "Secure transmission rate of short packets with queueing delay requirement," *IEEE Trans. Wireless Commun*, accepted on 30 June 2021, Early Access.

Chapter 2

Channel Training Strategies for SPC

2.1 Introduction

In this chapter, we compare the uplink channel training and downlink channel training in the context of SPC. We focus on investigating the requirement on channel reciprocity to activate uplink channel training, instead of downlink channel training, to achieve a higher data rate for the downlink transmission from a multi-antenna base station to a single-antenna user. We first derive novel closed-form expressions for the lower bounds on the data rates achieved by two channel training strategies by considering the impact of finite blocklength. The performance comparison result of these two strategies is determined by the amount of channel reciprocity that is utilized in the uplink channel training. We then derive an approximated expression for the minimum channel reciprocity that enables uplink channel training to outperform downlink channel training. Through numerical results, we demonstrate that this minimum channel reciprocity decreases as the blocklength decreases or the number of transmit antennas increases, which shows the necessity and benefits of activating uplink channel training for SPC with multiple transmit antennas. This work provides pivotal and unprecedented guidelines on choosing channel training strategies and channel reciprocity calibrations, offering valuable insights into latency reduction in SPC for URLLC applications.

This chapter is organized as follows. In Section 2.2, we describe the system model with two different channel training strategies. We present the achievable data rates of two channel training strategies in Section 2.3. In Section 2.4, we analyze the channel reciprocity for uplink channel training outperforming downlink channel training. Numerical results and conclusion are provided in Section 2.5 and 2.6, respectively.

2.2 System Model

We consider a MISO communications system where an N_{B}-antenna BS communicates with a single-antenna user. We denote $\mathbf{h}_{\mathrm{u}}$ as the $N_{\mathrm{B}} \times 1$ uplink channel vector from the user to the BS and denote $\mathbf{h}_{\mathrm{d}}$ as the $1 \times N_{\mathrm{B}}$ downlink channel vector from the BS to the user. All the

channels are subject to independent quasi-static Rayleigh fading with the finite blocklength T. We assume that the channels remain constant during one fading block. The entries of $\mathbf{h}_{\mathrm{u}}$ and $\mathbf{h}_{\mathrm{d}}$ are assumed to be independent and identically distributed (i.i.d.) circularly symmetric complex Gaussian random variables with zero mean and unit variance, i.e., $\mathbf{h}_{\mathrm{d}} \sim \mathcal{CN}(0, \mathbf{I}_{N_{\mathrm{B}}})$ and $\mathbf{h}_{\mathrm{u}} \sim \mathcal{CN}(0, \mathbf{I}_{N_{\mathrm{B}}})$, where $\mathcal{CN}(\mu, \nu)$ is the complex Gaussian distribution with the mean of μ and the variance of ν and $\mathbf{I}_{N_{\mathrm{B}}}$ is an $N_{\mathrm{B}} \times N_{\mathrm{B}}$ identity matrix. Furthermore, we assume that the transmit power P_{b} at the BS is fixed for each channel use. Additionally, we assume that the user and the BS have the knowledge about the statistical information of all the channels.

2.2.1 Channel Training

- **Uplink Channel Training:** In the uplink channel training, $\mathbf{h}_{\mathrm{u}}$ is obtained at the BS via uplink training where the user sends pilot sequences to the BS for estimating $\mathbf{h}_{\mathrm{u}}$. Considering the channel reciprocity between the uplink and the downlink, the downlink channel vector can be expressed as a function of the uplink channel vector, given by [72, 91]

$$\mathbf{h}_{\mathrm{d}} = \sqrt{\phi}\mathbf{h}_{\mathrm{u}}^{T} + \sqrt{1-\phi}\mathbf{e}^{T}, \tag{2.1}$$

  where ϕ is defined as the channel reciprocity coefficient between the uplink and the downlink, $\mathbf{h}_{\mathrm{u}}^{T}$ represents the transpose of $\mathbf{h}_{\mathrm{u}}$, and $\mathbf{e}$ is the $N_{\mathrm{B}} \times 1$ vector which reflects the uncertain part of $\mathbf{h}_{\mathrm{u}}$. The entries of $\mathbf{e}$ are i.i.d. and each of them follows $\mathcal{CN}(0,1)$.

  We note that the value of ϕ quantifies the level of channel reciprocity, where $0 \leq \phi \leq 1$. In practical scenarios, the level of channel reciprocity is determined by the uplink channel estimation error and the frequency offset between the transmitter and receiver [92]. Specifically, $\phi = 1$ indicates that the perfect channel reciprocity is achieved such that the downlink channel is exactly the same as the uplink channel. When ϕ decreases, the channel reciprocity becomes less reliable. When $\phi = 0$, the channel reciprocity does not exist such that the downlink channel is independent of the uplink channel.

- **Downlink Channel Training:** In the downlink channel training, $\mathbf{h}_{\mathrm{d}}$ is obtained at the BS via downlink training and uplink feedback where the BS sends pilot sequences to the user for estimating $\mathbf{h}_{\mathrm{d}}$ and then the user feeds back the estimate. When the BS sends pilot sequences in T_{tr} symbol periods, the received signal at the user is given by

$$\mathbf{y}_{\mathrm{d}} = \sqrt{\Lambda}\mathbf{h}_{\mathrm{d}}\mathbf{S}_{\mathrm{d}} + \mathbf{n}_{\mathrm{d}}, \tag{2.2}$$

  where $\Lambda \triangleq T_{\mathrm{tr}}P_{\mathrm{b}}/N_{\mathrm{B}}$, $\mathbf{y}_{\mathrm{d}}$ is the $1 \times T_{\mathrm{tr}}$ received signal vector, $\mathbf{S}_{\mathrm{d}}$ is the $N_{\mathrm{B}} \times T_{\mathrm{tr}}$ pilot sequence matrix transmitted by the BS which satisfies $\mathbf{S}_{\mathrm{d}}\mathbf{S}_{\mathrm{d}}^{H} = \mathbf{I}_{N_{\mathrm{B}}}$, and $\mathbf{n}_{\mathrm{d}}$ is the $1 \times T_{\mathrm{tr}}$

additive white Gaussian noise (AWGN) vector at the user with i.i.d entries following $\mathcal{CN}\left(0,\sigma_{\mathrm{u}}^2\right)$. We assume that the linear minimum mean square error (MMSE) estimator is adopted at the user. Based on the known pilot sequences, the user obtains the estimates of $\mathbf{h}_{\mathrm{d}}$ as [60, 93]

$$\hat{\mathbf{h}}_{\mathrm{d}} = \frac{\sqrt{\Lambda}}{\Lambda+\sigma_{\mathrm{u}}^2}\mathbf{y}_{\mathrm{d}}\mathbf{S}_{\mathrm{d}}^H. \tag{2.3}$$

As per the rules of the linear MMSE estimator, the entries of $\hat{\mathbf{h}}_{\mathrm{d}}$ are i.i.d. and each of them follows $\mathcal{CN}\left(0,\sigma_{\hat{\mathrm{h}}_{\mathrm{d}}}^2\right)$, where $\sigma_{\hat{\mathrm{h}}_{\mathrm{d}}}^2 = \Lambda/\left(\Lambda+\sigma_{\mathrm{u}}^2\right)$. We note that the estimation error, given by $\hat{\mathbf{e}}_{\mathrm{d}} = \mathbf{h}_{\mathrm{d}} - \hat{\mathbf{h}}_{\mathrm{d}}$, is independent of the estimate $\hat{\mathbf{h}}_{\mathrm{d}}$. We also note that the entries of $\hat{\mathbf{e}}_{\mathrm{d}}$ are i.i.d. and each follows $\mathcal{CN}\left(0,\sigma_{\hat{\mathrm{e}}_{\mathrm{d}}}^2\right)$, where $\sigma_{\hat{\mathrm{e}}_{\mathrm{d}}}^2 = \sigma_{\mathrm{u}}^2/\left(\Lambda+\sigma_{\mathrm{u}}^2\right)$. We note that $T_{\mathrm{tr}} \geq N_{\mathrm{B}}$ needs to be ensured in the system, in order to obtain a reliable estimate of $\mathbf{h}_{\mathrm{d}}$.

2.2.2 Data Transmission

After obtaining the downlink channel vector through either the uplink channel training or the downlink channel training, the BS selects an $N_{\mathrm{B}} \times 1$ normalized beamforming vector $\mathbf{v}$ to transmit signals to the user. The BS uses the obtained CSI as it is perfect. Therefore, the transmitted signal $\mathbf{x}$ is written as $\mathbf{x} = \mathbf{v}u$, where u is the information signal transmitted from the BS to the user. The received signal at the user in one symbol period is given by

$$y = \sqrt{P_{\mathrm{b}}}\mathbf{h}_{\mathrm{d}}\mathbf{x} + n = \sqrt{P_{\mathrm{b}}}\mathbf{h}_{\mathrm{d}}\mathbf{v}u + n, \tag{2.4}$$

where n is the AWGN at the user with zero mean and variance σ_{u}^2, while $\mathbf{x}$ is subject to the average power constraint $\mathbb{E}\left[\|\mathbf{x}\|^2\right] = 1$.

2.2.3 Data Rate with Finite Blocklength

Considering finite-blocklength transmission, the achievable data rate in the fading channel can be tightly approximated as $R(T,\varepsilon,\gamma)$ which is a function of the blocklength (i.e., the number of channel use) T, the decoding error probability ε, and the SNR γ [25]. Mathematically, this function is given by [27]

$$R(T,\varepsilon,\gamma) \approx C(\gamma) - \sqrt{\frac{1}{T}V(\gamma)}f_Q^{-1}(\varepsilon), \tag{2.5}$$

where $C(\gamma) = \log_2(1+\gamma)$ is the channel capacity, $V(\gamma) = \left(\log_2 e\right)^2\left(1-(1+\gamma)^{-2}\right)$ is the channel dispersion, and $f_Q^{-1}(\cdot)$ is the inverse Gaussian Q-function. We note that (2.5) is tight, even for a relatively small T, e.g., $T = 100$ [27].

2.3 Achievable Data Rates of Uplink and Downlink Channel Training Strategies

In this section, we focus on an ideal scenario, where the uplink channel training is perfect (i.e., no channel estimation error) and does not cost any time slot, meanwhile the feedback in the downlink channel training is perfect (i.e., no feedback error) and of no cost in terms of time slots. We would like to clarify that in this scenario, the ignored cost of time slots in two channel training strategies may not be the same. Notably, in general this cost is higher for the downlink channel training than that for the uplink channel training. In the uplink channel training, the user can use only one time slot to send pilot sequences and the BS only has to feed $||\mathbf{h}||$, but not $\mathbf{h}$, back to the user. In the downlink channel training, however, the user has to feed $\mathbf{h}$ (i.e., N_{B} complex numbers) back to the BS. We next derive lower bounds on the data rates achieved by uplink channel training and downlink channel training.

2.3.1 Achievable Data Rate of Uplink Channel Training

Under the assumption of perfect uplink channel training, the BS has the perfect knowledge about the uplink channel. As such, the beamforming vector is selected as $\mathbf{v} = \mathbf{h}_{\mathrm{u}} / \|\mathbf{h}_{\mathrm{u}}\|$ and the received signal at the user in one symbol period is given by

$$\begin{aligned} y &= \sqrt{P_{\mathrm{b}}}\mathbf{h}_{\mathrm{d}}\mathbf{x} + n = \sqrt{P_{\mathrm{b}}}\left(\sqrt{\phi}\ \mathbf{h}_{\mathrm{u}}^T + \sqrt{1-\phi}\ \mathbf{e}^T\right)\mathbf{v}u + n \\ &= \sqrt{P_{\mathrm{b}}\phi}\mathbf{h}_{\mathrm{u}}^T \frac{\mathbf{h}_{\mathrm{u}}}{\|\mathbf{h}_{\mathrm{u}}\|}u + \underbrace{\sqrt{P_{\mathrm{b}}\left(1-\phi\right)}\mathbf{e}^T \frac{\mathbf{h}_{\mathrm{u}}}{\|\mathbf{h}_{\mathrm{u}}\|}u + n}_{\tilde{n}}. \end{aligned} \tag{2.6}$$

Following [60], in this work we consider the worst-case scenario for decoding at the user, where $\tilde{n}$ in (2.6) is approximated as the zero-mean Gaussian noise. Under this approximation, the achievable data rate derived below is a lower bound. As per (2.6), the signal-to-interference-plus-noise ratio (SINR) at the user is given by

$$\gamma_{\mathrm{u}} = \frac{P_{\mathrm{b}}\phi\|\mathbf{h}_{\mathrm{u}}\|^2}{P_{\mathrm{b}}\left(1-\phi\right)\frac{|\mathbf{e}^T\mathbf{h}_{\mathrm{u}}|^2}{\|\mathbf{h}_{\mathrm{u}}\|^2} + \sigma_{\mathrm{u}}^2} = \frac{P_{\mathrm{b}}\phi\ \|\mathbf{h}_{\mathrm{u}}\|^2}{\sigma_{\tilde{\mathrm{n}}}^2}, \tag{2.7}$$

where $\sigma_{\tilde{n}}^2$ is the variance of $\tilde{n}$, given by $\sigma_{\tilde{n}}^2 = P_b(1-\phi) + \sigma_u^2$. Considering finite-blocklength transmission, for a given ε the lower bound on the data rate can be approximated by [27]

$$\begin{aligned} R_u &= \mathbb{E}_{\|\mathbf{h}_u\|^2}\left[C(\gamma_u) - \sqrt{\frac{1}{T}V(\gamma_u)}\, f_Q^{-1}(\varepsilon)\right] \\ &= \mathbb{E}_{\|\bar{\mathbf{h}}_u\|^2}\left[C\left(\gamma_{\text{eff}}^u \|\bar{\mathbf{h}}_u\|^2\right)\right] - \mathbb{E}_{\|\bar{\mathbf{h}}_u\|^2}\left[\sqrt{\frac{1}{T}V\left(\gamma_{\text{eff}}^u \|\bar{\mathbf{h}}_u\|^2\right)}\, f_Q^{-1}(\varepsilon)\right], \end{aligned} \tag{2.8}$$

where $\bar{\mathbf{h}}_u \triangleq \mathbf{h}_u / \sigma_{h_u}$ is the normalized channel vector, σ_{h_u} is the standard deviation of $\mathbf{h}_u$, $\bar{\mathbf{h}}_u \sim \mathcal{CN}(0, \mathbf{I}_{N_B})$, $\gamma_{\text{eff}}^u = \frac{\rho_b \phi}{(1-\phi)\rho_b + 1}$ is the effective SNR, and $\rho_b = P_b / \sigma_u^2$ is the average SNR.

In the following theorem, we derive a closed-form expression for the lower bound on the data rate achieved by the uplink channel training.

Theorem 2.1. The lower bound on the data rate achieved by uplink channel training is derived as

$$R_u = \Phi(\gamma_{\text{eff}}^u, N_B) - \Psi(\gamma_{\text{eff}}^u, N_B, T), \tag{2.9}$$

where the functions $\Phi(\gamma_{\text{eff}}^u, N_B)$ and $\Psi(\gamma_{\text{eff}}^u, N_B, T)$ are given by (2.10) and (2.11), respectively.

$$\Phi(\gamma_{\text{eff}}, N_B) = \frac{e^{\frac{1}{\gamma_{\text{eff}}}}}{\ln 2\, \Gamma(N_B)\, \gamma_{\text{eff}}^{N_B}} \sum_{i=0}^{N_B-1} \binom{N_B-1}{i} (-1)^{N_B-1-i}\, \mathbf{G}_{2,3}^{3,0}\left(\begin{matrix} -i, -i \\ 0, -1-i, -1-i \end{matrix} \middle| \frac{1}{\gamma_{\text{eff}}} \right). \tag{2.10}$$

$$\Psi(\gamma_{\text{eff}}, N_B, T) = \sqrt{\frac{2\pi}{T}}\, \frac{f_Q^{-1}(\varepsilon)}{\Gamma(N_B)\, \ln 2}\, e^{-(N_B-1)}\, (N_B-1)^{N_B-\frac{1}{2}} \sqrt{1 - (1+\gamma_{\text{eff}}(N_B-1))^{-2}}. \tag{2.11}$$

Proof: See Appendix *A.1*. ■

It is noted that Theorem 2.1 presents a channel-independent and accurate expression for the lower bound on the data rate achieved by the uplink channel training. This expression allows us to compare the performance of the uplink channel training and downlink channel training efficiently.

2.3.2 Achievable Data Rate of Downlink Channel Training

As assumed in the ideal scenario, the feedback from the user to the BS is perfect. As such, the BS has $\hat{\mathbf{h}}_d$ and the beamforming vector is selected as $\mathbf{v} = \hat{\mathbf{h}}_d / \|\hat{\mathbf{h}}_d\|$. Then, the received signal

at the user in one symbol period is given by

$$\begin{aligned} y &= \sqrt{P_{\mathrm{b}}}\mathbf{h}_{\mathrm{d}}\mathbf{x}+n = \sqrt{P_{\mathrm{b}}}\left(\hat{\mathbf{h}}_{\mathrm{d}}+\hat{\mathbf{e}}_{\mathrm{d}}\right)\mathbf{v}u+n \\ &= \sqrt{P_{\mathrm{b}}}\hat{\mathbf{h}}_{\mathrm{d}}\frac{\hat{\mathbf{h}}_{\mathrm{d}}}{\left\|\hat{\mathbf{h}}_{\mathrm{d}}\right\|}u+\underbrace{\sqrt{P_{\mathrm{b}}}\hat{\mathbf{e}}_{\mathrm{d}}\frac{\hat{\mathbf{h}}_{\mathrm{d}}}{\left\|\hat{\mathbf{h}}_{\mathrm{d}}\right\|}u+n}_{\hat{n}}. \end{aligned} \tag{2.12}$$

Once again, we consider the worst-case scenario for decoding at the user where $\hat{n}$ in (2.12) is approximated as Gaussian. Accordingly, the SINR at the user is given by

$$\gamma_{\mathrm{d}} = \frac{P_{\mathrm{b}}\left\|\hat{\mathbf{h}}_{\mathrm{d}}\right\|^2}{P_{\mathrm{b}}\frac{\left|\hat{\mathbf{e}}_{\mathrm{d}}\hat{\mathbf{h}}_{\mathrm{d}}\right|^2}{\left\|\hat{\mathbf{h}}_{\mathrm{d}}\right\|^2}+\sigma_{\mathrm{u}}^2} = \frac{P_{\mathrm{b}}\|\hat{\mathbf{h}}_{\mathrm{d}}\|^2}{\sigma_{\hat{\mathrm{n}}}^2}, \tag{2.13}$$

where $\sigma_{\hat{\mathrm{n}}}^2$ is the variance of $\hat{n}$, given by $\sigma_{\hat{\mathrm{n}}}^2 = P_{\mathrm{b}}\sigma_{\hat{\mathrm{e}}_{\mathrm{d}}}^2+\sigma_{\mathrm{u}}^2$. Then, the lower bound on the data rate achieved by the downlink channel training is written as

$$\begin{aligned} R_{\mathrm{d}} &= \left(1-\frac{T_{\mathrm{tr}}}{T}\right)\mathbb{E}_{\left\|\hat{\mathbf{h}}_{\mathrm{d}}\right\|^2}\left[C\left(\gamma_{\mathrm{d}}\right)-\sqrt{\frac{1}{T}V\left(\gamma_{\mathrm{d}}\right)}\,f_Q^{-1}(\varepsilon)\right] \\ &= \left(1-\frac{T_{\mathrm{tr}}}{T}\right)\mathbb{E}_{\left\|\bar{\mathbf{h}}_{\mathrm{d}}\right\|^2}\left[C\left(\gamma_{\mathrm{eff}}^{\mathrm{d}}\left\|\bar{\mathbf{h}}_{\mathrm{d}}\right\|^2\right)\right] \\ &\quad -\left(1-\frac{T_{\mathrm{tr}}}{T}\right)\mathbb{E}_{\left\|\bar{\mathbf{h}}_{\mathrm{d}}\right\|^2}\left[\sqrt{\frac{1}{T}V\left(\gamma_{\mathrm{eff}}^{\mathrm{d}}\left\|\bar{\mathbf{h}}_{\mathrm{d}}\right\|^2\right)}\,f_Q^{-1}(\varepsilon)\right], \end{aligned} \tag{2.14}$$

where $\bar{\mathbf{h}}_{\mathrm{d}} \triangleq \hat{\mathbf{h}}_{\mathrm{d}}/\sigma_{\hat{\mathrm{h}}_{\mathrm{d}}}$ is the normalized channel estimate, $\sigma_{\hat{\mathrm{h}}_{\mathrm{d}}}$ is the standard deviation of $\hat{\mathbf{h}}_{\mathrm{d}}$, $\bar{\mathbf{h}}_{\mathrm{d}} \sim \mathcal{CN}(0,\mathbf{I}_{N_{\mathrm{B}}})$, and $\gamma_{\mathrm{eff}}^{\mathrm{d}} = \frac{\rho_{\mathrm{b}}\sigma_{\hat{\mathrm{h}}_{\mathrm{d}}}^2}{\rho_{\mathrm{b}}\sigma_{\hat{\mathrm{e}}_{\mathrm{d}}}^2+1}$ is the effective SNR.

We next derive a closed-form expression for the lower bound on the data rate achieved by the downlink channel training in the following theorem.

Theorem 2.2. The lower bound on the data rate achieved by the downlink channel training in (2.14) is derived as

$$R_{\mathrm{d}} = \left(1-\frac{T_{\mathrm{tr}}}{T}\right)\left[\Phi\left(\gamma_{\mathrm{eff}}^{\mathrm{d}},N_{\mathrm{B}}\right)-\Psi\left(\gamma_{\mathrm{eff}}^{\mathrm{d}},N_{\mathrm{B}},T\right)\right], \tag{2.15}$$

where the functions of $\Phi\left(\gamma_{\mathrm{eff}}^{\mathrm{d}},N_{\mathrm{B}}\right)$ and $\Psi\left(\gamma_{\mathrm{eff}}^{\mathrm{d}},N_{\mathrm{B}},T\right)$ are given by (2.10) and (2.11), respectively.

Proof: The proof is similar to the proof of Theorem 2.1 and thus omitted here. ■

2.4 Determination of Channel Reciprocity for Uplink Channel Training Outperforming Downlink Channel Training

In this section, we examine the minimum channel reciprocity coefficient (i.e., the minimum value of ϕ, which is denoted by ϕ^*) that enables the uplink channel training to outperform the downlink channel training. To this end, we derive a closed-form expression to approximate ϕ^* in the following proposition, which is channel-independent and can be used to select the better strategy between the uplink and downlink channel training in practice.

Proposition 2.1. The minimum channel reciprocity coefficient ϕ^* that enables the uplink channel training to outperform the downlink channel training is approximated as

$$\phi^* = \frac{(\rho_\mathrm{b}+1)(\kappa-1)}{\rho_\mathrm{b}(N_\mathrm{B}+\kappa-1)}, \tag{2.16}$$

where $\kappa = \left(1+\gamma_{\mathrm{eff}}^{\mathrm{d}} N_\mathrm{B}\right)^{\frac{T-T_{\mathrm{tr}}^*}{T}}$ and T_{tr}^* is the optimal value of T_{tr} that maximizes R_d in the downlink channel training.

Proof: See Appendix *A.2*. ■

2.5 Numerical Results

In this section, we present numerical results to examine the effectiveness of our analysis and solution, including our newly derived closed-form expressions for the lower bounds on the achievable data rates and the approximation of the minimum channel reciprocity coefficient.

In Fig. 2.1, we demonstrate the accuracy of our newly derived closed-form expression for the lower bound on the data rate achieved by the uplink channel training. The simulated and theoretical results are obtained from (2.8) and (2.9), respectively. In Fig. 2.1, we first observe that the theoretical curves precisely match the simulated ones, which confirms the correctness of (2.9) in Theorem 2.1. Moreover, as expected, in this figure we observe that the data rate significantly increases with ϕ. Furthermore, we observe that the data rate approaches a constant (but not infinity) as $\rho_b \to \infty$ when $\phi < 1$, while this data rate increases to infinity as $\rho_b \to \infty$ when $\phi = 1$. This is due to the fact that the lower bound on the data rate is a linear function of ρ_b when $\phi = 1$, since the effective SNR $\gamma_{\mathrm{eff}}^{\mathrm{u}}$ becomes ρ_b as $\rho_b \to \infty$ for $\phi = 1$. Differently, the lower bound is limited by the interference caused by the imperfect channel reciprocity, since $\gamma_{\mathrm{eff}}^{\mathrm{u}}$ becomes $\phi/(1-\phi)$ as $\rho_b \to \infty$ for $\phi < 1$.

Fig. 2.2 plots the lower bounds on the data rates achieved by the uplink and downlink channel training versus ϕ for different values of N_B. The curves for the uplink and downlink channel training are obtained from (2.9) and (2.15), respectively. In this figure, we first observe that the date rate achieved by the uplink channel training increases with ϕ, which meets

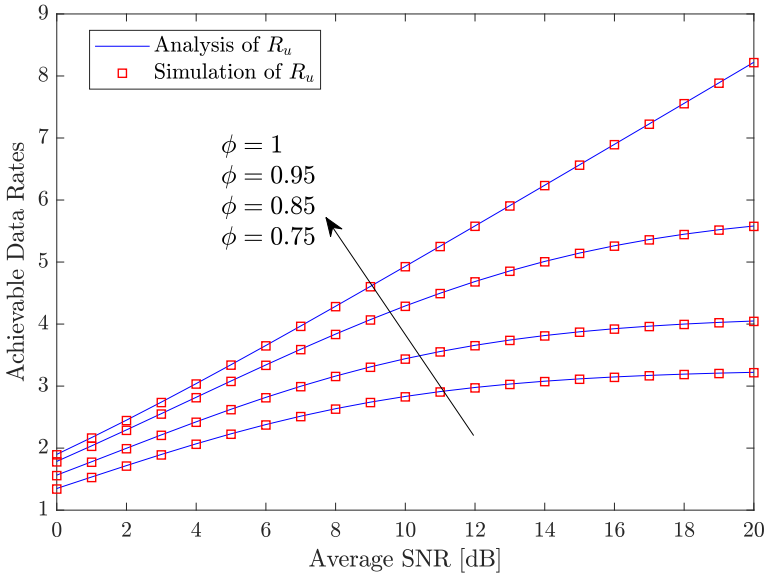

Figure 2.1: The lower bound on the data rate achieved by the uplink channel training versus the average SNR ρ_{b} for different values of ϕ with $N_{\mathrm{B}} = 5$, $\varepsilon = 10^{-9}$, and $T = 200$.

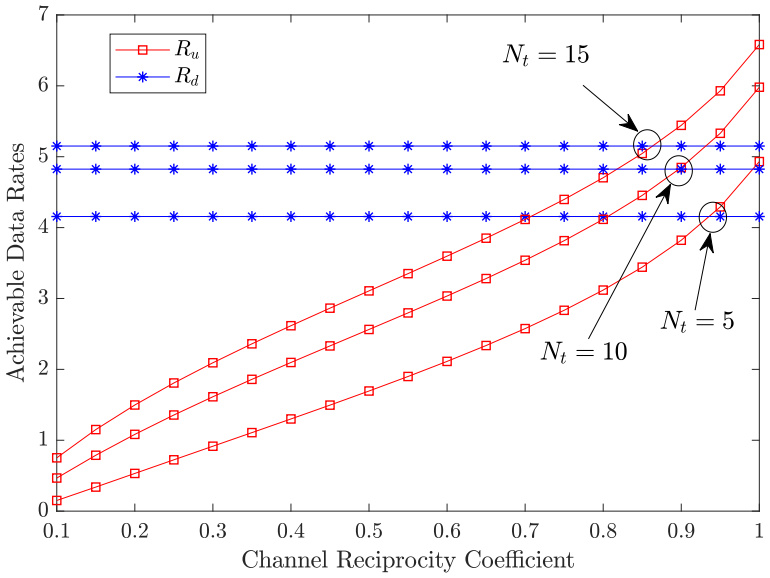

Figure 2.2: The lower bounds on the data rates achieved by the uplink and downlink channel training strategies versus the channel reciprocity coefficient ϕ for different value of N_{B} with $\rho_{\mathrm{b}} = 10$ dB, $\varepsilon = 10^{-9}$, and $T = 200$.

our expectation. Importantly, the date rate achieved by the uplink channel training becomes higher than that achieved by the downlink channel training when ϕ is greater than a specific value, which is ϕ^*. We also observe that ϕ^* decreases as the number of transmit antennas N_{B} increases. This is due to the fact that when N_{B} increases, more time slots need to be used to conduct downlink channel training, while the number of time slots used for the uplink channel

training does not change (since N_{B} is the number of receive antennas in the uplink).

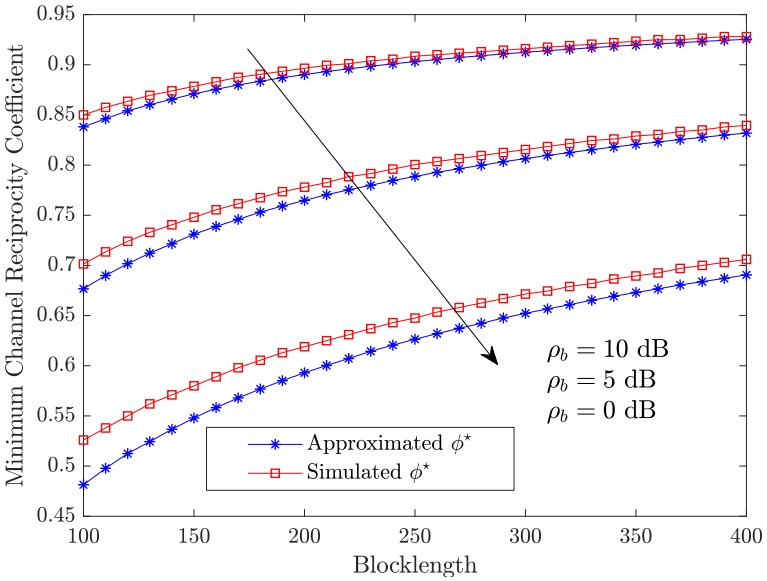

Figure 2.3: The minimum channel reciprocity coefficient ϕ^* versus the blocklength T for different values of ρ_{b} with $N_{\mathrm{B}} = 10$ and $\varepsilon = 10^{-5}$.

In Fig. 2.3, we examine the accuracy of our approximation of the minimum channel reciprocity coefficient ϕ^*, for which the uplink channel training outperforms the downlink channel training. To this end, we compare the simulated ϕ^* obtained based on (A.7) and the approximated ϕ^* obtained from (2.16). In Fig. 2.3, we first observe that the approximated curves are very close to the simulated ones. Also, we observe that the approximation accuracy improves when ρ_{b} increases, which is due to the fact that the rate loss caused by the finite blocklength becomes negligible when ρ_{b} tends to be large and this rate loss is not considered in our approximation. In this figure, we further observe that ϕ^* increases with T and ρ_{b}. This is due to the fact that the number of time slots (at least $N_{\mathrm{B}} - 1$) or the power saved by the uplink channel training relative to the downlink channel training becomes less significant when T or ρ_{b} increases, respectively.

2.6 Summary

In this chapter, we first fully examined the performance of uplink and downlink channel training strategies. In doing so, we derived closed-form expressions for the lower bounds on the data rates achieved by these two strategies, in which the impact of finite blocklength and channel dispersion was considered. Aided by these expressions, we analytically determined an expression to approximate the minimum channel reciprocity coefficient which enables the uplink channel training to achieve a higher data rate than the downlink channel training. Our

examination demonstrated that this minimum channel reciprocity coefficient decreases as the blocklength decreases or the number of transmit antennas increases, revealing the benefits of the uplink channel training in SPC with multiple transmit antennas.

Chapter 3

Optimal Resource Allocation for SPC

3.1 Introduction

In this chapter, we study the optimal SPC strategy which maximizes the average achievable data rate of a MISO system. In this system, an N_A-antenna AP transmits to a single-antenna user with finite blocklength T after estimating the AP-user channel via downlink training and uplink feedback. We determine the optimal allocation of the finite resource (e.g., the total transmit power and a finite number of symbol periods) for downlink training, uplink feedback, and data transmission to maximize the average data rate. Specifically, we derive an approximate closed-form lower bound on the average data rate, an explicit result for the optimal number of symbol periods for downlink training, an easy-to-implement method to find the optimal number of symbol periods for uplink feedback, and a simple expression for the optimal power allocation between data transmission and downlink training. By using numerical results, we demonstrate the effectiveness of our analytical solutions and examine the impact of system parameters, e.g., N_A and T, on the optimal strategy.

This chapter is organized as follows. In Section 3.2, we describe the system model. In Section 3.3, we first present the performance metrics of the considered MISO system. Then, we formulate the optimization problem and analyze the optimal resource allocation to maximize the average achievable data rate. Numerical results and conclusion are provided in Section 3.4 and 3.5, respectively.

3.2 System Model

We consider a MISO communication system where an N_A-antenna AP transmits small packets to a single-antenna user. We denote $\mathbf{h}_d$ as the $1 \times N_A$ channel vector from the AP to the user, the entries of which are subject to independent quasi-static Rayleigh fading. Therefore, the entries of $\mathbf{h}_d$ are i.i.d. circularly symmetric complex Gaussian random variables with zero mean and unit variance, i.e., $\mathbf{h}_d \sim \mathcal{CN}(0, \mathbf{I}_{N_A})$. We assume that the entries of $\mathbf{h}_d$ remain constant during one fading block. We also assume that the total duration of each fading block consists of T

symbol periods (i.e., T channel uses), including T_t symbol periods used for downlink training, T_f symbol periods used for uplink feedback, and T_d symbol periods used for data transmission. Therefore, we have $T_t + T_f + T_d = T$. In the finite blocklength regime, the maximum achievable rate is tightly approximated as

$$R \approx C(\gamma) - \sqrt{V(\gamma)/T} f_Q^{-1}(\varepsilon), \tag{3.1}$$

where T is the blocklength, ε is the decoding error probability, γ is the SNR, $C(\gamma) = \log_2(1+\gamma)$ is the Shannon capacity, $V(\gamma) = (\log_2 e)^2 \left(1 - 1/(1+\gamma)^2\right)$ is the channel dispersion, and $f_Q^{-1}(\cdot)$ is the inverse Gaussian Q-function.

According to [27] and [25], the approximation in (3.1) is tight even when T is as low as 100. We denote P_t and P_d as the transmit power per channel use at the AP for downlink training and data transmission, respectively. We further denote P as the average transmit power per channel use at the AP. Here, an average power constraint is considered over a fading block [60], i.e., $P_t T_t + P_d T_d \leq PT$. Additionally, we assume that the user and the AP have the knowledge about the statistical information of $\mathbf{h}_d$. The channel estimation in the considered MISO system is performed as follows: First, the AP sends pilot sequences to the user for estimating $\mathbf{h}_d$, referred to as downlink training. Second, the user feeds back the estimate to the AP, referred to as uplink feedback. We next formulate downlink training and uplink feedback in the following.

3.2.1 Downlink Training

When the AP sends pilot sequences in T_t symbol periods, the received signal vector at the user is given by $\mathbf{y}_d = \sqrt{\Lambda}\mathbf{h}_d\mathbf{S}_d + \mathbf{n}_d$, where $\Lambda \triangleq P_t T_t / N_A$, $\mathbf{S}_d$ is the $N_A \times T_t$ pilot sequence matrix transmitted by the AP which satisfies $\mathbf{S}_d\mathbf{S}_d^\dagger = \mathbf{I}_{N_A}$, and $\mathbf{n}_d$ is the $1 \times T_t$ AWGN vector at the user with i.i.d entries, each of which follows the complex Gaussian distribution with zero mean and variance σ^2.

By adopting the MMSE estimator based on the known $\mathbf{S}_d$, the user obtains the estimate of $\mathbf{h}_d$ as $\hat{\mathbf{h}}_d = \frac{\sqrt{\Lambda}}{\Lambda+\sigma^2}\mathbf{y}_d\mathbf{S}_d^\dagger$. As per the property of MMSE, the channel estimation error, given by $\hat{\mathbf{e}}_d = \mathbf{h}_d - \hat{\mathbf{h}}_d$, is independent of the realizations of estimated channel [94]. We also note that $\hat{\mathbf{e}}_d$ and $\hat{\mathbf{h}}_d$ have i.i.d. entries. Specifically, each entry of $\hat{\mathbf{e}}_d$ follows the complex Gaussian distribution with zero mean and variance $\sigma_{\hat{e}_d}^2$ while each entry of $\hat{\mathbf{h}}_d$ follows the complex Gaussian distribution with zero mean and variance $\sigma_{\hat{h}_d}^2$, where $\sigma_{\hat{e}_d}^2 = \sigma^2/\left(\Lambda+\sigma^2\right)$ and $\sigma_{\hat{\mathrm{h}}_d}^2 = \Lambda/\left(\Lambda+\sigma^2\right)$. We assume that $T_t \geq N_A$ is ensured in the MISO system to obtain a reliable estimate of $\mathbf{h}_d$.

3.2.2 Uplink Feedback

After downlink training, the user captures the channel direction information (CDI) given by $\tilde{\mathbf{h}} = \hat{\mathbf{h}}_d / \|\hat{\mathbf{h}}_d\|$. Then, the user quantizes the CDI by selecting the best quantization vector from the pre-shared codebook and conveys its index back to the AP over a feedback channel with zero propagation delay. Here, the propagation delay means the physical transmission duration from the AP to the user, which is formulated as the ratio between the transmission distance and the speed of light. Typically, the communication distance in URLLC is less than a few kilometers. Therefore, the propagation delay in the order of μs can be negligible [64]. Here, the codebook $\mathcal{C}$ is an $N_A \times 2^B$ matrix, i.e, $\mathcal{C} = \{\mathbf{w}_1, \mathbf{w}_2, \cdots, \mathbf{w}_{2^B}\}$, where $\mathbf{w}_i$ refers to the $N_A \times 1$ channel vector and $i \in \{1, 2, \cdots, 2^B\}$. We clarify that the relationship between T_f and B is $B = T_f \log_2 M$, where M is the modulation order. The codebook is assumed to be designed offline and known to both the AP and the user. Given the codebook $\mathcal{C}$, the user chooses the quantization vector that maximizes the SNR as the best quantization vector, i.e., $\mathbf{w}_{\text{opt}} = \text{argmax}_{1 \le i \le 2^B} \left|\tilde{\mathbf{h}}\mathbf{w}_i\right|^2$. The user then feeds back the index of selected quantization vector to the AP. After obtaining the CDI, i.e., $\tilde{\mathbf{h}}$, through downlink training and uplink feedback, the AP sets the $N_A \times 1$ normalized beamforming vector as $\mathbf{w}_{\text{opt}}$ to transmit to the user. The transmitted signal $\mathbf{x}$ is written as $\mathbf{x} = \mathbf{w}_{\text{opt}} u$, where u is the information signal transmitted from the AP to the user. The received signal at the user in one symbol period is given by

$$y = \sqrt{P_d}\mathbf{h}_d \mathbf{x} + n = \sqrt{P_d}\hat{\mathbf{h}}_d \mathbf{w}_{\text{opt}} u + n_d. \tag{3.2}$$

We consider the worst-case scenario [60, 90] for the decoding process at the user where $n_d = \sqrt{P_d}\hat{\mathbf{e}}_d \mathbf{w}_{\text{opt}} u + n$ in (3.2) is approximated as a Gaussian random variable with the variance $\sigma_{n_d}^2$. Under this consideration, the SNR at the user is given by

$$\gamma = \left|\hat{\mathbf{h}}_d \mathbf{w}_{\text{opt}}\right|^2 P_d / \sigma_{n_d}^2 = \rho_e \left\|\bar{\mathbf{h}}_d\right\|^2 \cos^2\left(\angle(\tilde{\mathbf{h}}, \mathbf{w}_{\text{opt}})\right), \tag{3.3}$$

where $\sigma_{n_d}^2 = P_d \sigma_{\hat{e}_d}^2 + \sigma^2$ with $\sigma_{\hat{e}_d}^2 = \frac{N_A \sigma^2}{T_t P_t + N_A \sigma^2}$, $\rho_e = P_d \left(1 - \sigma_{\hat{e}_d}^2\right) / \sigma_{n_d}^2$, $\bar{\mathbf{h}}_d \triangleq \hat{\mathbf{h}}_d / \sigma_{\hat{h}_d}$ is the normalized channel vector with the standard deviation $\sigma_{\hat{h}_d}$, and $\cos^2\left(\angle(\tilde{\mathbf{h}}, \mathbf{w}_{\text{opt}})\right) = \left|\tilde{\mathbf{h}}\mathbf{w}_{\text{opt}}\right|^2$.

3.3 Performance Optimization

In this section, we perform the optimization of the symbol periods used for downlink training and uplink feedback, i.e., T_t and T_f, as well as the transmit power allocated to data transmission and channel training, aiming to maximize the average data rate under the average transmit power constraint. To this end, we denote η as the power allocation coefficient such that η and $1 - \eta$ are the fraction of total transmit power allocated to data transmission and channel training, respectively. Thus, we have $\rho_d T_d = \eta \rho T$ and $\rho_t T_t = (1 - \eta)\rho T$, where $\rho_d = P_d / \sigma^2$,

$\rho_t = P_t/\sigma^2$, and $\rho = P/\sigma^2$.

3.3.1 Lower Bound on Average Data Rate

We first derive a lower bound on the average data rate in the context of SPC. Considering n_d in (3.2) as a Gaussian random variable, a lower bound on the average data rate with limited channel estimation overhead for SPC is

$$R = \tau \mathbb{E}\left[C(\gamma) - \sqrt{V(\gamma)/T} f_Q^{-1}(\varepsilon)\right], \tag{3.4}$$

where $\tau = 1 - (T_t + T_f)/T$ and $\mathbb{E}[\cdot]$ denotes the expectation operation w.r.t. the channel gain. It is worth mentioning that (3.4) emphasizes the effects of the channel training and feedback overheads [95] for a given decoding error probability. We note that the average data rate is different from the average throughput $(1-\varepsilon)R$ defined in [49], where the throughput is averaged over different decoding error probabilities. In this work, we set the decoding error probability as a constraint that can satisfy the reliability requirement. In addition, (3.4) only focuses on the rate which is used to transmit data. That is why it is named as the average data rate, but not the average throughput. In the following theorem, we derive an approximate closed-form expression for this lower bound.

Theorem 3.1. The approximate closed-form expression for the lower bound on the average data rate with limited channel estimation overhead is derived as

$$R \approx \tau\left[\Phi(\tilde{\rho}_e, N_A) - \Psi(\tilde{\rho}_e, N_A, T)\right], \tag{3.5}$$

where $\tilde{\rho}_e = \mu\rho_e$, $\mu = 1 - (1 - \frac{1}{N_A})2^{-\frac{B}{N_A - 1}}$, and $\Phi(\tilde{\rho}_e, N_A)$ and $\Psi(\tilde{\rho}_e, N_A, T)$ are given by (3.6) and (3.7), respectively, with $\mathbf{G}_{2,3}^{3,0}(\cdot|\cdot)$ being the Meijer G-function [96, Eq. (9.301)].

$$\Phi(\tilde{\rho}_e, N_A) = \frac{e^{\frac{1}{\tilde{\rho}_e}}}{\ln 2\,\Gamma(N_A)\,\tilde{\rho}_e^{N_A}} \sum_{i=0}^{N_A-1} \binom{N_A-1}{i} (-1)^{N_A-1-i} \mathbf{G}_{2,3}^{3,0}\left(\begin{matrix} -i, -i \\ 0, -1-i, -1-i \end{matrix} \middle| \frac{1}{\tilde{\rho}_e} \right). \tag{3.6}$$

$$\Psi(\tilde{\rho}_e, N_A, T) = \sqrt{\frac{2\pi}{T}} \frac{f_Q^{-1}(\varepsilon)}{\ln 2\,\Gamma(N_A)} e^{-(N_A-1)} (N_A-1)^{N_A-\frac{1}{2}} \sqrt{1 - (1 + \tilde{\rho}_e(N_A-1))^{-2}}. \tag{3.7}$$

Proof: See Appendix *B.1*. ■

It is worth mentioning that the results in [86] cannot be directly used in this work, since this work considers a different system model from [86]. Specifically, in this work the AP (i.e., the transmitter) obtains the CSI by performing downlink channel training and asking the user

to feed back the index of the quantization vector in terms of the channel direction information. Differently, in [86] the transmitter obtains the CSI based on the channel reciprocity between uplink and downlink.

3.3.2 Formulating and Solving Optimization Problem

We now formulate and solve the optimization problem of our interest. First, we re-express the approximated expression for R given in (3.5) as $R(T_t, T_f, \eta)$, i.e., a function of T_t, T_f, and η. Then, we formulate the joint optimization of T_t, T_f, and η to maximize $R(T_t, T_f, \eta)$ under the average transmit power constraint as

$$\max_{T_t, T_f, \eta} \; R(T_t, T_f, \eta) \tag{3.8a}$$

$$\text{s.t. } \rho_t T_t + \rho_d T_d \leq \rho T. \tag{3.8b}$$

Considering the practical scenario and the accuracy of (3.1), we only focus on the case where $T_t \geq N_A$ and $T_d > N_A$. For given codebook, the beamforming vector given in (3.2) is optimal for the above optimization problem. Motivated by the results in [60], we derive the optimal value of T_t which maximizes $R(T_t, T_f, \eta)$ for given ρT, denoted by T_t^*, in the following theorem.

Theorem 3.2. For URLLC scenarios (i.e., SNR $>$ 10 dB [37, 54, 64]), the optimal T_t that maximizes $R(T_t, T_f, \eta)$ for given ρT in the case of $T_t \geq N_A$ and $T_d > N_A$ is derived as

$$T_t^* = N_A. \tag{3.9}$$

Proof: See Appendix *B.2*. ■

We note that the optimal T_t is the same as the number of transmit antennas N_A, which physically means that the channels associated with all transmit antennas can be estimated during the channel training phase.

Based on Theorem 3.2, it is clear that T_t^* is independent of η and T_f. Thus, the objective function in (3.8) is rewritten as

$$\max_{T_f, \eta} \; R(T_t^*, T_f, \eta) \tag{3.10a}$$

$$\text{s.t. } \rho_t T_t^* + \rho_d T_d \leq \rho T. \tag{3.10b}$$

To solve (3.10), we first determine the optimal η which maximizes $R(T_t^*, T_f, \eta)$ for given T_f with $T_t^* = N_A$, denoted by η^*. Then we perform a one-dimensional search to find the optimal T_f based on the obtained η^* and T_t^*. We note that the equality in (3.10b) is always guaranteed due to the fact that a larger T_d always leads to a higher R. This also indicates that we only need

to determine the optimal values of η and T_f to find the optimal value of T_d as $T_d^* = T - T_t^* - T_f^*$. We next present the details for solving (3.10) with $T_t^* = N_A$ using a two-step approach.

Step 1: Find the optimal η for given T_f.

We note that R in (3.4) is a monotonically increasing function of γ when R is positive. Also, the expectation in (3.4) is relevant to channel realizations but independent of $\tilde{\rho}_e$. That is, the maximum average data rate is achieved by maximizing $\tilde{\rho}_e$ for given T_t and T_f. Based on (3.3), the effective SNR is given by

$$\tilde{\rho}_e = \frac{\mu P_d \left(1 - \sigma_{\hat{e}_d}^2\right)}{P_d \sigma_{\hat{e}_d}^2 + \sigma^2} = \frac{\mu \rho T \eta (1-\eta)}{(T_d - N_A)(\nu - \eta)}, \tag{3.11}$$

where μ is defined below (3.5) and $\nu = \frac{\rho T + N_A}{\rho T (1 - N_A/T_d)}$. By taking the second derivative of $\tilde{\rho}_e$ with respect to η, we find that $\frac{\partial^2 \tilde{\rho}_e}{\partial \eta^2} = \frac{\mu \rho T 2\nu(\nu-1)}{(T_d - N_A)(\eta - \nu)^3} < 0$, which confirms that $\tilde{\rho}_e$ is a concave function of η. As such, η^* can be found by numerically solving for $\partial \tilde{\rho}_e / \partial \eta = 0$, which gives

$$\eta^* = \nu - \sqrt{\nu^2 - \nu}. \tag{3.12}$$

Step 2: Find the optimal T_f.

We note that η^* given in (3.12) is a function of T and T_d (or equivalently, $T_t + T_f$), which is independent of the individual value of T_t or T_f. Since the optimal value of T_t is obtained, we can efficiently perform a one-dimensional numerical search to find the optimal T_f.

Overall, we first simplify the optimization problem by using $T_t^* = N_A$. Then, we maximize R over η for given T_f with T_t^*. After this, we find the optimal T_f, i.e., T_f^*, by using one-dimensional search. The complexity of our proposed method for solving (3.10) is low. Specifically, T_t^* can be obtained directly when N_A and T are determined. Based on this, for given T_f, we can obtain η^* according to (3.12). Finally, we perform a one-dimensional numerical search to find T_f^* within a finite range $[T - N_A, T]$. Hence, when system parameters are determined, the optimization problem can be solved efficiently using our derived results with relatively low complexity. The effectiveness of our approach will be validated in Section 3.4.

3.4 Numerical Results

Throughout this section, we consider the use of binary phase shift keying modulation for the feedback from the user to the AP such that $T_f = B$.

In Fig. 3.1, we demonstrate the accuracy of our derived closed-form expression for the lower bound on the data rate. The simulated and theoretical results are obtained from (3.4) and (3.5), respectively. The simulated points are averaged over 10,000 channel realizations, and the quantization codebook is generated based on the design criterion in [97]. In Fig. 1, we observe

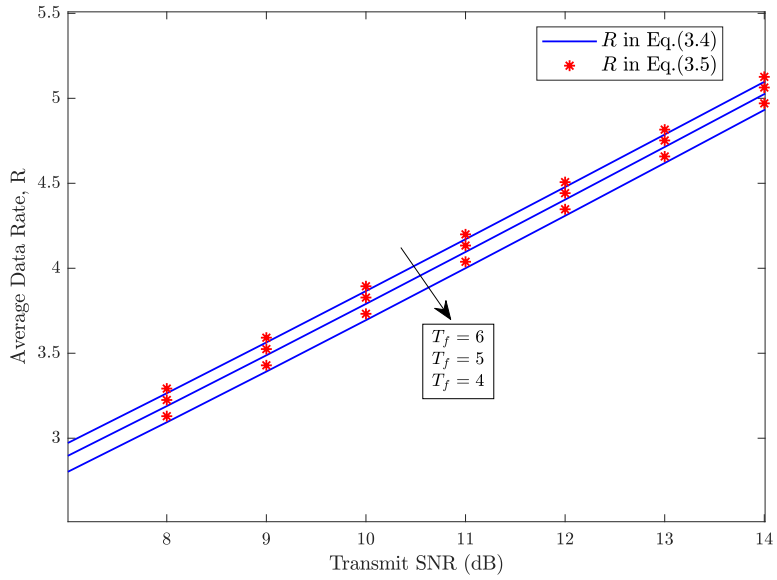

Figure 3.1: The average data rate R versus transmit SNR for different feedback symbol period T_f with $T = 200$, $N_A = 4$ and $\varepsilon = 10^{-6}$.

that the theoretical results precisely match the simulated ones during the whole SNR range, and the accuracy slightly increase when feedback symbol period increases. The observations imply that the quantization approximation has a almost negligible impact on the average data rate. Therefore, the closed-form expression derived in (3.5) serves as an accurate result for the average data rate with limited channel training and feedback under the consideration of the finite blocklength.

In Fig. 3.2(a), we plot the optimal symbol period for uplink feedback, T_f^*, versus T for different number of antennas at the AP, i.e., $N_A = 4$, 6, and 8. In this figure, we first observe that T_f^* increases as T increases. This observation is not surprising since more channel uses are allocated for downlink training and uplink feedback when T is larger. Also, we observe that T_f^* decreases as N_A decreases. This is due to the fact that decreasing N_A reduces the required channel uses for downlink training and uplink feedback. In Fig. 3.2(b), we plot the optimal power allocation coefficient, η^*, versus T for $N_A = 4$, 6, and 8. In this figure, we first confirm that the simulated curves exactly match the approximated values, demonstrating the correctness of our result derived in (3.12). We also observe that η^* increases as T increases. This is due to the fact that ρ_d remains stable and the ratio between T_d and T increases as T increases. Finally, we observe that η^* decreases as N_A increases. This is due to the fact that the number of channel uses for downlink training, T_t, increases with N_A, which reduces T_d.

In Fig. 3.3, we plot the transmit SNR for downlink training and data transmission versus T for different values of N_A, i.e., $N_A = 10$, 15, and 20. Here, we recall that $\rho_d = P_d/\sigma^2$ and $\rho_t = P_t/\sigma^2$. In this figure, we first observe that ρ_t gradually increases and ρ_d slightly

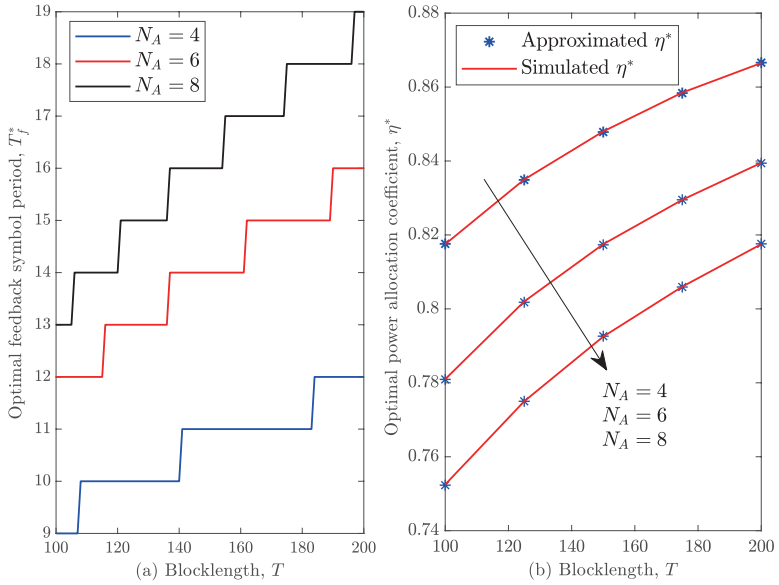

Figure 3.2: The optimal feedback symbol period T_f^* and the optimal power allocation coefficient η^* versus T with $\rho = 10$ dB and $\varepsilon = 10^{-9}$.

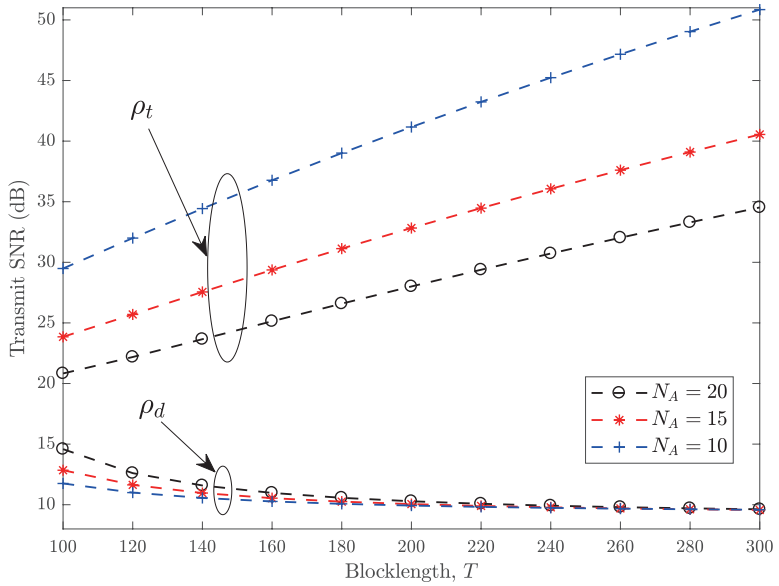

Figure 3.3: The transmit SNR for downlink training and data transmission versus T for different N_A with $\rho = 10$ dB and $\varepsilon = 10^{-9}$.

decreases and tends to be constant as T increases. However, we confirm that $\rho_t T_t^*$ decreases and $\rho_d T_d$ increases as T increases. This implies that the transmit power allocated to downlink training decreases while the transmit power allocated to data transmission increases when T is larger. We also observe that ρ_t increases as N_A decreases. We further observe that ρ_d slightly decreases as N_A decreases for small T but approaches almost the same value for large T. This

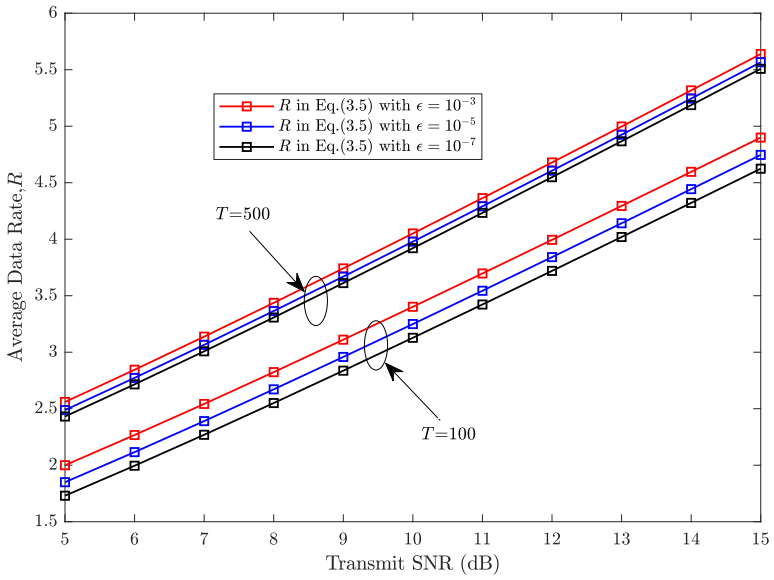

Figure 3.4: The average data rate R versus transmit SNR for different values of ε and T with optimal η^* and $N_A = 4$.

observation can be explained by the fact that smaller N_A reduces the required T_t^* but leads to a negligible increase in T_d. This results in an increase in ρ_t and a minor reduction in ρ_d in order to guarantee $\rho_t T_t + \rho_d T_d = \rho T$.

Fig. 3.4 plots the lower bound on the data rate versus the transmit SNR for different values of ε and T. The curves are obtained from (3.5) with the optimal power allocation coefficient η^*. In this figure, we first observe that, for given T, the data rate decreases when the decoding error probability ε increases. It implies that the more strict requirement for reliability leads to a larger rate loss. Moreover, for the same ε, the data rate increases when the blocklength T increases as expected. We also find that the difference in data rates with different values of ε becomes negligible when T increases.

3.5 Summary

In this chapter, we investigated the optimal resource allocation to maximize the average data rate in a MISO system which adopts SPC. We proved that the optimal number of symbol periods allocated to downlink training is equal to the number of transmit antennas at the AP. We also derived the optimal power allocation between downlink training and data transmission at the AP in closed form. Our outcomes provide a guideline to assist the URLLC designers with the fundamental problem of transmit power and symbol period allocation to guarantee the advantage of SPC in practice.

Chapter 4

Channel Inversion Power Control for One-Way URLLC

4.1 Introduction

In this chapter, we propose to use CIPC to achieve one-way URLLC, where only the transmission in one direction requires ultra reliability and low latency. Based on channel reciprocity, our proposed CIPC schemes guarantee the power of received signal that is used to decode the information to be a constant value Q, by varying the transmit signal and power, which relaxes the assumption of knowing CSI at the user. Thus, the CIPC schemes eliminate the overhead of CSI feedback, reduce communication latency, and explore the benefits of multiple antennas to significantly improve transmission reliability. We derive analytical expressions for the packet loss probability of the proposed CIPC schemes, based on which we determine a closed interval and a convex set for optimizing Q in CIPC with imperfect and perfect channel reciprocity, respectively. Our results show that CIPC is an effective means to achieve one-way URLLC. The tradeoff among reliability, latency, and required resources (e.g., transmit antennas) is further revealed, which provides novel principles for designing one-way URLLC systems.

This chapter is organized as follows. In Section 4.2, we first detail our considered scenario of one-way URLLC together with the adopted assumptions. Then, we present our proposed CIPC scheme and its associated performance metric. In Section 4.3, we analyze the packet loss probability of the truncated CIPC scheme with imperfect channel reciprocity. In Section 4.4, we examine the proposed CIPC scheme with perfect channel reciprocity. Numerical results and conclusion are provided in Section 4.5 and 4.6, respectively.

4.2 System Model

In this section, we first detail our considered scenario of one-way URLLC together with the adopted assumptions. Then, we present our proposed CIPC scheme and its associated performance metric, i.e., the packet loss probability.

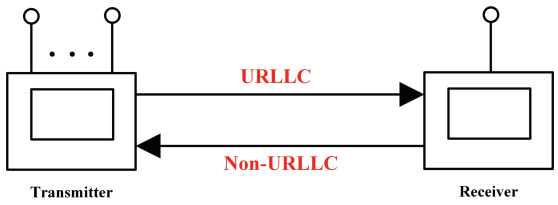

Figure 4.1: Illustration of the considered one-way URLLC scenario.

As shown in Fig. 4.1, in this work we consider a downlink one-way URLLC scenario in a TDD MISO communication system, where an N_t-antenna BS sends an urgent message triggered by the reception and processing of the uplink information to a single-antenna user with the stringent requirement of latency and reliability. Specifically, we consider the URLLC occurring in the downlink, while the uplink transmission is non-URLLC. The user periodically sends regular information in the uplink to the BS. Upon reception and processing of the uplink information, BS decides whether or not to send an urgent message to the user in the downlink. Hence, the downlink URLLC is actually triggered by the reception and processing of the uplink information. This means that the downlink URLLC does not happen at any arbitrary point in time, but it can only happen right after the reception and processing of a non-URLLC communication in the uplink. This is an practically important scenario. For example, in the context of wireless vehicular networks, a vehicle periodically reports its states and its observed surrounding information to BS. The transmitted packets consist of both pilots and useful information in order to enable BS to jointly perform channel estimation and information decoding. Then, BS immediately analyzes the received information to decide whether an urgent control information is required or not to be delivered to this vehicle. The processing task of analyzing the network could be completed by well-trained deep neural networks with proper online fine-tuning. It is noted that the processing delay could be one TTI ($0.125 \sim 1$ ms) in 5G NR [57]. As such, if the BS decides to immediately send out an urgent control message to the user, this downlink URLLC happens with very minimal time gap from the uplink communication that just happened. Therefore, it is reasonable to assume that the channel has not changed significantly from the uplink communication to the downlink communication. It is followed that, the BS can use the estimated channel information to perform downlink communication with channel inversion power control.

We denote $\mathbf{h}_u$ as the $N_t \times 1$ uplink channel vector from the user to the BS and denote $\mathbf{h}_d$ as the $1 \times N_t$ downlink channel vector from the BS to the user. Specifically, the downlink transmission considered in this work requires URLLC, i.e., the downlink transmission with a high reliability requirement needs to be performed within a finite blocklength T (or equivalently, T channel uses). All the channels are subject to independent quasi-static Rayleigh fading such that the entries of each channel vector are assumed to be i.i.d. circularly symmetric com-

plex Gaussian random variables with zero mean and unit variance, i.e., $\mathbf{h}_{\mathrm{d}} \sim \mathcal{CN}(0, \mathbf{I}_{N_{\mathrm{t}}})$ and $\mathbf{h}_{\mathrm{u}} \sim \mathcal{CN}(0, \mathbf{I}_{N_{\mathrm{t}}})$.

Considering the imperfect channel reciprocity, the downlink channel vector can be expressed as a function of the uplink channel vector, given by [72, 86]

$$\mathbf{h}_{\mathrm{d}} = \sqrt{\phi}\mathbf{h}_{\mathrm{u}}^{\mathcal{T}} + \sqrt{1-\phi}\mathbf{e}^{\mathcal{T}}, \tag{4.1}$$

where ϕ is defined as the channel reciprocity coefficient between the uplink and downlink channels, and $\mathbf{e}$ is the $N_{\mathrm{t}} \times 1$ vector that reflects the uncertain part of $\mathbf{h}_{\mathrm{u}}$. The entries of $\mathbf{e}$ are i.i.d. and each of them follows $\mathcal{CN}(0,1)$. We note that $\mathbf{e}$ is independent of $\mathbf{h}_{\mathrm{u}}$. The adoption of the channel reciprocity model in (4.1) is motivated by the fact that channel reciprocity requires appropriate hardware calibrations to compensate for the unknown amplitude scaling and phase shift between the downlink and uplink channels in practice [63]. The value of ϕ quantifies the level of channel reciprocity, where $0 \leq \phi \leq 1$. In practical scenarios, the level of channel reciprocity is affected by the uplink channel estimation error and the frequency offset between the BS and the user [63]. Specifically, $\phi = 1$ indicates that the perfect channel reciprocity is achieved such that the downlink channel is exactly the same as the uplink channel. As ϕ decreases, the channel reciprocity decreases. When $\phi = 0$, the channel reciprocity does not exist such that the downlink channel is independent of the uplink channel.

We assume that the BS knows $\mathbf{h}_{\mathrm{u}}$ perfectly. This is due to the fact that the uplink transmission does not have strict requirement on latency, which makes it possible for the user to periodically broadcast pilots for allowing the BS to estimate $\mathbf{h}_{\mathrm{u}}$. Even if the estimation is not perfect, the estimation error can be incorporated into the channel reciprocity coefficient ϕ in (4.1). In order to enable a user (e.g., a vehicle) to decode the information without knowing CSI, the CIPC scheme is used at the BS based on $\mathbf{h}_{\mathrm{u}}$, which will be detailed in the following subsection. The CIPC scheme can significantly reduce the communication latency and improve transmission reliability to meet the requirements of URLLC. This is due the fact that the CIPC scheme saves the signaling overhead used to feed back the estimated $\mathbf{h}_{\mathrm{u}}$ from BS to a user and allows all the downlink channel uses being available for data transmission when urgent information transmission is on demand.

4.2.1 Channel Inversion Power Control

In this work, the CIPC scheme is used at the BS to enable the user to decode the received signals without knowing $\mathbf{h}_{\mathrm{d}}$. The received signal in one channel use is given by

$$y = \sqrt{P_{\mathrm{a}}}\mathbf{h}_{\mathrm{d}}\mathbf{x} + w, \tag{4.2}$$

where w is the AWGN at the user with zero mean and variance σ_w^2, $\mathbf{x}$ is the transmitted signal which is subject to the average power constraint, i.e., $\mathbb{E}\left[\|\mathbf{x}\|^2\right] = 1$, and P_a is the transmit power. Following the imperfect channel reciprocity model given in (4.1), the received signal in (4.2) can be rewritten as

$$y = \sqrt{P_\mathrm{a}\phi}\mathbf{h}_\mathrm{u}^{\mathcal{T}}\mathbf{x} + \sqrt{P_\mathrm{a}(1-\phi)}\mathbf{e}^{\mathcal{T}}\mathbf{x} + w. \tag{4.3}$$

In order to counteract the impact of downlink channel phase at the user, the transmitted signal $\mathbf{x}$ is written as

$$\mathbf{x} = \frac{\mathbf{h}_\mathrm{u}^*}{\|\mathbf{h}_\mathrm{u}\|}u, \tag{4.4}$$

where u is the information signal transmitted from the BS to the user. Following (4.3) and (4.4), the SINR at the user can be written as

$$\gamma = \frac{P_\mathrm{a}\phi\|\mathbf{h}_\mathrm{u}\|^2}{P_\mathrm{a}(1-\phi)\frac{\left|\mathbf{e}^{\mathcal{T}}\mathbf{h}_\mathrm{u}^*\right|^2}{\|\mathbf{h}_\mathrm{u}\|^2} + \sigma_w^2}. \tag{4.5}$$

In order to counteract the impact of downlink channel gain at the user, the BS varies its transmit power to ensure

$$P_\mathrm{a}\|\mathbf{h}_\mathrm{u}\|^2 = Q, \tag{4.6}$$

where Q is a pre-determined constant value *a priori* agreed between the BS and the user. Then, the SINR at the user in (4.5) can be rewritten as

$$\gamma = \frac{\phi Q}{(1-\phi)\frac{Q\left|\mathbf{e}^{\mathcal{T}}\mathbf{h}_\mathrm{u}^*\right|^2}{\|\mathbf{h}_\mathrm{u}\|^2\|\mathbf{h}_\mathrm{u}\|^2} + \sigma_w^2}. \tag{4.7}$$

Considering Rayleigh fading for $\mathbf{h}_\mathrm{u}$, as per (4.6) we see that the transmit power P_a may be infinite to guarantee $P_\mathrm{a}\|\mathbf{h}_\mathrm{u}\|^2 = Q$ for some realizations of $\mathbf{h}_\mathrm{u}$. Without loss of generality, in this work we consider a maximum transmit power constraint, denoted by $P_\mathrm{a} \leq P_\mathrm{max}$ [68]. Specifically, the BS only transmits information to the user when the uplink channel gain, i.e., $\|\mathbf{h}_\mathrm{u}\|^2$, is greater than a specific value. Mathematically, the transmit power is given by

$$P_\mathrm{a} = \begin{cases} \frac{Q}{\|\mathbf{h}_\mathrm{u}\|^2}, & \|\mathbf{h}_\mathrm{u}\|^2 \geq \frac{Q}{P_\mathrm{max}}, \\ 0, & \|\mathbf{h}_\mathrm{u}\|^2 < \frac{Q}{P_\mathrm{max}}. \end{cases} \tag{4.8}$$

In this work, we refer to the CIPC scheme with a finite P_max as the truncated CIPC scheme, where the transmit power is truncated at a specific value. As $P_\mathrm{max} \to \infty$, the truncated CIPC

scheme converges to the conventional CIPC scheme, where transmission is always performed regardless of the channel quality. In this work, we first analyze the truncated CIPC scheme and then analyze the conventional CIPC scheme as a special case, which serves as a performance benchmark for the truncated CIPC scheme.

4.2.2 Fixed-Rate Transmission and Packet Loss Probability

As per (4.8), we see that the BS does not always transmit information to the user in the truncated CIPC scheme. The associated transmission probability, i.e., the probability that the BS sends information to the user, is given by

$$p_t(Q) = \Pr\{P_{\mathrm{a}} \leq P_{\max}\}. \tag{4.9}$$

We note that in the conventional CIPC scheme (i.e., where $P_{\max} \to \infty$), the transmission is always performed and thus, the transmission probability is one (i.e., $p_t(Q) = 1$).

In URLLC scenarios, the packet loss from the BS to the user is caused by not only the aforementioned transmission suspension induced by the considered maximum transmit power constraint. When the transmission is performed, the packet loss still occurs due to the non-zero decoding error probability for the finite blocklength [27]. In URLLC scenarios, the required QoS is normally predetermined in terms of a specific transmission rate or packet loss probability. In this work, we consider a fixed-rate transmission, where the information transmission rate R from the BS to the user is predetermined to meet a certain requirement on QoS. We note that adaptive-rate transmission can be considered in the context of URLLC, where the transmission rate can be adapted as per a predetermined packet loss probability (which represents a certain QoS in another form) and practical channel conditions. For fixed-rate transmission, based on a widely used asymptotic expression for the non-zero decoding error probability given in [27], the decoding error probability averaged over different channel realizations at the user is given by

$$\varepsilon = \mathbb{E}_{\{\mathbf{h}_{\mathrm{u}},\mathbf{e}\}}\left[f_Q\left(\left(\log_2(1+\gamma)-R\right)\sqrt{\frac{T}{V}}\right)\right] = \mathbb{E}_{\{\mathbf{h}_{\mathrm{u}},\mathbf{e}\}}\left[f_Q\left(\frac{\sqrt{T}\left(\ln(1+\gamma)-R\ln 2\right)}{\sqrt{1-(1+\gamma)^{-2}}}\right)\right], \tag{4.10}$$

where we recall that R is the information transmission rate, the SINR γ is given in (4.7), $V = (\log_2 e)^2\left(1-(1+\gamma)^{-2}\right)$ is the channel dispersion, and $f_Q(\cdot)$ denotes the Gaussian Q-function with $f_Q(x) = \frac{1}{\sqrt{2\pi}}\int_x^\infty e^{-\frac{t^2}{2}}dt$.

We note that a closed-form expression for (4.10) is intractable. Thus, we adopt the linear

approximation given by

$$f_Q\left((\log_2(1+\gamma)-R)\sqrt{\frac{T}{V}}\right)\approx\Omega(\gamma) \tag{4.11}$$

in this work, where [98, 99]

$$\Omega(\gamma)\triangleq\begin{cases}1, & 0\le\gamma\le\alpha\\ \frac{1}{2}-\delta(\gamma-\gamma_0), & \alpha<\gamma<\beta\\ 0, & \gamma\ge\beta,\end{cases} \tag{4.12}$$

with $\delta=\frac{\sqrt{T}}{2\pi\sqrt{2^{2R}-1}}$, $\gamma_0=2^R-1$, $\alpha=\gamma_0-\frac{1}{2\delta}$, and $\beta=\gamma_0+\frac{1}{2\delta}$. As such, the decoding error probability ε defined in (4.10) can be rewritten as

$$\varepsilon=\int_0^\infty f_Q\left(\frac{\sqrt{T}(\ln(1+\gamma)-R\ln 2)}{\sqrt{1-(1+\gamma)^{-2}}}\right)f_\gamma(\gamma)d\gamma \tag{4.13a}$$

$$\approx\int_0^\alpha f_\gamma(\gamma)d\gamma+\int_\alpha^\beta\left(\frac{1}{2}-\delta(\gamma-\gamma_0)\right)f_\gamma(\gamma)d\gamma \tag{4.13b}$$

$$=\int_0^\alpha f_\gamma(\gamma)d\gamma+\left(\frac{1}{2}+\delta\gamma_0\right)\int_\alpha^\beta f_\gamma(\gamma)d\gamma-\delta\int_\alpha^\beta\gamma f_\gamma(\gamma)d\gamma \tag{4.13c}$$

$$=F_\gamma(\alpha)+\left(\frac{1}{2}+\delta\gamma_0\right)(F_\gamma(\beta)-F_\gamma(\alpha))-\delta\int_\alpha^\beta\gamma f_\gamma(\gamma)d\gamma \tag{4.13d}$$

$$\overset{(a)}{=}\left(\frac{1}{2}-\delta\gamma_0+\delta\alpha\right)F_\gamma(\alpha)+\left(\frac{1}{2}+\delta\gamma_0-\delta\beta\right)F_\gamma(\beta)+\delta\int_\alpha^\beta F_\gamma(\gamma)d\gamma, \tag{4.13e}$$

where step (a) is obtained by $\int_\alpha^\beta\gamma f_\gamma(\gamma)d\gamma=\int_\alpha^\beta\gamma dF_\gamma(\gamma)=\beta F_\gamma(\beta)-\alpha F_\gamma(\alpha)-\int_\alpha^\beta F_\gamma(\gamma)d\gamma$.

In our considered truncated CIPC scheme, the non-zero decoding error occurs only when the transmission is performed. As such, for the truncated CIPC scheme, the decoding error probability is conditioned on that the transmit power is not zero (i.e., the channel condition satisfies $\|\mathbf{h}_\mathrm{u}\|^2\ge\frac{Q}{P_\mathrm{max}}$). Therefore, following (4.10), the conditional average decoding error probability of the truncated CIPC scheme is given by

$$\varepsilon\left(Q\middle|\|\mathbf{h}_\mathrm{u}\|^2\ge\frac{Q}{P_\mathrm{max}}\right)=\mathbb{E}_{\{\mathbf{h}_\mathrm{u},\mathbf{e}\}}\left[f_Q\left(\frac{\sqrt{T}(\ln(1+\gamma)-R\ln 2)}{\sqrt{1-(1+\gamma)^{-2}}}\middle|\|\mathbf{h}_\mathrm{u}\|^2\ge\frac{Q}{P_\mathrm{max}}\right)\right]. \tag{4.14}$$

Considering the packet loss caused by both the transmission suspension at the BS and the conditional non-zero decoding error probability at the user, the packet loss probability for our

considered truncated CIPC scheme is given by

$$P_{\varepsilon}(Q) = \varepsilon\left(Q\middle|\|\mathbf{h}_{\mathrm{u}}\|^2 \geq \frac{Q}{P_{\max}}\right) p_t(Q) + 1 - p_t(Q). \tag{4.15}$$

We first find that the packet loss probability $P_{\varepsilon}(Q)$ is a monotonically increasing function of the transmission rate R, since $\varepsilon\left(Q\middle|\|\mathbf{h}_{\mathrm{u}}\|^2 \geq \frac{Q}{P_{\max}}\right)$ monotonically increases with R and $p_t(Q)$ is not a function of R. Then, we find that $p_t(Q)$ monotonically decreases with Q and $\varepsilon\left(Q\middle|\|\mathbf{h}_{\mathrm{u}}\|^2 \geq \frac{Q}{P_{\max}}\right)$ decreases with Q. In other words, there exists an optimal value of Q that minimizes $P_{\varepsilon}(Q)$ for the truncated CIPC scheme, which will be tackled in Section 4.3. We further find that for the conventional CIPC scheme, we have $p_t(Q) = 1$ and the condition $\|\mathbf{h}_{\mathrm{u}}\|^2 \geq \frac{Q}{P_{\max}}$ is always satisfied, which leads to the fact that the packet loss probability of the conventional CIPC scheme is the same as the average decoding error probability given in (4.10).

4.3 Truncated and Conventional CIPC with Imperfect Channel Reciprocity

In this section, we analyze the packet loss probability of the truncated CIPC scheme with imperfect channel reciprocity (i.e., $0 < \phi < 1$). Specifically, we determine an upper bound on the receive signal power (i.e., the value of Q), which provides a closed interval for the optimal value of Q that minimizes the packet loss probability of the truncated CIPC scheme. Moreover, an easy-to-calculate expression for this packet loss probability P_{ε} is derived in this section. Furthermore, we analyze the conventional CIPC scheme where the BS is not subject to the maximum transmit power constraint, for the sake of performance comparison.

4.3.1 Packet Loss Probability of Truncated CIPC Scheme

When the maximum transmit power constraint is considered, the packet loss probability is affected by the transmission probability and the decoding error probability. We note that, for fixed R and T, the packet loss probability $P_{\varepsilon}(Q)$ given in (4.15) depends on Q heavily. Therefore, in the following we first derive an approximated but easy-to-calculate expression for $P_{\varepsilon}(Q)$ and then use it to determine the optimal value of Q that minimizes $P_{\varepsilon}(Q)$.

In order to derive the approximated expression for $P_{\varepsilon}(Q)$, we rewrite the SINR given in (4.7) as

$$\gamma = \frac{\phi Q}{Q(1-\phi)Z + \sigma_w^2}, \tag{4.16}$$

where we define $Z = \frac{Y}{X}$ with $X = \|\mathbf{h}_{\mathrm{u}}\|^2$ and $Y = \frac{\left|\mathbf{e}^{\mathcal{T}}\mathbf{h}_{\mathrm{u}}^*\right|^2}{\|\mathbf{h}_{\mathrm{u}}\|^2} = \left|\mathbf{e}^{\mathcal{T}}\frac{\mathbf{h}_{\mathrm{u}}^*}{\|\mathbf{h}_{\mathrm{u}}\|}\right|^2$. We note that X is

independent of Y. This is due to the fact that X depends on the norm of $\mathbf{h}_{\mathrm{u}}$ but not the phase, while Y depends on the phase of $\mathbf{h}_{\mathrm{u}}$ but not the norm. Since the norm and phase of $\mathbf{h}_{\mathrm{u}}$ are independent, we conclude that X and Y are independent.

We find that in order to calculate the decoding error probability $\varepsilon\left(Q\middle|\|\mathbf{h}_{\mathrm{u}}\|^2 \geq \frac{Q}{P_{\max}}\right)$, we need to derive the conditional CDF of the SINR. Thus, we next derive this conditional CDF with the maximum transmit power constraint, denoted by $F_\gamma\left(\gamma\middle|\|\mathbf{h}_{\mathrm{u}}\|^2 \geq \frac{Q}{P_{\max}}\right)$, and present it in the following lemma.

Lemma 4.1. The conditional CDF of the SINR given in (4.16) with the maximum transmit power constraint, $F_\gamma\left(\gamma\middle|\|\mathbf{h}_{\mathrm{u}}\|^2 \geq \frac{Q}{P_{\max}}\right)$, is given by

$$F_\gamma\left(\gamma\middle|\|\mathbf{h}_{\mathrm{u}}\|^2 \geq \frac{Q}{P_{\max}}\right) = \frac{\gamma_{\mathrm{up}}\left(N_{\mathrm{t}}, \frac{Q(1+\xi(\gamma))}{P_{\max}}\right)}{\gamma_{\mathrm{up}}\left(N_{\mathrm{t}}, \frac{Q}{P_{\max}}\right)(1+\xi(\gamma))^{N_{\mathrm{t}}}}, \tag{4.17}$$

where $\xi(\gamma) = \frac{Q\phi - \gamma\sigma_w^2}{Q\gamma(1-\phi)}$, $\gamma_{\mathrm{w}}(s,x) = \int_0^x e^{-t}t^{s-1}dt$ is the lower incomplete gamma function [96, Eq. (8.350.1)], $\gamma_{\mathrm{up}}(s,x) = \int_x^\infty e^{-t}t^{s-1}dt$ is the upper incomplete gamma function [96, Eq. (8.350.2)], and $\gamma_{\mathrm{w}}(s,x) + \gamma_{\mathrm{up}}(s,x) = \Gamma(s)$ [96, Eq. (8.356.3)].

Proof: See Appendix *C.1*. ■

We note that a closed-form expression for (4.14) is mathematically intractable. Therefore, in the following theorem, we derive an approximated but easy-to-calculate expression for the packet loss probability of the truncated CIPC scheme with the aid of Lemma 4.1.

Theorem 4.1. The packet loss probability of the truncated CIPC scheme with imperfect channel reciprocity in URLLC scenarios is approximated as

$$\begin{aligned} P_\varepsilon(Q) = \Bigg[&\left(\frac{1}{2} - \delta\gamma_0 + \delta\alpha\right)F_\gamma\left(\alpha\middle|\|\mathbf{h}_{\mathrm{u}}\|^2 \geq \frac{Q}{P_{\max}}\right) + \left(\frac{1}{2} + \delta\gamma_0 - \delta\beta\right)F_\gamma\left(\beta\middle|\|\mathbf{h}_{\mathrm{u}}\|^2 \geq \frac{Q}{P_{\max}}\right) \\ &+ \delta\int_\alpha^\beta F_\gamma\left(\gamma\middle|\|\mathbf{h}_{\mathrm{u}}\|^2 \geq \frac{Q}{P_{\max}}\right)d\gamma\Bigg]\left(1 - \frac{\gamma_{\mathrm{w}}\left(N_{\mathrm{t}}, \frac{Q}{P_{\max}}\right)}{\Gamma(N_{\mathrm{t}})}\right) + \frac{\gamma_{\mathrm{w}}\left(N_{\mathrm{t}}, \frac{Q}{P_{\max}}\right)}{\Gamma(N_{\mathrm{t}})}, \end{aligned} \tag{4.18}$$

where $F_\gamma\left(\gamma\middle|\|\mathbf{h}_{\mathrm{u}}\|^2 \geq \frac{Q}{P_{\max}}\right)$ is given in (4.17).

Proof: In order to prove Theorem 4.1 and derive the expression for P_ε, we need to derive the explicit expressions for $p_t(Q)$ and $\varepsilon\left(Q\middle|\|\mathbf{h}_{\mathrm{u}}\|^2 \geq \frac{Q}{P_{\max}}\right)$, which are detailed as below.

We first tackle the transmission probability $p_t(Q)$. By substituting (4.8) into (4.9), we express the transmission probability as

$$p_t(Q) = 1 - \Pr\left\{\|\mathbf{h}_{\mathrm{u}}\|^2 \leq \frac{Q}{P_{\max}}\right\} = 1 - \frac{\gamma_{\mathrm{w}}\left(N_{\mathrm{t}}, \frac{Q}{P_{\max}}\right)}{\Gamma(N_{\mathrm{t}})}, \tag{4.19}$$

where $f_X(x) = \frac{x^{N_t-1}e^{-x}}{\Gamma(N_t)}$ and $F_X(x) = \frac{\gamma_w(N_t,x)}{\Gamma(N_t)}$ are the PDF and CDF of $\|\mathbf{h}_u\|^2$, respectively.

We next write the expression for the decoding error probability in (4.14) as

$$\varepsilon\left(Q\middle|\|\mathbf{h}_u\|^2 \geq \frac{Q}{P_{\max}}\right) = \mathbb{E}_\gamma\left[f\left(\frac{\sqrt{T}\left(\ln(1+\gamma)-R\ln 2\right)}{\sqrt{1-(1+\gamma)^{-2}}}\middle|\|\mathbf{h}_u\|^2 \geq \frac{Q}{P_{\max}}\right)\right] \tag{4.20a}$$

$$\overset{(b)}{=} \int_0^\infty f\left(\frac{\sqrt{T}\left(\ln(1+\gamma)-R\ln 2\right)}{\sqrt{1-(1+\gamma)^{-2}}}\middle|\|\mathbf{h}_u\|^2 \geq \frac{Q}{P_{\max}}\right) f_\gamma\left(\gamma\middle|\|\mathbf{h}_u\|^2 \geq \frac{Q}{P_{\max}}\right) d\gamma \tag{4.20b}$$

$$\overset{(c)}{\approx} \int_0^\alpha f_\gamma\left(\gamma\middle|\|\mathbf{h}_u\|^2 \geq \frac{Q}{P_{\max}}\right) d\gamma + \int_\alpha^\beta \left(\frac{1}{2}-\delta\left(\gamma-\gamma_0\right)\right) f_\gamma\left(\gamma\middle|\|\mathbf{h}_u\|^2 \geq \frac{Q}{P_{\max}}\right) d\gamma \tag{4.20c}$$

$$\overset{(d)}{=} \left(\frac{1}{2}-\delta\gamma_0+\delta\alpha\right) F_\gamma\left(\alpha\middle|\|\mathbf{h}_u\|^2 \geq \frac{Q}{P_{\max}}\right) + \left(\frac{1}{2}+\delta\gamma_0-\delta\beta\right) F_\gamma\left(\beta\middle|\|\mathbf{h}_u\|^2 \geq \frac{Q}{P_{\max}}\right)$$
$$+ \delta\int_\alpha^\beta F_\gamma\left(\gamma\middle|\|\mathbf{h}_u\|^2 \geq \frac{Q}{P_{\max}}\right) d\gamma, \tag{4.20d}$$

where step (b) is obtained due to the fact that the transmission condition only has an impact on the distribution, but not the range, of γ. Steps (c) and (d) are achieved due to the results given in (4.13e). Finally, substituting (4.19) and (4.20d) into (4.15), we obtain the desired result in (4.18). ■

4.3.2 Optimization of Q for Truncated CIPC Scheme

In this subsection, we determine the optimal value of Q to minimize the packet loss probability $P_\varepsilon(Q)$ of the truncated CIPC scheme for given T, R, and $P_{\max}$. The optimization problem at the BS is given by

$$\min_Q \; P_\varepsilon(Q) \tag{4.21}$$

$$\text{s.t. } T \geq 100, \tag{4.21a}$$

where (4.21a) is the condition for achieving effective approximation for the maximal achievable rate in the finite blocklength regime [27]. We note that current practical codes have typical blocklength from 100 to 1000 for short-packet control information transmission, e.g., 168 in [25]. Hence, (4.21a) can be applied into practical scenarios.

Due to the high complexity involved in the expression for $P_\varepsilon(Q)$ in (4.18), it may not be easy to analytically solve the optimization problem in (4.21) by using (4.18). To cope with this, we present the following lemma to determine an upper bound on Q for the packet loss probability of the truncated CIPC scheme in the context of URLLC, which ultimately helps to numerically solve the optimization problem.

Lemma 4.2. In the context of URLLC, the value of Q in the truncated CIPC scheme is smaller than a specific value, i.e., $Q < P_{\max}(N_{\mathrm{t}}-1)$ with $N_t > 1$. It is noted that the value of Q is determined by the maximum transmit power and the number of transmit antennas.

Proof: We note that the transmission probability $p_t(Q)$ in (4.9) monotonically decreases when Q increases, which is due to the fact that the first-order partial derivative of $p_t(Q)$ w.r.t. Q is given by

$$\frac{\partial\{p_t(Q)\}}{\partial Q} = -\frac{e^{-\frac{Q}{P_{\max}}}\left(\frac{Q}{P_{\max}}\right)^{N_{\mathrm{t}}-1}}{P_{\max}\Gamma(N_{\mathrm{t}})} < 0. \tag{4.22}$$

We also note that the second-order partial derivative of $p_t(Q)$ w.r.t. Q is given by

$$\frac{\partial^2\{p_t(Q)\}}{\partial Q^2} = \frac{e^{-\frac{Q}{P_{\max}}}\left(\frac{Q}{P_{\max}}\right)^{N_{\mathrm{t}}+1}\left(Q-P_{\max}\left(N_{\mathrm{t}}-1\right)\right)}{Q^3\Gamma(N_{\mathrm{t}})}. \tag{4.23}$$

As such, we note that the sign of $\frac{\partial^2\{p_t(Q)\}}{\partial Q^2}$ has three possibilities, which are given by

$$\frac{\partial^2\{p_t(Q)\}}{\partial Q^2}\begin{cases} <0, & \text{when } 0<Q<P_{\max}(N_{\mathrm{t}}-1), \\ =0, & \text{when } Q=P_{\max}(N_{\mathrm{t}}-1), \\ >0, & \text{when } Q>P_{\max}(N_{\mathrm{t}}-1). \end{cases} \tag{4.24}$$

It is worth mentioning that Q needs to satisfy the condition of $0 < Q < P_{\max}(N_{\mathrm{t}}-1)$. This is due to the fact that when $Q = P_{\max}(N_{\mathrm{t}}-1)$, as per (4.19) the probability $p_t(Q)$ becomes a function of N_{t} only, which is given by

$$p_t(Q) = p_t(P_{\max}(N_{\mathrm{t}}-1)) = 1 - \frac{\gamma_{\mathrm{lw}}\left(N_{\mathrm{t}}, N_{\mathrm{t}}-1\right)}{\Gamma\left(N_{\mathrm{t}}\right)}. \tag{4.25}$$

We note that $p_t(P_{\max}(N_{\mathrm{t}}-1))$ is a monotonically decreasing function of N_{t} and thus $1 - p_t(P_{\max}(N_{\mathrm{t}}-1))$ increases and approaches a constant value (i.e., 0.5) as N_{t} increases. Following (4.15), we have $P_{\varepsilon}(Q) > 1 - p_t(P_{\max}(N_{\mathrm{t}}-1))$. As such, we note that using more transmit antennas is not beneficial to improve reliability when $Q = P_{\max}(N_{\mathrm{t}}-1)$. We also note that $p_t(Q) = 1 - \frac{\gamma_{\mathrm{lw}}\left(N_{\mathrm{t}}, \frac{Q}{P_{\max}}\right)}{\Gamma(N_{\mathrm{t}})}$ is a monotonically decreasing function of Q due to $\frac{\partial\{p_t(Q)\}}{\partial Q} < 0$ proved in (4.22). Thus, for $Q > P_{\max}(N_{\mathrm{t}}-1)$, $1 - p_t(Q)$ is larger than 0.5 which violates the requirement of URLLC. As such, for a given $P_{\max}$, we cannot meet the ultra-reliable requirement of URLLC by setting $Q = P_{\max}(N_{\mathrm{t}}-1)$ and we have to decrease Q in order to further increase the value of $p_t(Q)$ due to $\frac{\partial\{p_t(Q)\}}{\partial Q} < 0$. Therefore, reducing the value of Q is the only solution to meet the requirement of URLLC, e.g., satisfying $1 - p_t(Q) \leq 10^{-7}$. Therefore, in the truncated CIPC scheme, the bound of Q can be determined as $0 < Q < P_{\max}(N_{\mathrm{t}}-1)$, which

completes the proof. ■

With the aid of the upper bound on Q presented in Lemma 4.2, the optimization of Q in (4.21) can be numerically solved by searching the optimal value of Q over the closed interval $[0, P_{\max}(N_{\rm t}-1)]$. When the reliability requirement of URLLC is given, denoted as $P_{\varepsilon}^{\rm req}$, we can further explore the upper bound on Q by solving $1-p_t(Q) \leq P_{\varepsilon}^{\rm req}$. It is noted that $1-p_t(Q) = \frac{\gamma_{\rm w}\left(N_{\rm t}, \frac{Q}{P_{\max}}\right)}{\Gamma(N_{\rm t})}$ is a monotonically increasing function of Q due to $\frac{\partial\{p_t(Q)\}}{\partial Q} < 0$ proved in (4.22). As such, we can obtain an additional upper bound on Q, denoted by $Q_{\rm up}$, by solving $\frac{\gamma_{\rm w}\left(N_{\rm t}, \frac{Q_{\rm up}}{P_{\max}}\right)}{\Gamma(N_{\rm t})} = P_{\varepsilon}^{\rm req}$. Then by combining the closed interval in Lemma 4.2, we write the new closed interval as $0 < Q < \min\left(P_{\max}(N_{\rm t}-1), Q_{\rm up}\right)$. In addition, we provide a convex set to determine the optimal value of Q that minimizes the packet loss probability in our proposed truncated CIPC scheme with perfect channel reciprocity, which will be detailed in Section 4.4.

4.3.3 Packet Loss Probability of Conventional CIPC Scheme

The conventional CIPC scheme is the CIPC scheme without the maximum transmit power constraint, i.e., with $P_{\max} \to \infty$. This means that the BS can always transmit signals and guarantee $P_{\rm a}\|\mathbf{h}_{\rm u}\|^2 = Q$ in the conventional CIPC scheme. As such, as mentioned before, the transmission probability is one (i.e., $p_t(Q) = 1$) for the conventional CIPC scheme, which leads to the fact that the packet loss probability of the conventional CIPC scheme, i.e., $P_{\varepsilon}^{\infty}(Q)$, is same as the decoding error probability, i.e., $\varepsilon(\gamma)$ defined in (4.10). This enables us to derive an approximated but closed-form expression for the packet loss probability of the conventional CIPC scheme, denoted as $P_{\varepsilon}^{\infty}(Q)$, in the following corollary.

Corollary 4.1. For given finite blocklength T and transmission data rate R, the packet loss probability of the conventional CIPC scheme, $P_{\varepsilon}^{\infty}(Q)$, is approximated as

$$P_{\varepsilon}^{\infty}(Q) = \left(\frac{1}{2} - \delta\gamma_0 + \delta\alpha\right)\left(\frac{1}{1+\xi(\alpha)}\right)^{N_{\rm t}} + \left(\frac{1}{2} + \delta\gamma_0 - \delta\beta\right)\left(\frac{1}{1+\xi(\beta)}\right)^{N_{\rm t}} + \delta M_1^{N_{\rm t}}\left((-1)^{-N_{\rm t}} M_2\left(B_{-\frac{\alpha}{M_2}}(1+N_{\rm t}, 1-N_{\rm t}) - B_{-\frac{\beta}{M_2}}(1+N_{\rm t}, 1-N_{\rm t})\right)\right), \quad (4.26)$$

where $\xi(x) = \frac{Q\phi - x\sigma_w^2}{xQ(1-\phi)}$, $M_1 = \frac{Q(1-\phi)}{Q(1-\phi)-\sigma_w^2}$, $M_2 = \frac{Q\phi}{Q(1-\phi)-\sigma_w^2}$, and $B_x(a,b) = \int_0^x t^{a-1}(1-t)^{b-1}dt$ is the incomplete beta function [96, Eq. (8.391)].

Proof: See Appendix *C.2*. ■

We note that the closed-form expression for the packet loss probability of the conventional CIPC scheme offers an upper bound on the performance of the truncated CIPC scheme. This can be used to draw many useful insights with efficient calculations for practical communications scenarios.

4.4 Truncated CIPC with Perfect Channel Reciprocity

In this section, we examine the proposed CIPC scheme with perfect channel reciprocity (i.e., $\phi = 1$) in the context of URLLC. Specifically, we first derive the packet loss probability for the truncated CIPC scheme with perfect channel reciprocity, which is not a special case of that for the truncated CIPC scheme with imperfect channel reciprocity. We also prove that the packet loss probability of the truncated CIPC scheme with $\phi = 1$ is convex w.r.t. Q in a specific set, which significantly facilitates the optimization of Q for the truncated CIPC scheme with perfect channel reciprocity.

4.4.1 Packet Loss Probability of Truncated CIPC Scheme

The packet loss probability for the truncated CIPC scheme with perfect channel reciprocity ($\phi = 1$) is not a special case of that derived in Theorem 4.1 which is for the truncated CIPC scheme with imperfect channel reciprocity ($0 < \phi < 1$). In addition, the perfect channel reciprocity can exist in some ideal scenarios and can aid to obtain an upper bound on the performance of the truncated CIPC scheme in practical scenarios. This motivates us to consider the truncated CIPC scheme with perfect channel reciprocity in this subsection.

Applying perfect channel reciprocity into our proposed truncated CIPC scheme (i.e., $\phi = 1$) leads to $\mathbf{h}_{\mathrm{d}} = \mathbf{h}_{\mathrm{u}}^T$. As such, the received signal in (4.2) can be rewritten as

$$y_{\phi=1} = \sqrt{P_{\mathrm{a}}}\mathbf{h}_{\mathrm{u}}^T\mathbf{x} + w. \tag{4.27}$$

Given (4.27), the SINR in (4.5) converts into the SNR given by

$$\gamma_{\phi=1} = \frac{Q}{\sigma_w^2}. \tag{4.28}$$

Based on (4.28), we derive the packet loss probability of our proposed truncated CIPC scheme with perfect channel reciprocity in the following lemma.

Lemma 4.3. The packet loss probability of the truncated CIPC scheme with perfect channel reciprocity in URLLC scenarios is derived as

$$P_{\varepsilon}^{\phi=1}(Q) = 1 - \left(1 - \frac{\gamma_{\mathrm{w}}\left(N_{\mathrm{t}}, \frac{Q}{P_{\max}}\right)}{\Gamma(N_{\mathrm{t}})}\right)\left(1 - f_Q\left(\frac{\sqrt{T}\left(\ln\left(1+\frac{Q}{\sigma_w^2}\right) - R\ln 2\right)}{\sqrt{1-\left(1+\frac{Q}{\sigma_w^2}\right)^{-2}}}\right)\right). \tag{4.29}$$

Proof: In order to prove Lemma 4.3, we first convert $P_{\varepsilon}(Q)$ defined in (4.15) into

$P_{\varepsilon}^{\phi=1}(Q)$, which is given by

$$P_{\varepsilon}^{\phi=1}(Q) = \varepsilon(Q)\, p_t(Q) + 1 - p_t(Q). \tag{4.30}$$

We note that the transmission probability $p_t(Q)$ is derived in (4.19), i.e., $p_t(Q) = 1 - \frac{\gamma_{\text{lw}}\left(N_{\text{t}}, \frac{Q}{P_{\max}}\right)}{\Gamma(N_{\text{t}})}$, which is also valid for the perfect channel reciprocity. Then, substituting the SNR, i.e., $\gamma_{\phi=1}$ given by (4.28), into (4.10), the decoding error probability can be rewritten as

$$\varepsilon(Q) = f_Q\left(\frac{\sqrt{T}\left(\ln\left(1+\frac{Q}{\sigma_w^2}\right) - R\ln 2\right)}{\sqrt{1-\left(1+\frac{Q}{\sigma_w^2}\right)^{-2}}}\right), \tag{4.31}$$

where the expectation is eliminated, due to the fact that the SNR in (4.28) is independent of channel realizations.

Finally, substituting (4.19) and (4.31) into (4.30), we obtain the desired result in (4.29), which completes the proof. ■

We note that the packet loss probability $P_{\varepsilon}^{\phi=1}(Q)$ is a monotonically increasing function of the transmission rate R, since $\varepsilon(Q)$ monotonically increases with R and $p_t(Q)$ is not a function of R. Meanwhile, $P_{\varepsilon}^{\phi=1}(Q)$ monotonically decreases with $P_{\max}$, as $p_t(Q)$ increases with $P_{\max}$ and $\varepsilon(Q) < 1$ does not depend on $P_{\max}$. In the numerical results, we will examine the required maximum transmit power to achieve URLLC with a certain transmission rate and the maximum allowable packet loss probability.

4.4.2 Optimization of Q for Truncated CIPC Scheme

For given T, R and $P_{\max}$, the optimization of Q to minimize the packet loss probability in the truncated CIPC scheme with perfect channel reciprocity is given by

$$\begin{aligned} &\min_{Q} \; P_{\varepsilon}^{\phi=1}(Q) \\ &\text{s.t.} \;\; T \geq 100. \end{aligned} \tag{4.32}$$

Considering the complexity involved in the expression for $P_{\varepsilon}^{\phi=1}(Q)$ derived in Lemma 4.3, it still may not be easy to analytically solve the optimization problem (4.32). However, we prove that $P_{\varepsilon}^{\phi=1}(Q)$ is convex w.r.t. Q in a specific convex set for the optimization problem (4.32), which is detailed in the following proposition.

Proposition 4.1. The packet loss probability $P_{\varepsilon}^{\phi=1}(Q)$ of the truncated CIPC is a convex func-

tion of Q for $Q_0 < Q < P_{\max}(N_t - 1)$, where $Q_0 = \sigma_w^2 \gamma_a$ and γ_a is the solution to

$$\frac{\ln(1+\gamma_a)}{(1+\gamma_a)^2 - 1} = \frac{1}{3}. \tag{4.33}$$

Proof: See Appendix *C.3*. ■

With the aid of monotonicity and convexity of $P_\varepsilon^{\phi=1}(Q)$ w.r.t. Q presented in Proposition 4.1 and the closed-form expression for $P_\varepsilon^{\phi=1}(Q)$ derived in Lemma 4.3, the optimization of Q in (4.32) can be conducted by using some efficient numerical methods, e.g., finding the solution of Q to $\partial\{P_\varepsilon^{\phi=1}(Q)\}/\partial Q = 0$ subject to $Q_0 < Q < P_{\max}(N_t - 1)$ and then comparing the resultant value of $P_\varepsilon^{\phi=1}(Q)$ with the values of $P_\varepsilon^{\phi=1}(Q)$ in the region of $0 < Q \leq Q_0$.

4.5 Numerical Results

In this section, we present numerical results to examine the performance of the proposed CIPC schemes. Based on the numerical results, we draw useful insights into the impact of various system parameters on the performance of the proposed schemes in the considered one-way URLLC scenario. In the following, the value of noise variance is set to 1, i.e., $\sigma_w^2 = 1$.

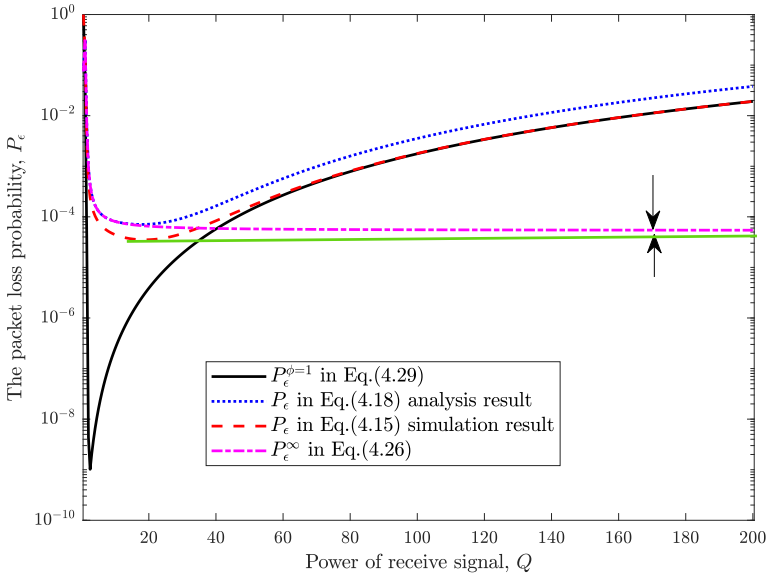

Figure 4.2: The packet loss probability $P_\varepsilon(Q)$ versus the power of received signals Q in the truncated CIPC scheme with $R = 0.8$, $\phi = 0.9$, $T = 100$, $N_t = 4$, and $P_{\max} = 23$ dBm.

Fig. 4.2 plots the packet loss probabilities, $P_\varepsilon(Q)$, of the truncated and conventional CIPC schemes versus the power of received signals, Q. The simulated and theoretical results are obtained from (4.15) and (4.18), respectively. The simulated results are obtained by averaging

over 10,000 channel realizations. We first observe that there indeed exists an optimal value of Q that minimizes $P_\varepsilon(Q)$ for the truncated CIPC scheme. As clarified in our analysis, this is mainly due to the maximum transmit power constraint, which results in that both the transmission probability and the decoding error probability decrease when Q increases. We also observe that the trend of theoretical results precisely match the simulated ones in the whole value range of Q, which leads to that the optimal value of Q can be precisely searched via our derived easy-to-calculate expression for the packet loss probability of the truncated CIPC scheme given in (4.18).

It is noted that in Fig. 4.2 the black solid curve (with "legend $P_\varepsilon^{\phi=1}$ in Eq. (4.29)") is the packet loss probability of the truncated CIPC scheme with perfect channel reciprocity (i.e., $\phi = 1$), while other curves are for imperfect channel reciprocity with $\phi = 0.9$. As expected, we observe that the reliability performance of the truncated CIPC scheme increases when ϕ increases and the performance of the truncated CIPC scheme with perfect channel reciprocity serves as an upper bound in practical scenarios where the channel reciprocity may not be perfect. Moreover, we observe that the packet loss probability of the conventional CIPC scheme where $P_{\max} \to \infty$, P_ε^∞, monotonically decreases with Q. This is due to the fact that when the transmit power is unbounded, the transmission always occurs and the transmission probability is one (i.e., $p_t(Q) = 1$). This leads to the fact that the packet loss probability of the conventional CIPC scheme is the same as the average decoding error probability given in (4.10). In fact, the decoding error probability is a monotonically decreasing function of Q, since the corresponding SINR monotonically increases with Q. Therefore, our second observation confirms that our proposed performance metric is more appropriate for one-way URLLC applications in practical wireless scenarios, since it considers the transmit power constraint. Furthermore, we observe that the gap between the minimum packet loss probability of the truncated CIPC scheme (with legend "P_ε in Eq. (4.15) simulation results" and shown in green solid curve) and the packet loss probability of the conventional CIPC scheme (with legend "P_ε^∞ in Eq. (4.26)") is not large and becomes smaller as Q increases. It is noted that infinite transmit power, i.e., $P_{\max} \to \infty$ is used in the conventional CIPC scheme, while its achievable minimum packet loss probability is not sensitive to the value of Q and eventually approaches the packet loss probability of the proposed truncated CIPC scheme for given $P_{\max}$ when Q is large enough. In other words, the maximum transmit power plays a critical role in our proposed truncated CIPC scheme for determining the achievable minimum packet loss probability.

Fig. 4.3 plots the packet loss probability $P_\varepsilon(Q)$ of the truncated CIPC scheme with imperfect channel reciprocity versus the power of received signal Q with different values of N_{t}. First, we observe from this figure the existence of the optimal value of Q that minimizes $P_\varepsilon(Q)$. Second, we observe that this optimal value is within the interval $(0, P_{\max}(N_{\mathrm{t}} - 1))$, which demonstrates the correctness of our Lemma 4.2. Third, we observe that the minimum value of $P_\varepsilon(Q)$ highly depends on the values of N_{t}, i.e., this minimum value decreases significantly with N_{t}.

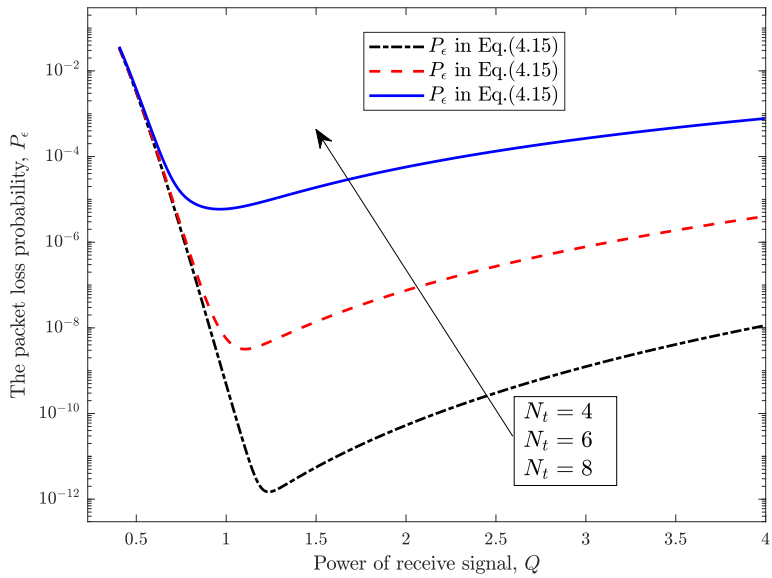

Figure 4.3: The packet loss probability $P_\varepsilon(Q)$ versus the power of received signal Q in the truncated CIPC scheme for different value of N_t with $R = 0.3$, $T = 150$, $\phi = 0.9$, and $P_{\max} = 10$ dBm.

This indicates that the reliability in URLLC can be improved by using more transmit antennas in the truncated CIPC scheme. We note that, without the considered CIPC scheme, increasing the number of transmit antennas may not improve reliability in URLLC. This is due to the fact that the traditional channel estimation overhead increases when there is a higher number of transmit antennas, which limits the reliability performance achieved by using multiple antennas. Fourth, we observe that in the low regime of Q, the values of $P_\varepsilon(Q)$ for different values of N_t are almost the same. Meanwhile, in the high regime of Q, the values of $P_\varepsilon(Q)$ are significantly different for different values of N_t. The main reason lies in the different impact of N_t on $P_\varepsilon(Q)$ for different Q. Specifically, $P_\varepsilon(Q)$ is dominated by the conditional decoding error probability $\varepsilon\left(Q\middle|\|\mathbf{h}_\mathrm{u}\|^2 \geq \frac{Q}{P_{\max}}\right)$ when $p_t(Q)$ approaches 1. It is noted that $\varepsilon\left(Q\middle|\|\mathbf{h}_\mathrm{u}\|^2 \geq \frac{Q}{P_{\max}}\right)$ and $p_t(Q)$ are the functions of N_t according to their definitions in (4.14) and (4.9), respectively. To achieve an ultra low decoding error probability, e.g., 10^{-7}, the value of $p_t(Q)$ needs to be close to 1 in order to make the packet loss probability $P_\varepsilon(Q)$ approach the target value. In addition, we note that $p_t(Q)$ and $\varepsilon\left(Q\middle|\|\mathbf{h}_\mathrm{u}\|^2 \geq \frac{Q}{P_{\max}}\right)$ are monotonically decreasing functions of Q. Therefore, when Q is small, the transmission condition $\|\mathbf{h}_\mathrm{u}\|^2 \geq \frac{Q}{P_{\max}}$ can be easily satisfied, which is not very sensitive to the value of N_t. However, when Q is high, $\|\mathbf{h}_\mathrm{u}\|^2$ needs to be very large to keep the same transmission condition for given $P_{\max}$. This is due to the fact that the value of $\|\mathbf{h}_\mathrm{u}\|^2$ significantly depends on the value of N_t. In other words, the value of Q heavily affects the impact of N_t on $P_\varepsilon(Q)$.

Fig. 4.4 plots the achievable minimum $P_\varepsilon(Q)$ of the truncated CIPC scheme versus the

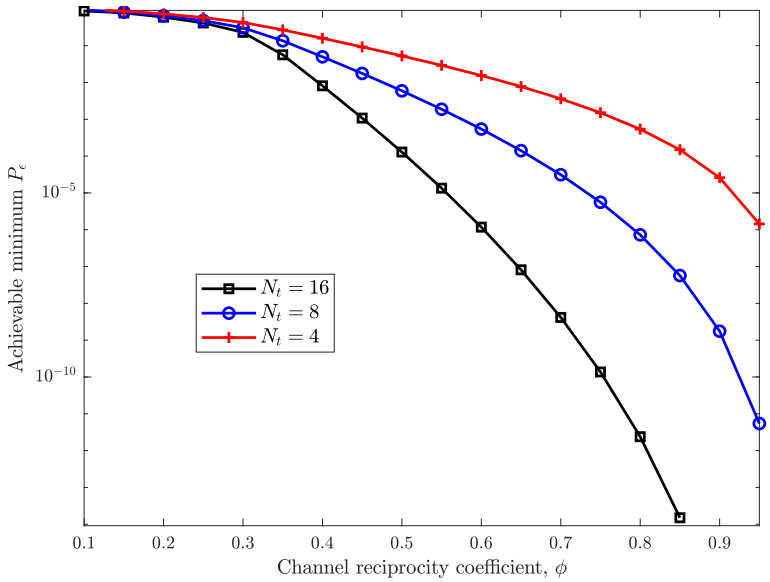

Figure 4.4: The achievable minimum $P_\varepsilon(Q)$ versus the channel reciprocity coefficient ϕ for different number of transmit antennas N_t with $R = 0.5$, $T = 150$, and $P_{\max} = 23$ dBm.

channel reciprocity coefficient ϕ for different values of N_t. We first observe that for a large number of transmit antennas, e.g., $N_\mathrm{t} = 16$, the minimum packet loss probability significantly decreases with ϕ. This shows the benefits of using multiple antennas at the BS in the considered CIPC schemes for achieving reliability improvement in URLLC scenarios. We also observe that the slope of the minimum packet loss probability with respect to ϕ increases as N_t increases, which demonstrates that the benefit of using channel reciprocity to achieve URLLC becomes more profound when the number of transmit antennas increases. Furthermore, in the simulations used to plot this figure, we confirm that the transmission probability $p_t(Q)$ increases and approaches one as the number of transmit antenna N_t increases.

Fig. 4.5 plots the packet loss probability of the truncated CIPC scheme with perfect channel reciprocity $P_\varepsilon^{\phi=1}(Q)$ versus the power of received signal Q. As shown in Fig. 4.5, we observe that the optimal value of Q that minimizes $P_\varepsilon^{\phi=1}(Q)$ is within the interval $(Q_0, P_{\max}(N_\mathrm{t}-1))$, where $P_{\max}(N_\mathrm{t}-1) = 30$ in this figure. More specifically, the figure shows that $P_\varepsilon^{\phi=1}(Q)$ first decreases and then increases when Q increases. The result demonstrates the correctness of Proposition 4.1, where $P_\varepsilon^{\phi=1}(Q)$ of the truncated CIPC is a convex function of Q for $Q_0 < Q < P_{\max}(N_\mathrm{t}-1)$.

Fig. 4.6 plots the maximum rate R versus the power of received signal Q in the truncated CIPC scheme with perfect channel reciprocity, i.e., $\phi = 1$, for different reliability requirements, where $P_\varepsilon^{\phi=1}(Q) = 10^{-5}, 10^{-7}$ and 10^{-9}. As shown in Fig. 4.6, the maximum achievable rate decreases when the reliability requirement becomes more stringent. Moreover, we find that the

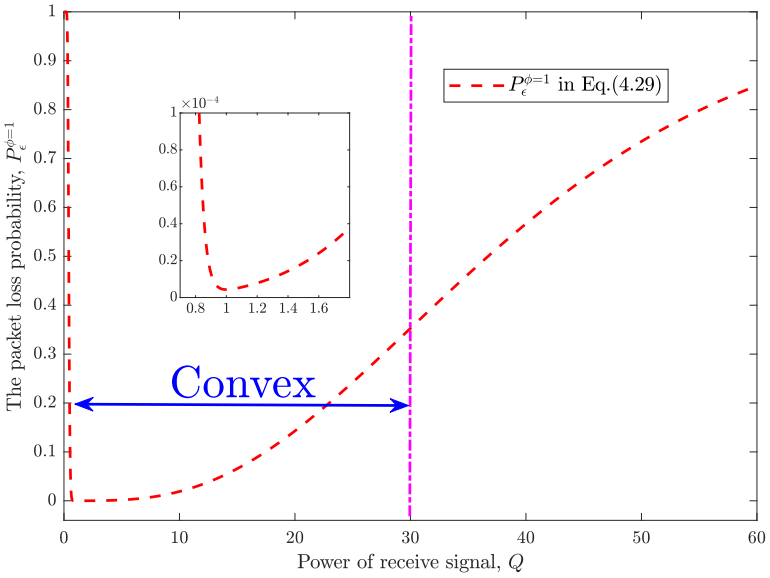

Figure 4.5: The packet loss probability with perfect channel reciprocity, $P_\varepsilon^{\phi=1}(Q)$, versus the power of receive signal Q in the truncated CIPC scheme with $R = 0.5$, $T = 150$, $\phi = 0.8$, $N_\mathrm{t} = 4$, and $P_\mathrm{max} = 10$ dBm.

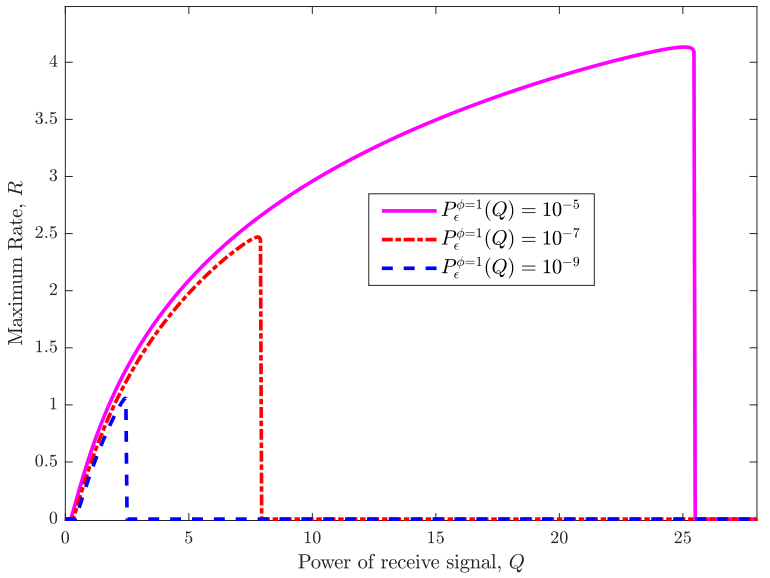

Figure 4.6: The maximum rate R versus the power of received signal Q in the truncated CIPC scheme with perfect channel reciprocity, i.e., $\phi = 1$, for different packet loss probabilities $P_\varepsilon^{\phi=1}(Q)$ with $T = 150$, $N_\mathrm{t} = 4$, and $P_\mathrm{max} = 23$ dBm.

maximum value of R that guarantees the target $P_\varepsilon^{\phi=1}(Q)$ first increases nonlinearly with Q and then immediately reduces to zero as Q becomes larger. This is due to the fact that $P_\varepsilon^{\phi=1}(Q)$

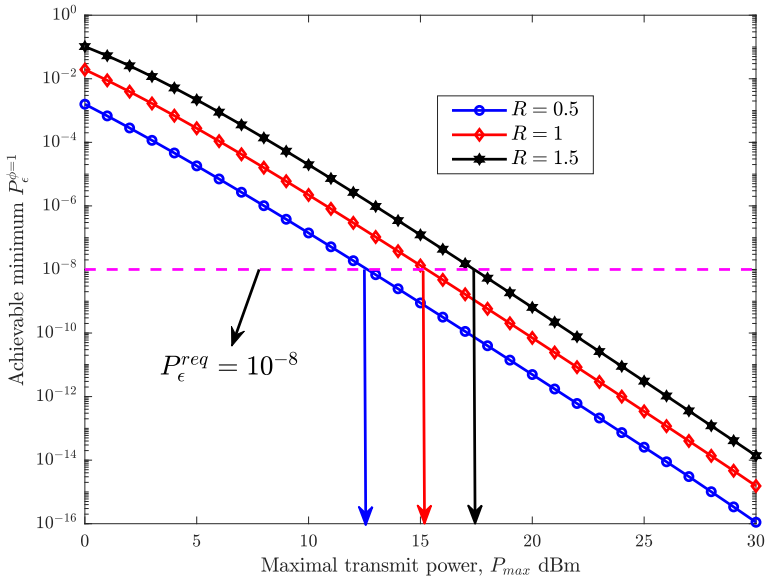

Figure 4.7: The minimum packet loss probability $P_\varepsilon^{*,\phi=1}(Q)$ versus the maximum transmit power $P_{\max}$ for different values of R with $N_t = 5$ and $T = 150$.

first decreases and then increases when Q increases. In other words, when Q is larger than the threshold that satisfying the reliability requirement, no achievable rate can be supported by current system parameters.

Fig. 4.7 plots the minimum packet loss probability of the truncated CIPC scheme with perfect channel reciprocity versus the maximum transmit power $P_{\max}$ for different values of the transmission rate R. As expected, we first observe that the minimum packet loss probability monotonically decreases when $P_{\max}$ increases, since increasing $P_{\max}$ enables the BS to send signals under more channel conditions and thus increases the transmission probability $p_t(Q)$. This demonstrates that the maximum transmit power plays a critical role in the truncated CIPC scheme. This figure also demonstrates that to guarantee a certain reliability, the required value of $P_{\max}$ increases when the transmission rate R increases, which can be explicitly determined by our examinations. This reveals one specific contribution of this work, i.e., determining system parameters (e.g., $P_{\max}$) for given requirements on the considered URLLC scenario. Furthermore, we observe that the minimum packet loss probability increases when R increases, which demonstrates the tradeoff between the transmission rate R and reliability in URLLC.

4.6 Summary

In this chapter, we proposed to use the CIPC schemes to achieve one-way URLLC with on-hand performance evaluation. Specifically, we first derived expressions for the packet loss

probabilities of the truncated and traditional CIPC schemes with imperfect channel reciprocity. Using these expressions, we determined a closed interval for the optimal value of the received signal power Q, which significantly facilitates the optimal design of the CIPC schemes. Then, we analyzed the performance of the truncated CIPC scheme with perfect channel reciprocity, which provides an upper bound on the performance of truncated CIPC in practical scenarios. Based on this analysis, we proved that the optimal Q lies in a convex set in the case with perfect channel reciprocity. Our examination explicitly determined the trade-off among reliability, latency, and required communication resources (e.g., transmit antennas and transmit power), which provides novel design guidelines into achieving one-way URLLC with the CIPC schemes.

Chapter 5

Secure Transmission Rate of Short Packets

5.1 Introduction

This chapter studies how to realize secure SPC subject to a statistical QoS requirement and an average power constraint. It is noted that physical layer security (PLS) is promising for secure short-packet transmissions in URLLC. The bottlenecks of applying PLS in practice include 1) lack of accurate CSI of both the intended user and the eavesdropper; 2) high computational complexity for solving optimization problems. To address the first issue, we compare the secure transmission rates of short packets in different scenarios (i.e., with/without eavesdropper's instantaneous CSI and with/without channel estimation errors) and derive the closed-form optimal power control policy in a special case. To find numerical solutions in general cases, we apply an unsupervised deep learning method for solving constrained functional optimization problems, which has low complexity after the training stage. Through numerical results, we obtain the following three key findings: 1) The learning-based power control policy approaches the closed-form optimal policy in the special case and outperforms two existing power control policies in general cases, 2) Knowing the instantaneous CSI of the eavesdropper only provides a marginal gain of the secure data rate in the high signal-to-noise ratio regime, and 3) In the presence of channel estimation errors, the learning-based policy trained by the estimated channels can guarantee the average transmit power constraint, while the closed-form policy cannot.

This chapter is organized as follows. The system models and performance metrics are given in Section 5.2. In Section 5.3, we formulate the optimization problem. In Section 5.4 and 5.5, we analyze the normalized optimal power control policy that maximizes the effective secrecy throughput in the perfect full and partial CSI scenarios and derive the closed-form solution and learning-based solution in special and general cases, respectively. In Section 5.6, we investigate the estimation error of CSI for the optimal solutions in special and general cases. Numerical results and conclusions are given in Section 5.7 and 5.8, respectively.

5.2 System Model and Performance Metrics

5.2.1 System Model

In this chapter, we consider the downlink transmission in a wireless network, in which a single-antenna AP transmits confidential short packets to an intended user in the presence of an eavesdropper. We assume that the intended user and the eavesdropper are each equipped with a single antenna, due to size limitation. The wireless channels are assumed to be block fading channels, i.e., small-scale channels are constant within each frame but vary among different frames according to independent and identically distributed (i.i.d.) Rayleigh fading. Thus, small-scale channel gains from the AP to the intended user and the eavesdropper in the ith frame, denoted by $g_b[i]$ and $g_e[i]$, respectively, follow an exponential distribution with unit mean. The duration of each frame is T_c, which is the channel coherence time. The large-scale channel gains from the AP to the intended user and the eavesdropper are denoted by α_b and α_e, respectively.

5.2.2 Performance Metrics

In this chapter, we aim to analyze the effective secrecy throughput in the finite blocklength regime under statistical QoS constraints. We extend the definition of the effective secrecy throughput in [78] to the finite blocklength regime, i.e., the effective capacity [100] of a queueing system, where the service rate is characterized by the maximal achievable secrecy rate with short blocklength codes [44, 76]. In the following, we briefly introduce the preliminary concepts of effective secrecy throughput.

- **Secrecy Rate in Finite Blocklength Regime:** To reduce transmission delay, the duration of a coding block (slot), denoted by T_b, is assumed to be shorter than T_c, i.e., $T_b < T_c$. The number of symbols transmitted in each slot, which is also referred to as the blocklength of channel coding, is determined by the allocated bandwidth B and the transmission duration T_b, i.e., T_bB. Since $T_b < T_c$, the wireless channel is quasi-static. The SNRs at the intended user and the eavesdropper, denoted by $\gamma_b[i]$ and $\gamma_e[i]$, are given by

$$\gamma_b[i] = \frac{\alpha_b g_b[i]P[i]}{N_bB} \text{ and } \gamma_e[i] = \frac{\alpha_e g_e[i]P[i]}{N_eB}, \tag{5.1}$$

  respectively, where $P[i]$ is the transmit power in the ith frame, and N_b and N_e are the single-sided noise spectral densities at the intended user and the eavesdropper, respectively.

  Let us denote the instantaneous secrecy rate in the ith frame by $R_s[i]$. According to [44, 76], a lower bound on the maximal achievable secrecy rate (bits/s/Hz) for a given

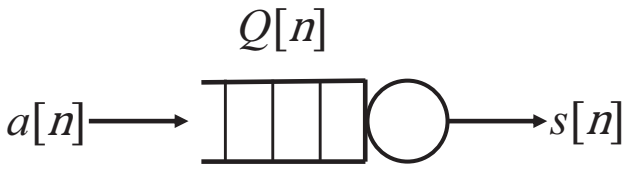

Figure 5.1: Queueing model.

decoding error probability ε_c and the information leakage δ is expressed as

$$R_s[i] > \begin{cases} C_s[i] - \sqrt{\frac{V_b[i]}{T_b B}} \frac{f_Q^{-1}(\varepsilon_c)}{\ln 2} - \sqrt{\frac{V_e[i]}{T_b B}} \frac{f_Q^{-1}(\delta)}{\ln 2}, & \gamma_b[i] > \gamma_e[i], \\ 0, & \gamma_b[i] \leq \gamma_e[i], \end{cases} \tag{5.2}$$

where $C_s[i] = \log_2(1+\gamma_b[i]) - \log_2(1+\gamma_e[i])$ is the secrecy capacity in the infinite blocklength regime, $V_x[i] = 1-(1+\gamma_x[i])^{-2}$, $x \in \{b,e\}$, is the channel dispersion, and $f_Q^{-1}(\cdot)$ is the inverse Q-function. In the sequel, we use the lower bound in (5.2) to characterize the service rate.

- **Effective Capacity and Statistical QoS Requirement:** The statistical QoS requirement is defined as a queueing delay bound and the maximum tolerable delay bound violation probability, (D_q, ε_q). To meet the requirement, the steady state queueing delay, denoted by D_∞, needs to satisfy the following constraint

$$\Pr\{D_\infty > D_q\} \leq \varepsilon_q. \tag{5.3}$$

We apply the *effective capacity* to characterize the statistical QoS requirement in wireless communications. It is defined as [54, 100]

$$\mathrm{E_C}(\theta) = -\lim_{N_f \to \infty} \frac{1}{\theta N_f T_c} \ln\left(\mathbb{E}\left[e^{-\theta \sum_{i=1}^{N_f} T_c B R_s[i]}\right]\right) \text{ bits/s}, \tag{5.4}$$

where $\mathbb{E}[\cdot]$ denotes the expectation operation, θ is the QoS exponent and N_f is the number of frames.

It is noted that the effective capacity is used to analyze the performance of the queueing system. Thus, it is independent on the blocklength. We also note that it is normal to adopt the effective capacity to analyze the delay performance of a communication system in the finite blocklength regime, such as [65, 101, 102]. According to the definition [100], the effective capacity is defined as the maximum constant arrival rate $a[n]$ that a given service process $s[n]$ can support to guarantee a statistical queueing requirement. In Fig. 5.1, we see that there is no restriction on the nature of the service process. Thus, the

service process can be the secrecy capacity, the Shannon capacity, the achievable rate in finite blocklength regime, or any other performance metric that is related to the physical-layer technologies. For our considered system, the service process is characterized by the secrecy capacity in the finite blocklength regime, which is used to obtain the effective capacity. Moreover, in order to analyze the end-to-end performance, we consider the statistical QoS requirement in the Medium Access Control (MAC) layer in our work. Since the effective capacity can be applied into any physical-layer service process, we use it to characterize the statistical QoS requirement in our system.

In this work, we consider a constant arrival rate, $a[n]$. If $\mathrm{E_C}(\theta) = a[n]$, the tail probability of the steady state queueing delay can be expressed as [100]

$$\Pr\{D_\infty > D_q\} \approx e^{-\theta a[n] D_q}, \tag{5.5}$$

where the approximation is accurate when $D_q \gg T_c$ or $\Pr\{D_\infty > D_q\}$ is extremely small [54]. By substituting (5.5) into (5.3), we derive the expression for the QoS exponent as $\theta = \frac{\ln(1/\varepsilon_q)}{a[n]D_q}$, which decreases when D_q and ε_q increase. By using the results in [54], the analysis in this subsection can be easily extended to other packet arrival processes, such as the Poisson arrival process, interrupted Poisson process, and switched Poisson processes.

- **Effective Secrecy Throughout:** Since the wireless channels are i.i.d. among different frames, $R_s[i]$ and $R_s[j]$ are uncorrelated for all $j \neq i$. By substituting (5.2) into (5.4), the effective capacity is re-expressed as

$$\begin{aligned}
\mathrm{E_C}(\theta) &= -\lim_{N_f\to\infty} \frac{1}{\theta N_f T_c} \ln\left(\mathbb{E}\left[e^{-\theta\sum_{i=1}^{N_f} T_c B R_s[i]}\right]\right) \\
&= -\lim_{N_f\to\infty} \frac{1}{\theta T_c N_f} \ln \Pi_{i=1}^{N_f}\left(\mathbb{E}\left[e^{-\theta T_c B R_s[i]}\right]\right) \\
&= -\lim_{N_f\to\infty} \frac{1}{\theta T_c N_f} N_f \ln\left(\mathbb{E}\left[e^{-\theta T_c B R_s[i]}\right]\right) \\
&= -\frac{1}{\theta T_c} \ln\left(\mathbb{E}\left[e^{-\theta T_c B R_s[i]}\right]\right) \text{ bits/s.}
\end{aligned} \tag{5.6}$$

Since $R_s[i]$ is i.i.d, we remove index i in the remaining of this paper for notational simplicity. By normalizing the effective capacity with the bandwidth B, we obtain the normalized effective secrecy throughput as

$$\mathrm{E_{SC}} = -\frac{1}{\theta T_c B} \ln\left(\mathbb{E}\left[e^{-\theta T_c B R_s}\right]\right) \text{ bits/s/Hz.} \tag{5.7}$$

5.3 Problem Formulation

To investigate the impact of eavesdropper's CSI on the effective secrecy throughput, we formulate the optimization problems that maximize the effective secrecy throughput subject to an average transmit power constraint in two different scenarios, i.e., the full CSI and the partial CSI scenarios. In the full CSI scenario, the small-scale channel gains of the intended user and the eavesdropper are available at the AP. In the partial CSI scenario, the AP only knows the small-scale channel gain of the intended user. In both scenarios, we assume that the large-scale channel gains and the distributions of small-scale channel gains of the intended user and the eavesdropper are known by the AP.

5.3.1 Problem Formulation in Full CSI Scenario

In the full CSI scenario, the AP adjusts transmit power according to g_b and g_e. We define the normalized power control policy as $\mu(g_b, g_e) \triangleq P/\overline{P}$, where $\overline{P}$ is the maximum average transmit power of the AP. Then, the average transmit power constraint is given by

$$\mathbb{E}[\mu(g_b, g_e)] = \int_0^\infty \int_0^\infty \mu(g_b, g_e) f_{g_b}(g_b) f_{g_e}(g_e) dg_b dg_e \leq 1, \tag{5.8}$$

where $f_{g_b}(g_b)$ and $f_{g_e}(g_e)$ are the PDFs of g_b and g_e, respectively.

Given the definition of $\mu(g_b, g_e)$, the SNRs at the intended user and the eavesdropper can be re-expressed as

$$\gamma_b = \frac{P}{\overline{P}} \times \frac{\overline{P}\alpha_b}{N_b B} g_b = \mu(g_b, g_e) \varphi_b g_b; \tag{5.9}$$

$$\gamma_e = \frac{P}{\overline{P}} \times \frac{\overline{P}\alpha_e}{N_e B} g_e = \mu(g_b, g_e) \varphi_e g_e, \tag{5.10}$$

respectively, where $\varphi_x \triangleq \overline{P}\alpha_x / N_x B$, $x \in \{b, e\}$, is the average SNR.

We note that the achievable rate in (5.2) is zero when $\gamma_b \leq \gamma_e$. It means that when $\varphi_b g_b < \varphi_e g_e$, $R_s = 0$ for any power control policy. Thus, the optimal power control policy is $\mu(g_b, g_e) = 0$ in the region of $\{(g_b, g_e) | \varphi_b g_b < \varphi_e g_e\}$, and the average power constraint in (5.8) can be re-expressed as

$$\int_0^\infty \int_{\frac{\varphi_e}{\varphi_b} g_e}^\infty \mu(g_b, g_e) f_{g_b}(g_b) f_{g_e}(g_e) dg_b dg_e \leq 1. \tag{5.11}$$

Similar to (5.11), the effective secrecy throughput in (5.7) can be rewritten as

$$\begin{aligned}\mathrm{E_{SC}} &= -\frac{1}{\theta T_c B}\ln\Bigg(\int_0^{\infty}\int_0^{\frac{\varphi_e}{\varphi_b}g_e} f_{g_b}(g_b) f_{g_e}(g_e)\, dg_b dg_e \\ &\quad + \int_0^{\infty}\int_{\frac{\varphi_e}{\varphi_b}g_e}^{\infty} \Phi\left(\mu(g_b,g_e), g_b, g_e\right) f_{g_b}(g_b) f_{g_e}(g_e)\, dg_b dg_e\Bigg) \\ &= -\frac{1}{\theta T_c B}\ln\Big(C_0 + \Psi\left(\mu(g_b,g_e), g_b, g_e\right)\Big), \end{aligned} \tag{5.12}$$

where $C_0 \triangleq \int_0^{\infty}\int_0^{\frac{\varphi_e}{\varphi_b}g_e} f_{g_b}(g_b) f_{g_e}(g_e)\, dg_b dg_e$. $\Phi\left(\mu(g_b,g_e), g_b, g_e\right)$ and $\Psi\big(\mu(g_b,g_e), g_b, g_e\big)$ are defined as follows,

$$\begin{aligned}\Psi\big(\mu(g_b,g_e), g_b, g_e\big) &= \int_0^{\infty}\int_{\frac{\varphi_e}{\varphi_b}g_e}^{\infty} \underbrace{\underbrace{\left(\frac{1+\mu(g_b,g_e)\,\varphi_b g_b}{1+\mu(g_b,g_e)\,\varphi_e g_e}\right)^{-\beta}}_{\Phi_1(\mu(g_b,g_e),g_b,g_e)} \underbrace{e^{\frac{\beta\left(\sqrt{V_b} f_Q^{-1}(\varepsilon_c)+\sqrt{V_e} f_Q^{-1}(\delta)\right)}{\sqrt{T_b B}}}}_{\Phi_2(\mu(g_b,g_e),g_b,g_e)}}_{\Phi(\mu(g_b,g_e),g_b,g_e)} \\ &\quad \times f_{g_b}(g_b) f_{g_e}(g_e)\, dg_b dg_e \\ &= \int_0^{\infty}\int_{\frac{\varphi_e}{\varphi_b}g_e}^{\infty} \Phi(\mu(g_b,g_e), g_b, g_e) f_{g_b}(g_b) f_{g_e}(g_e)\, dg_b dg_e, \end{aligned} \tag{5.13}$$

where $\beta \triangleq \frac{\theta T_c B}{\ln 2}$.

The optimal power control policy that maximizes the effective secrecy throughput under QoS and average transmit power constraints can be obtained from the following problem,

$$\begin{aligned} \max_{\mu(g_b,g_e)} \quad & \mathrm{E_{SC}} \\ \text{s.t.} \quad & \mu(g_b,g_e) \geq 0 \text{ and (5.11).} \end{aligned} \tag{5.14}$$

Since C_0 in (5.12) is a constant and $\mathrm{E_{SC}}$ decreases with $\Psi\big(\mu(g_b,g_e), g_b, g_e\big)$, maximizing $\mathrm{E_{SC}}$ is equivalent to minimizing $\Psi\big(\mu(g_b,g_e), g_b, g_e\big)$. Therefore, the problem in (5.14) can be further transformed as

$$\begin{aligned} \min_{\mu(g_b,g_e)} \quad & \Psi\big(\mu(g_b,g_e), g_b, g_e\big) \\ \text{s.t.} \quad & \mu(g_b,g_e) \geq 0 \text{ and (5.11).} \end{aligned} \tag{5.15}$$

5.3.2 Problem Formulation in Partial CSI Scenario

In the partial CSI scenario, the transmitter can only adjust the transmit power according to the value of g_b. Thus, the normalized power control policy can be simplified as $\mu(g_b)$. The

average power constraint can be rewritten as

$$\mathbb{E}\left[\mu(g_b)\right] = \int_0^{\infty} \mu(g_b) f_{g_b}(g_b) dg_b \leq 1. \tag{5.16}$$

Similarly, the SNRs at the intended user and the eavesdropper can be re-expressed as follows:

$$\gamma_b = \frac{P}{\overline{P}} \times \frac{\overline{P}\alpha_b}{N_b B} g_b = \mu(g_b)\varphi_b g_b; \tag{5.17}$$

$$\gamma_e = \frac{P}{\overline{P}} \times \frac{\overline{P}\alpha_e}{N_e B} g_e = \mu(g_b)\varphi_e g_e. \tag{5.18}$$

Since $R_s = 0$ when $\phi_b g_b < \phi_e g_e$, the normalized effective secrecy throughput in (5.7) can be rewritten as

$$\begin{aligned} \mathrm{E_{SC}} &= -\frac{1}{\theta T_c B} \ln\left\{ \int_0^{\infty} \int_{\frac{\varphi_b}{\varphi_e} g_b}^{\infty} f_{g_b}(g_b) f_{g_e}(g_e) dg_e dg_b + \int_0^{\infty} \int_0^{\frac{\varphi_b}{\varphi_e} g_b} \Upsilon(\mu(g_b), g_b) f_{g_b}(g_b) f_{g_e}(g_e) dg_e dg_b \right\} \\ &= -\frac{1}{\theta T_c B} \ln\left\{ C_1 + \Omega\big(\mu(g_b), g_b\big) \right\}, \end{aligned} \tag{5.19}$$

where $C_1 \triangleq \int_0^{\infty} \int_{\frac{\varphi_b}{\varphi_e} g_b}^{\infty} f_{g_b}(g_b) f_{g_e}(g_e) dg_e dg_b$. $\Upsilon(\mu(g_b), g_b)$ and $\Omega\big(\mu(g_b), g_b\big)$ are defined as follows,

$$\begin{aligned} \Omega\big(\mu(g_b), g_b\big) &= \int_0^{\infty} \int_0^{\frac{\varphi_b}{\varphi_e} g_b} \underbrace{\underbrace{\left(\frac{1+\mu(g_b)\varphi_b g_b}{1+\mu(g_b)\varphi_e g_e}\right)^{-\beta}}_{\Upsilon_1(\mu(g_b), g_b)} \underbrace{e^{\frac{\beta\left(\sqrt{V_b} f_Q^{-1}(\varepsilon_C) + \sqrt{V_e} f_Q^{-1}(\delta)\right)}{\sqrt{T_b B}}}}_{\Upsilon_2(\mu(g_b), g_b)}}_{\Upsilon(\mu(g_b), g_b)} f_{g_b}(g_b) f_{g_e}(g_e) dg_e dg_b \\ &= \int_0^{\infty} \int_0^{\frac{\varphi_b}{\varphi_e} g_b} \Upsilon(\mu(g_b), g_b) f_{g_b}(g_b) f_{g_e}(g_e) dg_e dg_b. \end{aligned} \tag{5.20}$$

Then, the optimization problem in the partial CSI scenario is given by

$$\begin{aligned} \max_{\mu(g_b)} \ & \mathrm{E_{SC}} \\ \text{s.t.} \ & \mu\left(g_b\right) \geq 0 \text{ and (5.16)}. \end{aligned} \tag{5.21}$$

Since C_1 in (5.19) is a constant and $\mathrm{E_{SC}}$ decreases with $\Omega\big(\mu\left(g_b\right), g_b\big)$, maximizing $\mathrm{E_{SC}}$ is equivalent to minimizing $\Omega\big(\mu\left(g_b\right), g_b\big)$. Therefore, problem (5.21) is equivalent to the

following problem,

$$\min_{\mu(g_b)} \ \Omega\big(\mu\left(g_b\right), g_b\big) \tag{5.22}$$
$$\text{s.t. } \mu\left(g_b\right) \geq 0 \text{ and (5.16).}$$

In both full and partial CSI scenarios, problems in (5.15) and (5.22) are functional optimization problems, which lead to the fact that the optimal power control policies, $\mu\left(g_b, g_e\right)$ and $\mu\left(g_b\right)$, do not have closed-form expressions in general. To obtain useful insights, we first derive the closed-form expressions of $\mu\left(g_b, g_e\right)$ and $\mu\left(g_b\right)$ in a special case. Then, we apply an unsupervised learning algorithm to find the optimal power control policy numerically in general cases.

5.4 Closed-form Solution in Special Case

In this section, we derive the closed-form solution of the normalized optimal power control policy that maximizes the effective secrecy throughput in a special case, where $V_x \approx 1$, $x \in \{b, e\}$, and $\beta = 1$ in both full and partial CSI scenarios. We note that the channel dispersion, given by $V_x = 1 - (1+\gamma_x)^{-2}$ is strictly smaller than 1. By substituting $V_x \approx 1$ into (5.2), we obtain a lower bound of the achievable secrecy rate. Thus, the QoS requirement can be satisfied if the lower bound is used in the optimization. In addition, the approximation of $V_x \approx 1$ is accurate when the SNR is large, e.g., $\gamma_x > 10$ dB [36, 37], which is a prerequisite for achieving low latency and high reliability.

5.4.1 Special Case in Full CSI Scenario

When $V_x \approx 1$, the term $\Phi_2\left(\mu\left(g_b, g_e\right), g_b, g_e\right) = e^{\frac{\beta}{\sqrt{T_b B}}\left(f_Q^{-1}(\varepsilon_c) + f_Q^{-1}(\delta)\right)}$ in (5.13) is a constant that does not depend on $\mu\left(g_b, g_e\right)$. As such, the problem in (5.15) can be further reduced as

$$\min_{\mu(g_b,g_e)} \int_0^{\infty} \int_{\frac{\varphi_e}{\varphi_b} g_e}^{\infty} \Phi_1\left(\mu\left(g_b, g_e\right), g_b, g_e\right) f_{g_b}(g_b) f_{g_e}(g_e)\, dg_b dg_e \tag{5.23}$$
$$\text{s.t.} \quad \mu\left(g_b, g_e\right) \geq 0 \text{ and (5.11),}$$

where $\Phi_1\left(\mu\left(g_b,g_e\right),g_b,g_e\right)=\left(\frac{1+\mu(g_b,g_e)\varphi_b g_b}{1+\mu(g_b,g_e)\varphi_e g_e}\right)^{-\beta}$. The optimal solution to this problem satisfies the first order necessary conditions [78, 103], given by

$$\frac{\partial\mathcal{L}_1}{\partial\mu\left(g_b,g_e\right)}=0, \tag{5.24}$$

$$\lambda_1\left(\int_0^{\infty}\int_{\frac{\varphi_e}{\varphi_b}g_e}^{\infty}\mu\left(g_b,g_e\right)f_{g_b}\left(g_b\right)f_{g_e}\left(g_e\right)dg_b dg_e-1\right)=0, \tag{5.25}$$

$$\lambda_1\geq 0,\mu\left(g_b,g_e\right)\geq 0, \text{ and (5.11)},$$

where $\mathcal{L}_1$ is the Lagrangian function defined as [103]

$$\begin{aligned}\mathcal{L}_1\triangleq&\int_0^{\infty}\int_{\frac{\varphi_e}{\varphi_b}g_e}^{\infty}\left(\frac{1+\mu\left(g_b,g_e\right)\varphi_b g_b}{1+\mu\left(g_b,g_e\right)\varphi_e g_e}\right)^{-\beta}f_{g_b}(g_b)\,f_{g_e}(g_e)\,dg_b dg_e\\&+\lambda_1\left(\int_0^{\infty}\int_{\frac{\varphi_e}{\varphi_b}g_e}^{\infty}\mu\left(g_b,g_e\right)f_{g_b}(g_b)\,f_{g_e}(g_e)\,dg_b dg_e-1\right)\end{aligned} \tag{5.26}$$

and λ_1 is the Lagrangian multiplier. For Rayleigh fading channels, the partial derivative of $\mathcal{L}_1$ w.r.t. the normalized power control policy $\mu\left(g_b,g_e\right)$ can be derived as [78]

$$\begin{aligned}\frac{\partial\mathcal{L}_1}{\partial\mu\left(g_b,g_e\right)}&=\left[\frac{\partial}{\partial\mu\left(g_b,g_e\right)}\left\{\left(\frac{1+\mu\left(g_b,g_e\right)\varphi_b g_b}{1+\mu\left(g_b,g_e\right)\varphi_e g_e}\right)^{-\beta}\right\}+\lambda_1\right]f_{g_b}\left(g_b\right)f_{g_e}\left(g_e\right)\\&=\left[\lambda_1-\frac{\beta\left(\varphi_b g_b-\varphi_e g_e\right)\left(\frac{1+\mu(g_b,g_e)\varphi_b g_b}{1+\mu(g_b,g_e)\varphi_e g_e}\right)^{1-\beta}}{\left(1+\mu\left(g_b,g_e\right)\varphi_b g_b\right)^2}\right]f_{g_b}\left(g_b\right)f_{g_e}\left(g_e\right).\end{aligned} \tag{5.27}$$

The value of β depends on the QoS requirement, channel coherence time, and bandwidth. To derive the closed-form solution, we adjust the value of B to satisfy $\beta=1$. When $\beta=1$, (5.24) can be simplified as

$$\left[\lambda_1-\frac{\varphi_b g_b-\varphi_e g_e}{\left(1+\mu\left(g_b,g_e\right)\varphi_b g_b\right)^2}\right]f_{g_b}\left(g_b\right)f_{g_e}\left(g_e\right)=0. \tag{5.28}$$

The optimal solution satisfies (5.28) for all the values of g_b and g_e. Thus, $\lambda_1>0$ and the closed-form expression for the optimal solution can be derived as

$$\mu^*_{\beta=1}\left(g_b,g_e\right)=\begin{cases}\tau_1, & g_b-\frac{\varphi_e}{\varphi_b}g_e>\frac{\lambda_1}{\varphi_b},\\ 0, & g_b-\frac{\varphi_e}{\varphi_b}g_e\leq\frac{\lambda_1}{\varphi_b},\end{cases} \tag{5.29}$$

where

$$\tau_1 = \frac{1}{\varphi_b g_b}\left(\sqrt{\frac{\varphi_b g_b - \varphi_e g_e}{\lambda_1}} - 1\right). \tag{5.30}$$

The optimal policy is a "water-filling" policy, and value of λ_1 should satisfy the average transmit power constraint,

$$\int_0^{\infty}\int_{\frac{\varphi_e}{\varphi_b}g_e+\frac{\lambda_1}{\varphi_b}}^{\infty} \tau_1 f_{g_b}(g_b) f_{g_e}(g_e)\, dg_b dg_e = 1, \tag{5.31}$$

which is obtained by substituting (5.29) into (5.25). Since $\frac{\varphi_e}{\varphi_b}g_e + \frac{\lambda_1}{\varphi_b}$ strictly increases with λ_1 and τ_1 strictly decreases with λ_1, the left-hand-side of (5.31) strictly decreases with λ_1. Thus, the value of λ_1 that satisfies (5.31) is unique and can be obtained by binary search. We denote it by λ_1^*.

5.4.2 Special Case in Partial CSI Scenario

When $V_x \approx 1$, the term $\mathrm{Y}_2(\mu(g_b), g_b) = e^{\frac{\beta}{\sqrt{T_b B}}\left(f_Q^{-1}(\varepsilon_c)+f_Q^{-1}(\delta)\right)}$ in (5.20) is a constant. The optimization problem in (5.22) can be re-expressed as

$$\begin{aligned}\min_{\mu(g_b)} & \int_0^{\infty}\int_0^{\frac{\varphi_b}{\varphi_e}g_b}\left(\frac{1+\mu(g_b)\varphi_b g_b}{1+\mu(g_b)\varphi_e g_e}\right)^{-1} f_{g_b}(g_b) f_{g_e}(g_e) dg_e dg_b \\ \text{s.t.} \quad & \mu(g_b) \geq 0 \text{ and (5.16).}\end{aligned} \tag{5.32}$$

The optimal solution to problem (5.32) should satisfy the following conditions [78, 103],

$$\frac{\partial \mathcal{L}_2}{\partial \mu(g_b)} = 0, \tag{5.33}$$

$$\lambda_2\left(\int_0^{\infty}\mu(g_b) f_{g_b}(g_b) dg_b - 1\right) = 0, \tag{5.34}$$

$$\lambda_2 \geq 0, \mu(g_b) \geq 0 \text{ and (5.16),}$$

where $\mathcal{L}_2$ is the Lagrangian function defined as [103]

$$\mathcal{L}_2 \triangleq \int_0^{\infty}\int_0^{\frac{\varphi_b}{\varphi_e}g_b}\left(\frac{1+\mu(g_b)\varphi_b g_b}{1+\mu(g_b)\varphi_e g_e}\right)^{-1} f_{g_b}(g_b) f_{g_e}(g_e) dg_e dg_b + \lambda_2\left(\int_0^{\infty}\mu(g_b) f_{g_b}(g_b) dg_b - 1\right), \tag{5.35}$$

and λ_2 is the Lagrangian multiplier. For Rayleigh fading channel, the partial derivative of the Lagrangian function $\mathcal{L}_2$ w.r.t the normalized power control policy $\mu(g_b)$ can be derived as

follows,

$$\frac{\partial \mathcal{L}_2}{\partial \mu(g_b)} = \left[\lambda_2 - \int_0^{\frac{\varphi_b}{\varphi_e} g_b} \frac{\varphi_b g_b - \varphi_e g_e}{\left(1+\mu(g_b)\varphi_b g_b\right)^2} f_{g_e}(g_e) dg_e\right] f_{g_b}(g_b)$$
$$= \left[\lambda_2 - \frac{\varphi_b g_b + \left(e^{-\frac{\varphi_b}{\varphi_e} g_b} - 1\right)\varphi_e}{\left(1+\mu(g_b)\varphi_b g_b\right)^2}\right] f_{g_b}(g_b). \tag{5.36}$$

As such, (5.33) can be simplified as

$$\left[\lambda_2 - \frac{\varphi_b g_b + \left(e^{-\frac{\varphi_b}{\varphi_e} g_b} - 1\right)\varphi_e}{\left(1+\mu(g_b)\varphi_b g_b\right)^2}\right] f_{g_b}(g_b) = 0. \tag{5.37}$$

The optimal solution should satisfy (5.37) for all the values of g_b. Thus, $\lambda_2 > 0$ and the closed-form expression for the optimal solution can be derived as

$$\mu^{\star}_{\beta=1}(g_b) = \begin{cases} \tau_2, & g_b > g_b^{\text{th}} \\ 0, & g_b \leq g_b^{\text{th}}, \end{cases} \tag{5.38}$$

where

$$\tau_2 = \frac{1}{\varphi_b g_b}\left(\frac{\sqrt{\varphi_b g_b + \left(e^{-\frac{\varphi_b}{\varphi_e} g_b} - 1\right)\varphi_e}}{\lambda_2} - 1\right), \tag{5.39}$$

and g_b^{th} is the solution of $\tau_2 = 0$, i.e.,

$$\frac{\varphi_b}{\varphi_e} g_b^{\text{th}} + \left(e^{-\frac{\varphi_b}{\varphi_e} g_b^{\text{th}}} - 1\right) = \frac{\lambda_2^2}{\varphi_e}. \tag{5.40}$$

The optimal policy is again a "water-filling" policy, and λ_2 should satisfy the average transmit power constraint,

$$\int_{g_b^{\text{th}}}^{\infty} \tau_2 f_{g_b}(g_b) dg_b = 1, \tag{5.41}$$

which is obtained by substituting (5.38) into (5.34). Since g_b^{th} in (5.40) strictly increases with λ_2 and τ_2 in (5.39) strictly decreases with λ_2, the left-hand-side of (5.41) strictly decreases with λ_2. Thus, there is a unique value of λ_2 that satisfies (5.41). We can obtain the unique solution λ_2^* by binary search. Given the value of λ_2^*, the unique solution of g_b^{th} can be obtained from (5.40).

It is noted that [78] proved the above problems in the special case to be convex when $\beta = 1$

and $V_x \approx 1$. Therefore, our obtained closed-form solutions are globally optimal. Moreover, no closed-form optimal solution has been obtained when queuing delay and security requirement are considered [78, 79, 81, 104]. For example, [78] developed a numerical method to obtain the optimal power control policy, but did not obtain closed-form optimal solutions. It is also worth mentioning that our motivation of deriving the closed-form solution in the special case is to use it as a benchmark to demonstrate the effectiveness of our learning-based solutions. Therefore, it is very important and necessary to analyze the case with $V_x \approx 1$.

5.5 An Unsupervised Learning-Based Solution in General Cases

It is noted that although the closed-form solution is available in the special case, the threshold needs to be obtained by the binary search to satisfy the average transmit power constraint. With the proposed unsupervised learning method, there is no need to search the threshold with the binary search. Also, in the general case, it is very difficult, if not impossible, to derive closed-form solutions for the first-order necessary conditions. To overcome this difficulty, we apply an unsupervised learning method to find the solution numerically [84]. The underlying idea is to use a DNN to approximate the normalized power control policy and apply the primal-dual method to update the parameters of the DNN and the Lagrangian multiplier. After the training stage, near-optimal solutions can be obtained from the output of the DNN by using the forward-propagation algorithm, which has low computational complexity.

5.5.1 General Case in Full CSI Scenario

With the primal-dual method, problem (5.15) in the full CSI scenario can be converted into

$$\begin{aligned} \max_{\lambda_f} \min_{\mu(g_b,g_e)} \mathcal{L}_f &\triangleq \Psi\left(\mu\left(g_b,g_e\right),g_b,g_e\right)+\lambda_f\left(\mathbb{E}\left[\mu\left(g_b,g_e\right)\right]-1\right) \\ \text{s.t.} \quad & (5.13),\ \mu\left(g_b,g_e\right)\geq 0, \text{ and } \lambda_f \geq 0, \end{aligned} \tag{5.42}$$

where $\mathcal{L}_f$ is the Lagrangian function of (5.15) and λ_f is the Lagrangian multiplier.

The DNN used to approximate $\mu\left(g_b,g_e\right)$ in the full CSI scenario is denoted by $\hat{\mu}\left(g_b,g_e;\omega_f\right)$, where g_b and g_e are the inputs and ω_f represents the parameters of the DNN (i.e., weights and bias). Then, problem (5.42) can be rewritten as

$$\begin{aligned} \max_{\lambda_f} \min_{\omega_f} \hat{\mathcal{L}}_f &\triangleq \Psi\left(\hat{\mu}\left(g_b,g_e;\omega_f\right),g_b,g_e\right)+\lambda_f\left(\mathbb{E}\left[\hat{\mu}\left(g_b,g_e;\omega_f\right)\right]-1\right) \\ \text{s.t.} \quad & (5.13),\ \hat{\mu}\left(g_b,g_e;\omega_f\right)\geq 0, \text{ and } \lambda_f \geq 0, \end{aligned} \tag{5.43}$$

where ω_f and λ_f are updated iteratively. In the tth iteration, the system generates N training samples, $\{(g_b^{(t,n)},g_e^{(t,n)}),n=1,\cdots,N\}$, according to the distributions of g_b and g_e. From these

realizations of small-scale channel gains, the estimated Lagrangian function is given by

$$\hat{\mathcal{L}}_f^{(t)} \triangleq \frac{1}{N}\sum_{n=1}^{N}\left[\Phi\left(\hat{\mu}\left(g_b^{(t,n)}, g_e^{(t,n)}; \omega_f^{(t)}\right), g_b^{(t,n)}, g_e^{(t,n)}\right) + \lambda_f^{(t)}\left(\hat{\mu}\left(g_b^{(t,n)}, g_e^{(t,n)}; \omega_f^{(t)}\right) - 1\right)\right]. \tag{5.44}$$

With the unsupervised learning approach in [84], the Lagrangian multiplier can be updated according to

$$\lambda_f^{(t+1)} = \left[\lambda_f^{(t)} + \phi^{(t)}\frac{\partial \hat{\mathcal{L}}_f^{(t)}}{\partial \lambda_f^{(t)}}\right]^+ = \left[\lambda_f^{(t)} + \phi^{(t)}\left(\frac{1}{N}\sum_{n=1}^{N}\hat{\mu}\left(g_b^{(t,n)}, g_e^{(t,n)}; \omega_f^{(t)}\right) - 1\right)\right]^+, \tag{5.45}$$

where $[x]^+ \triangleq \max\{x, 0\}$ and $\phi^{(t)}$ is the learning rate.
In the primal domain, the stochastic gradient descent (SGD) algorithm is applied to minimize the objective function in (5.43) by optimizing the parameters of the DNN, i.e.,

$$\omega_f^{(t+1)} = \omega_f^{(t)} - \phi^{(t)}\nabla_{\omega_f}\hat{\mathcal{L}}_f^{(t)}, \tag{5.46}$$

where

$$\nabla_{\omega_f}\hat{\mathcal{L}}_f^{(t)} = \frac{1}{N}\sum_{n=1}^{N}\left[\nabla_{\omega_f}\hat{\mu}\left(g_b^{(t,n)}, g_e^{(t,n)}; \omega_f^{(t)}\right)\frac{\partial \hat{\mathcal{L}}_f^{(t,n)}}{\partial \hat{\mu}\left(g_b^{(t,n)}, g_e^{(t,n)}; \omega_f^{(t)}\right)}\right]. \tag{5.47}$$

We note that $\nabla_{\omega_f}\hat{\mu}\left(g_b^{(t,n)}, g_e^{(t,n)}; \omega_f^{(t)}\right)$ can be computed via backward propagation. The partial derivative of $\hat{\mathcal{L}}_f^{(t,n)}$ w.r.t $\hat{\mu}\left(g_b^{(t,n)}, g_e^{(t,n)}; \omega_f^{(t)}\right)$ can be obtained from

$$\frac{\partial \hat{\mathcal{L}}_f^{(t,n)}}{\partial \hat{\mu}\left(g_b^{(t,n)}, g_e^{(t,n)}; \omega_f^{(t)}\right)} = \lambda_f^{(t+1)} + \frac{\partial \Phi\left(\hat{\mu}\left(g_b^{(t,n)}, g_e^{(t,n)}; \omega_f^{(t)}\right), g_b^{(t,n)}, g_e^{(t,n)}\right)}{\partial \hat{\mu}\left(g_b^{(t,n)}, g_e^{(t,n)}; \omega_f^{(t)}\right)}. \tag{5.48}$$

The second term in (5.48) can be obtained by substituting the values of $\hat{\mu}\left(g_b^{(t,n)}, g_e^{(t,n)}; \omega_f^{(t)}\right)$,

$g_b^{(t,n)}$ and $g_e^{(t,n)}$ into the following expression,

$$\frac{\partial\Phi\left(\mu\left(g_b,g_e\right),g_b,g_e\right)}{\partial\mu\left(g_b,g_e\right)}=\left[\left(\frac{\beta\varphi_b g_b\frac{f_Q^{-1}(\varepsilon_c)}{\sqrt{T_bBV_b}}}{\left(1+\mu\left(g_b,g_e\right)\varphi_b g_b\right)^3}+\frac{\beta\varphi_e g_e\frac{f_Q^{-1}(\delta)}{\sqrt{T_bBV_e}}}{\left(1+\mu\left(g_b,g_e\right)\varphi_e g_e\right)^3}\right)-\frac{\beta\left(\varphi_b g_b-\varphi_e g_e\right)}{\left(1+\mu\left(g_b,g_e\right)\varphi_b g_b\right)\left(1+\mu\left(g_b,g_e\right)\varphi_e g_e\right)}\right]\times\left(\frac{1+\mu\left(g_b,g_e\right)\varphi_b g_b}{1+\mu\left(g_b,g_e\right)\varphi_e g_e}\right)^{-\beta}e^{\beta\left(\sqrt{\frac{V_b}{T_bB}}f_Q^{-1}(\varepsilon_c)+\sqrt{\frac{V_e}{T_bB}}f_Q^{-1}(\delta)\right)}. \quad (5.49)$$

5.5.2 General Case in Partial CSI Scenario

In the partial CSI scenario, problem (5.22) can be converted into

$$\max_{\lambda_p}\min_{\mu(g_b)}\ \mathcal{L}_p\triangleq\Omega\left(\mu\left(g_b\right),g_b\right)+\lambda_p\left(\mathbb{E}\left[\mu\left(g_b\right)\right]-1\right) \quad (5.50)$$
$$\text{s.t.}\quad (5.20),\ \mu\left(g_b\right)\geq 0,\ \text{and}\ \lambda_p\geq 0,$$

where $\mathcal{L}_p$ is the Lagrangian function of problem (5.22) and λ_p is the Lagrangian multiplier.

When the normalized power control policy is approximated by a DNN denoted by $\hat{\mu}\left(g_b;\omega_p\right)$, where ω_p represents the parameters of the DNN (i.e., weights and bias), problem (5.50) can be rewritten as

$$\max_{\lambda_p}\min_{\omega_p}\ \hat{\mathcal{L}}_p\triangleq\Omega\left(\hat{\mu}\left(g_b;\omega_p\right),g_b\right)+\lambda_p\left(\mathbb{E}\left[\hat{\mu}\left(g_b;\omega_p\right)\right]-1\right) \quad (5.51)$$
$$\text{s.t.}\quad (5.20),\ \hat{\mu}\left(g_b;\omega_p\right)\geq 0,\ \text{and}\ \lambda_p\geq 0.$$

The estimated Lagrangian function in the tth iteration, denoted by $\hat{\mathcal{L}}_p^{(t)}$, is given by

$$\hat{\mathcal{L}}_p^{(t)}\triangleq\frac{1}{N}\sum_{n=1}^{N}\left[\int_0^{\frac{\varphi_b}{\varphi_e}g_b}\Upsilon\left(\hat{\mu}\left(g_b^{(t,n)};\omega_p^{(t)}\right),g_b^{(t,n)}\right)f_{g_e}(g_e)dg_e+\lambda_p^{(t)}\left(\hat{\mu}\left(g_b^{(t,n)};\omega_p^{(t)}\right)-1\right)\right]. \quad (5.52)$$

The Lagrangian multiplier $\lambda_p^{(t+1)}$ and the parameters of DNN $\omega_p^{(t+1)}$ can be updated according to the following method [84],

$$\lambda_p^{(t+1)}=\left[\lambda_p^{(t)}+\phi^{(t)}\frac{\partial\hat{\mathcal{L}}_p^{(t)}}{\partial\lambda_p^{(t)}}\right]^+=\left[\lambda_p^{(t)}+\phi^{(t)}\left(\frac{1}{N}\sum_{n=1}^{N}\hat{\mu}\left(g_b^{(t,n)};\omega_p^{(t)}\right)-1\right)\right]^+ \quad (5.53)$$

and

$$\omega_p^{(t+1)} = \omega_p^{(t)} - \phi^{(t)} \nabla_{\omega_p} \hat{\mathcal{L}}_p^{(t)} = \omega_p^{(t)} - \phi^{(t)} \left(\frac{1}{N} \sum_{n=1}^{N} \left[\nabla_{\omega_p} \hat{\mu} \left(g_b^{(t,n)}; \omega_p^{(t)} \right) \frac{\partial \hat{\mathcal{L}}_p^{(t,n)}}{\partial \hat{\mu} \left(g_b^{(t,n)}; \omega_p^{(t)} \right)} \right] \right), \tag{5.54}$$

where $\nabla_{\omega_p} \hat{\mu} \left(g_b^{(t,n)}; \omega_p^{(t)} \right)$ can be computed via backward propagation and $\frac{\partial \hat{\mathcal{L}}_p^{(t,n)}}{\partial \hat{\mu} \left(g_b^{(t,n)}; \omega_p^{(t)} \right)}$ can be derived as follows,

$$\frac{\partial \hat{\mathcal{L}}_p^{(t,n)}}{\partial \hat{\mu} \left(g_b^{(t,n)}; \omega_p^{(t)} \right)} = \int_0^{\frac{\varphi_b}{\varphi_e} g_b} \frac{\partial \Upsilon \left(\hat{\mu} \left(g_b^{(t,n)}; \omega_p^{(t)} \right), g_b^{(t,n)} \right)}{\partial \hat{\mu} \left(g_b^{(t,n)}; \omega_p^{(t)} \right)} f_{g_e}(g_e) dg_e + \lambda_p^{(t+1)}. \tag{5.55}$$

The first term in (5.55) can be obtained by the following two steps. First, substitute the values of $\hat{\mu} \left(g_b^{(t,n)}; \omega_p^{(t)} \right)$ and $g_b^{(t,n)}$ into the following expression,

$$\begin{aligned} \frac{\partial \Upsilon \left(\mu \left(g_b \right), g_b \right)}{\partial \mu \left(g_b \right)} = & \left(\frac{1 + \mu \left(g_b \right) \varphi_b g_b}{1 + \mu \left(g_b \right) \varphi_e g_e} \right)^{-\beta} \left[\left(\frac{\beta \varphi_b g_b \frac{f_Q^{-1}(\varepsilon_c)}{\sqrt{T_b B V_b}}}{\left(1 + \mu \left(g_b \right) \varphi_b g_b \right)^3} + \frac{\beta \varphi_e g_e \frac{f_Q^{-1}(\delta)}{\sqrt{T_b B V_e}}}{\left(1 + \mu \left(g_b \right) \varphi_e g_e \right)^3} \right) \right. \\ & \left. - \frac{\beta \left(\varphi_b g_b - \varphi_e g_e \right)}{\left(1 + \mu \left(g_b \right) \varphi_b g_b \right) \left(1 + \mu \left(g_b \right) \varphi_e g_e \right)} \right] e^{\beta \left(\sqrt{\frac{V_b}{T_b B}} f_Q^{-1}(\varepsilon_c) + \sqrt{\frac{V_e}{T_b B}} f_Q^{-1}(\delta) \right)}. \end{aligned} \tag{5.56}$$

Second, evaluating the integral term by generating multiple realizations of g_e according to its distribution.

5.6 Power Control Policy with Imperfect CSI

In this section, we investigate the impacts of channel estimation errors on the normalized power control policies in the full and partial CSI scenarios. We consider the imperfect channel estimation at the receiver and assume that the feedback to the AP is perfect. More specifically, the AP broadcasts pilots to the receivers, where the MMSE estimator is applied for channel estimation. After that, the receivers will feed the estimated CSI back to the AP. Finally, the AP adjusts the transmit power according to the estimated CSI.

In the following, we consider channel estimation errors in the following two scenarios:

- **Channel Estimation Error in Full CSI Scenario:** The AP knows the estimated CSI of the main channel and the eavesdropper's channel. The eavesdropper is assumed to be an ordinary user of the network. For example, the AP transmits the packets consisting of

1) non-confidential messages for the eavesdropper and 2) confidential messages for the intended user. In this case, both of the receivers feed back the estimated CSI to the AP.

- **Channel Estimation Error in Partial CSI Scenario:** The AP only knows the estimated CSI of the main channel. For this scenario, the eavesdropper is a malicious user that does not cooperate with the AP. In this case, the eavesdropper will not feed back the estimated CSI, but we assume distribution of the eavesdropper's channel is available at the AP.

5.6.1 Channel Estimation Error Model

According to [60, 105], the actual CSI, h_x, $x \in \{b,e\}$, can be obtained from the estimated main channel and the estimation error according to

$$h_x = \hat{h}_x + \Delta h_x, \tag{5.57}$$

where $\hat{h}_x$ and Δh_x are the estimated channel coefficient and the estimation error, respectively.

Recall that, in this work, we assume that h_x, $x \in \{b,e\}$ follows complex Gaussian distributions with zero mean and unit variance, i.e., $h_x \sim \mathcal{CN}(0,1)$. As per the rules of the MMSE estimator in the Bayesian linear model [106], $\hat{h}_x$ and Δh_x follow complex Gaussian distributions, i.e., $\hat{h}_x \sim \mathcal{CN}\left(0, \sigma^2_{\hat{h}_x}\right)$ and $\Delta h_x \sim \mathcal{CN}\left(0, \sigma^2_{\Delta h_x}\right)$, where $\sigma^2_{\hat{h}_b} = 1 - \sigma^2_{\Delta h_b}$ and $\sigma^2_{\hat{h}_e} = 1 - \sigma^2_{\Delta h_e}$. For simplicity, we assume that the estimation error at the intended user and the eavesdropper follow the same complex Gaussian distribution, i.e., $\sigma^2_e \triangleq \sigma^2_{\Delta h_b} = \sigma^2_{\Delta h_e}$.

As such, the received signal at the intended user and the eavesdropper can be expressed as

$$y_b = \sqrt{\alpha_b}\sqrt{P}\hat{h}_b s + \sqrt{\alpha_b}\sqrt{P}\Delta h_b s + n_b; \tag{5.58}$$

$$y_e = \sqrt{\alpha_e}\sqrt{P}\hat{h}_e s + \sqrt{\alpha_e}\sqrt{P}\Delta h_e s + n_e, \tag{5.59}$$

where s is the transmitted signal with $\mathbb{E}[|s|^2] = 1$, $|s|$ denotes the modulus of s, and n_b and n_e are the additive white noise at the intended user and the eavesdropper, respectively. The SINR at the intended user and the eavesdropper are

$$\gamma_b = \frac{\alpha_b|\hat{h}_b|^2 P}{\alpha_b|\Delta h_b|^2 P + N_b B} = \frac{\alpha_b \hat{g}_b P}{\alpha_b z_b P + N_b B}; \tag{5.60}$$

$$\gamma_e = \frac{\alpha_e|\hat{h}_e|^2 P}{\alpha_e|\Delta h_e|^2 P + N_e B} = \frac{\alpha_e \hat{g}_e P}{\alpha_e z_e P + N_e B}, \tag{5.61}$$

where $\hat{g}_b \triangleq |\hat{h}_b|^2$, $\hat{g}_e \triangleq |\hat{h}_e|^2$, $z_b \triangleq |\Delta h_b|^2$, and $z_e \triangleq |\Delta h_e|^2$. Since $\hat{h}_x$ and Δh_x follow complex Gaussian distributions, $\hat{g}_x$ and z_x are exponentially distributed, i.e., $\hat{g}_x \sim \text{Exp}[1/(1-\sigma^2_e)]$ and $z_x \sim \text{Exp}(1/\sigma^2_e)$.

To obtain the effective secrecy throughput with estimation errors, we consider the worst

case that the channel estimation errors are treated as one part of the additive noise [60]. As such, the SINRs at the intended user and the eavesdropper are converted into SNRs, which are given by

$$\gamma_b = \frac{\alpha_b P \hat{g}_b}{\alpha_b P \sigma_e^2 + N_b B} = \frac{\frac{P}{\overline{P}} \hat{g}_b}{\frac{P}{\overline{P}} \sigma_e^2 + \frac{1}{\varphi_b}}; \tag{5.62}$$

$$\gamma_e = \frac{\alpha_e P \hat{g}_e}{\alpha_b P \sigma_e^2 + N_e B} = \frac{\frac{P}{\overline{P}} \hat{g}_e}{\frac{P}{\overline{P}} \sigma_e^2 + \frac{1}{\varphi_e}}, \tag{5.63}$$

where $\varphi_x = \overline{P}\alpha_x / N_x B$, $x \in \{b, e\}$, is the average SNR. Based on the expressions of SNRs, we can futher derive the effective secrecy throughput in full and partial CSI scenarios, respectively.

5.6.2 Full CSI Scenario

To meet the average transmit power constraint, the normalized power control policy, $\mu\left(\hat{g}_b, \hat{g}_e\right)$, should satisfy the following constraint,

$$\mathbb{E}\left[\mu\left(\hat{g}_b, \hat{g}_e\right)\right] = \int_0^\infty \int_0^\infty \mu\left(\hat{g}_b, \hat{g}_e\right) f_{\hat{g}_b}\left(\hat{g}_b\right) f_{\hat{g}_e}\left(\hat{g}_e\right) d\hat{g}_b d\hat{g}_e \leq 1, \tag{5.64}$$

where $f_{\hat{g}_b}\left(\hat{g}_b\right)$ and $f_{\hat{g}_e}\left(\hat{g}_e\right)$ are the PDFs of $\hat{g}_b$ and $\hat{g}_e$, respectively.

Like (5.12), the effective secrecy throughput can be rewritten as

$$\begin{aligned} \mathrm{E_{SC}} &= -\frac{1}{\theta T_c B} \ln\Big(C_2 + \int_0^\infty \int_{\frac{\varphi_e}{\varphi_b}\hat{g}_e}^\infty \Xi\big(\mu\left(\hat{g}_b, \hat{g}_e\right), \hat{g}_b, \hat{g}_e\big) f_{\hat{g}_b}\left(\hat{g}_b\right) f_{\hat{g}_e}\left(\hat{g}_e\right) d\hat{g}_b d\hat{g}_e\Big) \\ &= -\frac{1}{\theta T_c B} \ln\Big(C_2 + \Theta\big(\mu\left(\hat{g}_b, \hat{g}_e\right), \hat{g}_b, \hat{g}_e\big)\Big), \end{aligned} \tag{5.65}$$

where $C_2 \triangleq \int_0^\infty \int_0^{\frac{\varphi_e}{\varphi_b}\hat{g}_e} f_{\hat{g}_b}\left(\hat{g}_b\right) f_{\hat{g}_e}\left(\hat{g}_e\right) d\hat{g}_b d\hat{g}_e$. $\Xi\big(\mu\left(\hat{g}_b, \hat{g}_e\right), \hat{g}_b, \hat{g}_e\big)$ and $\Theta\big(\mu\left(\hat{g}_b, \hat{g}_e\right), \hat{g}_b, \hat{g}_e\big)$ are defined as follows,

$$\begin{aligned} \Theta\big(\mu\left(\hat{g}_b, \hat{g}_e\right), \hat{g}_b, \hat{g}_e\big) = \int_0^\infty \int_{\frac{\varphi_e}{\varphi_b}\hat{g}_e}^\infty & \underbrace{\underbrace{\left(\frac{1 + \frac{\mu(\hat{g}_b,\hat{g}_e)\hat{g}_b}{\mu(\hat{g}_b,\hat{g}_e)\sigma_e^2 + 1/\varphi_b}}{1 + \frac{\mu(\hat{g}_b,\hat{g}_e)\hat{g}_e}{\mu(\hat{g}_b,\hat{g}_e)\sigma_e^2 + 1/\varphi_e}}\right)^{-\beta}}_{\Xi_1\left(\mu(\hat{g}_b,\hat{g}_e),\hat{g}_b,\hat{g}_e\right)} \underbrace{\frac{e^{\beta\left(\sqrt{\frac{V_b}{T_b B}} f_Q^{-1}(\varepsilon_c) + \sqrt{\frac{V_e}{T_b B}} f_Q^{-1}(\delta)\right)}}{\Xi_2\left(\mu(\hat{g}_b,\hat{g}_e),\hat{g}_b,\hat{g}_e\right)}}_{\Xi\left(\mu(\hat{g}_b,\hat{g}_e),\hat{g}_b,\hat{g}_e\right)}} \\ & \times f_{\hat{g}_b}\left(\hat{g}_b\right) f_{\hat{g}_e}\left(\hat{g}_e\right) d\hat{g}_b d\hat{g}_e \\ = \int_0^\infty \int_{\frac{\varphi_e}{\varphi_b}\hat{g}_e}^\infty & \Xi\big(\mu\left(\hat{g}_b, \hat{g}_e\right), \hat{g}_b, \hat{g}_e\big) f_{\hat{g}_b}\left(\hat{g}_b\right) f_{\hat{g}_e}\left(\hat{g}_e\right) d\hat{g}_b d\hat{g}_e, \end{aligned} \tag{5.66}$$

where $V_x = 1 - (1 + \gamma_x)^{-2}$. From (5.62), the SNRs at the intended user and the eavesdropper

with channel estimation errors are given by

$$\gamma_b = \frac{\mu\left(\hat{g}_b, \hat{g}_e\right)\hat{g}_b}{\mu\left(\hat{g}_b, \hat{g}_e\right)\sigma_e^2 + \frac{1}{\varphi_b}} \text{ and } \gamma_e = \frac{\mu\left(\hat{g}_b, \hat{g}_e\right)\hat{g}_e}{\mu\left(\hat{g}_b, \hat{g}_e\right)\sigma_e^2 + \frac{1}{\varphi_e}}, \tag{5.67}$$

respectively.

As we can see from (5.67), the power control policy affects both of the signal power and the noise power, which is different from the scenarios with the perfect CSI. This makes it more challenging to find the optimal solutions, and the closed-form solutions are not available even with the approximation $V_x \approx 1$. Moreover, with the perfect CSI, the problems are convex when $V_x \approx 1$ is applied. With the imperfect CSI, the problems are non-convex.

Similar to the problem formulation in Section 5.3.1, C_2 is a constant and $\mathrm{E_{SC}}$ decreases with $\Theta\big(\mu\left(\hat{g}_b, \hat{g}_e\right), \hat{g}_b, \hat{g}_e\big)$. Thus, maximizing $\mathrm{E_{SC}}$ is equivalent to minimize $\Theta\big(\mu\left(\hat{g}_b, \hat{g}_e\right), \hat{g}_b, \hat{g}_e\big)$. The optimal power control policy that maximizes the effective secrecy throughput can be obtained by solving the following problem,

$$\begin{aligned} \min_{\mu(\hat{g}_b, \hat{g}_e)} \ & \Theta\big(\mu\left(\hat{g}_b, \hat{g}_e\right), \hat{g}_b, \hat{g}_e\big) \\ \text{s.t.} \ & \mu\left(\hat{g}_b, \hat{g}_e\right) \geq 0 \text{ and (5.64)}. \end{aligned} \tag{5.68}$$

5.6.2.1 Closed-form Solution in Special Case

With channel estimation errors, one can hardly derive the closed-form solution of problem (5.68). As a benchmark, the AP can apply the closed-form solution in (5.29) by treating the estimated CSI as the actual CSI. In the special case, where $V_x \approx 1$, $x \in \{b, e\}$, and $\beta = 1$, the normalized power control policy can be obtained by substituting $\hat{g}_b$ and $\hat{g}_e$ into (5.29).

5.6.2.2 Unsupervised Learning for Power Control in General Case

With the primal-dual method, problem (5.68) can be converted into

$$\begin{aligned} \max_{\lambda_{if}} \min_{\mu(\hat{g}_b, \hat{g}_e)} \ & \mathcal{L}_{if} \triangleq \Theta\big(\mu\left(\hat{g}_b, \hat{g}_e\right), \hat{g}_b, \hat{g}_e\big) + \lambda_{if}\left(\mathbb{E}\left[\mu\left(\hat{g}_b, \hat{g}_e\right)\right] - 1\right) \\ \text{s.t.} \ & (5.66),\ \mu\left(\hat{g}_b, \hat{g}_e\right) \geq 0, \text{ and } \lambda_{if} \geq 0, \end{aligned} \tag{5.69}$$

where $\mathcal{L}_{if}$ is the Lagrangian function of (5.68) and λ_{if} is the Lagrangian multiplier. By approximating $\mu\left(\hat{g}_b, \hat{g}_e\right)$ with a DNN, i.e., $\hat{\mu}\left(\hat{g}_b, \hat{g}_e; \omega_{if}\right)$, the functional optimization problem in

(5.69) can be re-expressed as a variable optimization problem,

$$\max_{\lambda_{if}} \min_{\omega_{if}} \hat{\mathcal{L}}_{if} \triangleq \Theta\big(\hat{\mu}\left(\hat{g}_b, \hat{g}_e; \omega_{if}\right), \hat{g}_b, \hat{g}_e\big) + \lambda_{if}\left(\mathbb{E}\left[\hat{\mu}\left(\hat{g}_b, \hat{g}_e; \omega_{if}\right)\right] - 1\right) \tag{5.70}$$
$$\text{s.t.} \quad (5.66),\ \hat{\mu}\left(\hat{g}_b, \hat{g}_e; \omega_{if}\right) \geq 0, \text{ and } \lambda_{if} \geq 0,$$

where the parameters of the DNN ω_{if} and the Lagrangian multiplier λ_{if} are updated iteratively. In the tth iteration, N training samples are used to estimate the Lagrangian function,

$$\hat{\mathcal{L}}_{if}^{(t)} \triangleq \frac{1}{N}\sum_{n=1}^{N}\left[\Xi\left(\hat{\mu}\left(\hat{g}_b^{(t,n)}, \hat{g}_e^{(t,n)}; \omega_{if}^{(t)}\right), \hat{g}_b^{(t,n)}, \hat{g}_e^{(t,n)}\right) + \lambda_{if}^{(t)}\left(\hat{\mu}\left(\hat{g}_b^{(t,n)}, \hat{g}_e^{(t,n)}; \omega_{if}^{(t)}\right) - 1\right)\right]. \tag{5.71}$$

Then, the Lagrangian multiplier $\lambda_{if}^{(t+1)}$ and the parameters of DNN $\omega_{if}^{(t+1)}$ can be updated iteratively according to

$$\lambda_{if}^{(t+1)} = \left[\lambda_{if}^{(t)} + \phi^{(t)}\frac{\partial \hat{\mathcal{L}}_{if}^{(t)}}{\partial \lambda_{if}^{(t)}}\right]^{+} = \left[\lambda_{if}^{(t)} + \phi^{(t)}\left(\frac{1}{N}\sum_{n=1}^{N}\hat{\mu}\left(\hat{g}_b^{(t,n)}, \hat{g}_e^{(t,n)}; \omega_{if}^{(t)}\right) - 1\right)\right]^{+}; \tag{5.72}$$

$$\begin{aligned}\omega_{if}^{(t+1)} &= \omega_{if}^{(t)} - \phi^{(t)}\nabla_{\omega_{if}}\hat{\mathcal{L}}_{if}^{(t)} \\ &= \omega_{if}^{(t)} - \phi^{(t)}\frac{1}{N}\sum_{n=1}^{N}\left[\nabla_{\omega_{if}}\hat{\mu}\left(\hat{g}_b^{(t,n)}, \hat{g}_e^{(t,n)}; \omega_{if}^{(t)}\right)\frac{\partial \hat{\mathcal{L}}_{if}^{(t,n)}}{\partial \hat{\mu}\left(\hat{g}_b^{(t,n)}, \hat{g}_e^{(t,n)}; \omega_{if}^{(t)}\right)}\right],\end{aligned} \tag{5.73}$$

where $\nabla_{\omega_{if}}\hat{\mu}\left(\hat{g}_b^{(t,n)}, \hat{g}_e^{(t,n)}; \omega_{if}^{(t)}\right)$ can be computed via backward propagation and

$$\frac{\partial \hat{\mathcal{L}}_{ip}^{(t,n)}}{\partial \hat{\mu}\left(\hat{g}_b^{(t,n)}, \hat{g}_e^{(t,n)}; \omega_{if}^{(t)}\right)} = \lambda_{if}^{(t+1)} + \frac{\partial \Xi\left(\hat{\mu}\left(\hat{g}_b^{(t,n)}, \hat{g}_e^{(t,n)}; \omega_{if}^{(t)}\right), \hat{g}_b^{(t,n)}, \hat{g}_e^{(t,n)}\right)}{\partial \hat{\mu}\left(\hat{g}_b^{(t,n)}, \hat{g}_e^{(t,n)}; \omega_{if}^{(t)}\right)}. \tag{5.74}$$

The second term in (5.74) can be obtained by substituting the values of $\hat{\mu}\left(\hat{g}_b^{(t,n)}, \hat{g}_e^{(t,n)}; \omega_{if}^{(t)}\right)$, $\hat{g}_b^{(t,n)}$ and $\hat{g}_e^{(t,n)}$ into the following expression,

$$\begin{aligned}\frac{\partial \Xi\left(\mu\left(\hat{g}_b, \hat{g}_e\right), \hat{g}_b, \hat{g}_e\right)}{\partial \mu\left(\hat{g}_b, \hat{g}_e\right)} &= \frac{\partial \Xi_1\left(\mu\left(\hat{g}_b, \hat{g}_e\right), \hat{g}_b, \hat{g}_e\right)}{\partial \mu\left(\hat{g}_b, \hat{g}_e\right)}\Xi_2\big(\mu\left(\hat{g}_b, \hat{g}_e\right), \hat{g}_b, \hat{g}_e\big) \\ &\quad + \frac{\partial \Xi_2\left(\mu\left(\hat{g}_b, \hat{g}_e\right), \hat{g}_b, \hat{g}_e\right)}{\partial \mu\left(\hat{g}_b, \hat{g}_e\right)}\Xi_1\big(\mu\left(\hat{g}_b, \hat{g}_e\right), \hat{g}_b, \hat{g}_e\big).\end{aligned} \tag{5.75}$$

According to the definitions of $\Xi_1\big(\mu\left(\hat{g}_b, \hat{g}_e\right), \hat{g}_b, \hat{g}_e\big)$ and $\Xi_2\big(\mu\left(\hat{g}_b, \hat{g}_e\right), \hat{g}_b, \hat{g}_e\big)$ in (5.66), the partial derivatives of $\Xi_1\left(\mu\left(\hat{g}_b, \hat{g}_e\right), \hat{g}_b, \hat{g}_e\right)$ and $\Xi_2\left(\mu\left(\hat{g}_b, \hat{g}_e\right), \hat{g}_b, \hat{g}_e\right)$ w.r.t $\mu\left(\hat{g}_b, \hat{g}_e\right)$ can be derived as (5.76) and (5.77), respectively.

$$\frac{\partial \Xi_1\left(\mu\left(\hat{g}_b,\hat{g}_e\right),\hat{g}_b,\hat{g}_e\right)}{\partial \mu\left(\hat{g}_b,\hat{g}_e\right)} = -\left(\frac{\frac{\hat{g}_b/\varphi_b}{\left(\mu(\hat{g}_b,\hat{g}_e)\sigma_e^2+1/\varphi_b\right)^2}}{1+\frac{\mu(\hat{g}_b,\hat{g}_e)\hat{g}_e}{\mu(\hat{g}_b,\hat{g}_e)\sigma_e^2+1/\varphi_e}} - \frac{\left(1+\frac{\mu(\hat{g}_b,\hat{g}_e)\hat{g}_b}{\mu(\hat{g}_b,\hat{g}_e)\sigma_e^2+1/\varphi_b}\right)\left(\frac{\hat{g}_e/\varphi_e}{\left(\mu(\hat{g}_b,\hat{g}_e)\sigma_e^2+1/\varphi_e\right)^2}\right)}{\left(1+\frac{\mu(\hat{g}_b,\hat{g}_e)\hat{g}_e}{\mu(\hat{g}_b,\hat{g}_e)\sigma_e^2+1/\varphi_e}\right)^2}\right) \times \beta\left(\frac{1+\frac{\mu(\hat{g}_b,\hat{g}_e)\hat{g}_b}{\mu(\hat{g}_b,\hat{g}_e)\sigma_e^2+1/\varphi_b}}{1+\frac{\mu(\hat{g}_b,\hat{g}_e)\hat{g}_e}{\mu(\hat{g}_b,\hat{g}_e)\sigma_e^2+1/\varphi_e}}\right)^{-\beta-1}. \tag{5.76}$$

$$\frac{\partial \Xi_2\left(\mu\left(\hat{g}_b,\hat{g}_e\right),\hat{g}_b,\hat{g}_e\right)}{\partial \mu\left(\hat{g}_b,\hat{g}_e\right)} = \left(\frac{\frac{\beta f_Q^{-1}(\varepsilon_c)}{\sqrt{T_bB}}\frac{\hat{g}_b/\varphi_b}{\left(\mu(\hat{g}_b,\hat{g}_e)\sigma_e^2+1/\varphi_b\right)^2}}{\sqrt{V_b}\left(1+\frac{\mu(\hat{g}_b,\hat{g}_e)\hat{g}_b}{\mu(\hat{g}_b,\hat{g}_e)\sigma_e^2+1/\varphi_b}\right)^3} + \frac{\frac{\beta f_Q^{-1}(\delta)}{\sqrt{T_bB}}\frac{\hat{g}_e/\varphi_e}{\left(\mu(\hat{g}_b,\hat{g}_e)\sigma_e^2+1/\varphi_e\right)^2}}{\sqrt{V_e}\left(1+\frac{\mu(\hat{g}_b,\hat{g}_e)\hat{g}_e}{\mu(\hat{g}_b,\hat{g}_e)\sigma_e^2+1/\varphi_e}\right)^3}\right) \times e^{\frac{\beta}{\sqrt{T_bB}}\left(\sqrt{V_b}f_Q^{-1}(\varepsilon_c)+\sqrt{V_e}f_Q^{-1}(\delta)\right)}. \tag{5.77}$$

5.6.3 Partial CSI Scenario

In this scenario, the transmit power is adjusted according to the estimated CSI of the intended user. The constraint on the normalized power control policy, $\mu(\hat{g}_b)$, is given by

$$\mathbb{E}\left[\mu(\hat{g}_b)\right] = \int_0^\infty \mu(\hat{g}_b) f_{\hat{g}_b}(\hat{g}_b) d\hat{g}_b \le 1. \tag{5.78}$$

The effective secrecy throughput can be rewritten as

$$\begin{aligned} \mathrm{E_{SC}} &= -\frac{1}{\theta T_c B}\ln\Big(C_3 + \int_0^\infty \int_0^{\frac{\varphi_b}{\varphi_e}\hat{g}_b} \Pi\big(\mu\left(\hat{g}_b\right),\hat{g}_b\big) f_{\hat{g}_b}\left(\hat{g}_b\right) f_{\hat{g}_e}\left(\hat{g}_e\right) d\hat{g}_e d\hat{g}_b\Big) \\ &= -\frac{1}{\theta T_c B}\ln\Big(C_3 + \Lambda\big(\mu\left(\hat{g}_b\right),\hat{g}_b\big)\Big), \end{aligned} \tag{5.79}$$

where $C_3 \triangleq \int_0^\infty \int_{\frac{\varphi_b}{\varphi_e}\hat{g}_b}^\infty f_{\hat{g}_b}\left(\hat{g}_b\right) f_{\hat{g}_e}\left(\hat{g}_e\right) d\hat{g}_e d\hat{g}_b$. $\Pi\big(\mu\left(\hat{g}_b\right),\hat{g}_b\big)$ and $\Lambda\big(\mu\left(\hat{g}_b\right),\hat{g}_b\big)$ are defined as follows,

$$\begin{aligned} \Lambda\big(\mu\left(\hat{g}_b\right),\hat{g}_b\big) &= \int_0^\infty \int_0^{\frac{\varphi_b}{\varphi_e}\hat{g}_b} \underbrace{\underbrace{\left(\frac{1+\mu\left(\hat{g}_b\right)\varphi_b\hat{g}_b}{1+\mu\left(\hat{g}_b\right)\varphi_e\hat{g}_e}\right)^{-\beta}}_{\Pi_1\left(\mu(\hat{g}_b),\hat{g}_b\right)} \underbrace{e^{\beta\frac{\left(\sqrt{V_b}f_Q^{-1}(\varepsilon_c)+\sqrt{V_e}f_Q^{-1}(\delta)\right)}{\sqrt{T_bB}}}}_{\Pi_2\left(\mu(\hat{g}_b),\hat{g}_b\right)} f_{\hat{g}_b}\left(\hat{g}_b\right) f_{\hat{g}_e}\left(\hat{g}_e\right) d\hat{g}_e d\hat{g}_b}_{\Pi\left(\mu(\hat{g}_b),\hat{g}_b\right)} \\ &= \int_0^\infty \int_0^{\frac{\varphi_b}{\varphi_e}\hat{g}_b} \Pi\big(\mu\left(\hat{g}_b\right),\hat{g}_b\big) f_{\hat{g}_b}\left(\hat{g}_b\right) f_{\hat{g}_e}\left(\hat{g}_e\right) d\hat{g}_e d\hat{g}_b, \end{aligned} \tag{5.80}$$

where $V_x = 1-(1+\gamma_x)^{-2}$, $x \in \{b,e\}$. From (5.62), the SNRs at the intended user and the

eavesdropper can be derived as

$$\gamma_b = \frac{\mu\left(\hat{g}_b\right)\hat{g}_b}{\mu\left(\hat{g}_b\right)\sigma_e^2 + \frac{1}{\varphi_b}} \text{ and } \gamma_e = \frac{\mu\left(\hat{g}_b\right)\hat{g}_e}{\mu\left(\hat{g}_b\right)\sigma_e^2 + \frac{1}{\varphi_e}}. \tag{5.81}$$

Similar to the problem formulation in Section 5.3.2, C_3 is a constant and $\mathrm{E_{SC}}$ decreases with $\Lambda\big(\mu\left(\hat{g}_b\right), \hat{g}_b\big)$. Thus, maximizing $\mathrm{E_{SC}}$ is equivalent to minimizing $\Lambda\big(\mu\left(\hat{g}_b\right), \hat{g}_b\big)$. Then, the optimal power control policy can be obtained by solving the following problem,

$$\begin{aligned} &\min_{\mu(\hat{g}_b)} \ \Lambda\big(\mu\left(\hat{g}_b\right), \hat{g}_b\big) \\ &\text{s.t.} \quad \mu\left(\hat{g}_b\right) \geq 0 \text{ and (5.78).} \end{aligned} \tag{5.82}$$

5.6.3.1 Closed-form Solution in Special Case

Similar to the full CSI scenario, we can obtain a benchmark by treating the estimated CSI as the actual CSI. In the special case, where $V_x \approx 1$, $x \in \{b, e\}$, and $\beta = 1$, the normalized power control policy can be obtained by substituting $\hat{g}_b$ into (5.38).

5.6.3.2 Unsupervised Learning for Power Control in General Case

With the primal-dual method, problem (5.82) can be converted into

$$\begin{aligned} &\max_{\lambda_{ip}} \min_{\mu(\hat{g}_b)} \ \mathcal{L}_{ip} \triangleq \Pi\big(\mu\left(\hat{g}_b\right), \hat{g}_b\big) + \lambda_{ip}\left(\mathbb{E}\left[\mu\left(\hat{g}_b\right)\right] - 1\right) \\ &\text{s.t.} \quad (5.80),\ \mu\left(\hat{g}_b\right) \geq 0, \text{ and } \lambda_{ip} \geq 0, \end{aligned} \tag{5.83}$$

where $\mathcal{L}_{ip}$ is the Lagrangian function of (5.82) and λ_{ip} is the Lagrangian multiplier. By approximating $\mu\left(\hat{g}_b\right)$ with a DNN, i.e., $\hat{\mu}\left(\hat{g}_b; \omega_{ip}\right)$, the functional optimization problem in (5.83) can be re-expressed as a variable optimization problem,

$$\begin{aligned} &\max_{\lambda_{ip}} \min_{\omega_{ip}} \ \hat{\mathcal{L}}_{ip} \triangleq \Pi\big(\mu\left(\hat{g}_b; \omega_{ip}\right), \hat{g}_b\big) + \lambda_{ip}\left(\mathbb{E}\left[\mu\left(\hat{g}_b; \omega_{ip}\right)\right] - 1\right) \\ &\text{s.t.} \quad (5.80),\ \mu\left(\hat{g}_b; \omega_{ip}\right) \geq 0, \text{ and } \lambda_{ip} \geq 0, \end{aligned} \tag{5.84}$$

where the parameters of the DNN ω_{ip} and the Lagrangian multiplier λ_{ip} are updated iteratively. In the tth iteration, N training samples are used to estimated the Lagrangian function,

$$\hat{\mathcal{L}}_{ip}^{(t)} \triangleq \frac{1}{N}\sum_{n=1}^{N}\left[\int_0^{\frac{\varphi_b}{\varphi_e}\hat{g}_b} \Pi\left(\hat{\mu}\left(\hat{g}_b^{(t,n)}; \omega_{ip}^{(t)}\right), \hat{g}_b^{(t,n)}\right) f_{\hat{g}_e}\left(\hat{g}_e\right) d\hat{g}_e + \lambda_{ip}^{(t)}\left(\hat{\mu}\left(\hat{g}_b^{(t,n)}; \omega_{ip}^{(t)}\right) - 1\right)\right]. \tag{5.85}$$

Then, the Lagrangian multiplier $\lambda_{ip}^{(t+1)}$ and the parameters of DNN $\omega_{ip}^{(t+1)}$ can be updated iteratively according to

$$\lambda_{ip}^{(t+1)} = \left[\lambda_{ip}^{(t)} + \phi^{(t)} \frac{\partial \hat{\mathcal{L}}_{ip}^{(t)}}{\partial \lambda_{ip}^{(t)}}\right]^{+} = \left[\lambda_{ip}^{(t)} + \phi^{(t)} \left(\frac{1}{N}\sum_{n=1}^{N} \hat{\mu}\left(\hat{g}_b^{(t,n)}; \omega_{ip}^{(t)}\right) - 1\right)\right]^{+}; \tag{5.86}$$

$$\omega_{ip}^{(t+1)} = \omega_{ip}^{(t)} - \phi^{(t)} \nabla_{\omega_{ip}} \hat{\mathcal{L}}_{ip}^{(t)} = \omega_{ip}^{(t)} - \phi^{(t)} \frac{1}{N}\sum_{n=1}^{N} \left[\nabla_{\omega_{ip}} \hat{\mu}\left(\hat{g}_b^{(t,n)}; \omega_{ip}^{(t)}\right) \frac{\partial \hat{\mathcal{L}}_{ip}^{(t,n)}}{\partial \hat{\mu}\left(\hat{g}_b^{(t,n)}; \omega_{ip}^{(t)}\right)}\right], \tag{5.87}$$

where $\nabla_{\omega_{ip}} \hat{\mu}\left(\hat{g}_b^{(t,n)}; \omega_{ip}^{(t)}\right)$ can be computed via backward propagation and

$$\frac{\partial \hat{\mathcal{L}}_{ip}^{(t,n)}}{\partial \hat{\mu}\left(\hat{g}_b^{(t,n)}; \omega_{ip}^{(t)}\right)} = \int_0^{\frac{\varphi_b}{\varphi_e}\hat{g}_b} \frac{\partial \Pi\left(\hat{\mu}\left(\hat{g}_b^{(t,n)}; \omega_{ip}^{(t)}\right), \hat{g}_b^{(t,n)}\right)}{\partial \hat{\mu}\left(\hat{g}_b^{(t,n)}; \omega_{ip}^{(t)}\right)} f_{\hat{g}_e}(\hat{g}_e)\, d\hat{g}_e + \lambda_{ip}^{(t+1)}. \tag{5.88}$$

Similar to (5.55), the first term in (5.88) can be obtained by following two steps. First, substitute the values of $\hat{\mu}\left(\hat{g}_b^{(t,n)}; \omega_{ip}^{(t)}\right)$ and $\hat{g}_b^{(t,n)}$ into (5.75). Second, evaluating the integral term by generating multiple realizations of g_e according to its distribution.

It is worth mentioning that our unsupervised learning method does not require the information of channel distribution, but only needs some samples of the channel realizations to perform the SGD algorithm, where a batch of CSI estimated from the receiver is used. Moreover, in order to ensure the pre-train DNN working well in practical systems, transfer learning can be applied into the fine-tune pre-trained DNN, based on the estimated CSI in practical systems. As such, the initial performance of the pre-trained DNN is better than the one initialized with random parameters, in terms of the initial achievable rate and the convergence time [40, 75, 107, 108].

5.7 Numerical Results

In this section, we provide numerical results to reveal some useful insights and demonstrate the effectiveness of the unsupervised learning method (with legend "DNN"). In the special case when $\beta = 1$ and $V_x = 1$, we compare the proposed learning-based power control policy with the closed-form optimal power control policy (with legend "Closed Form"). In other general cases, we compare the learning-based power control policy with two baselines in the existing literature. The first one is the "water-filling" policy that maximizes the Shannon's capacity of the intended user [38] (with legend "Basedline 1"). The second one is the constant transmit power policy, $\mu = P/\overline{P} = 1$ (with legend "Basedline 2"). It is worth mentioning that the water-filling policy obtained in our work is different from the water-filling policy [38] and

the low-complexity on/off power allocation policy [109]. The low-complexity on/off power allocation policy in [109] can achieve the near-optimal performance as the average SNR goes to infinity with the main channel CSI only. However, it does not guarantee the statistical QoS constraint in the finite blocklength regime, and hence is not a reasonable baseline.

Table 5.1: Simulation Parameters and Hyper-Parameters

Duration of each frame, T_c	1 ms
Duration of each block (slot), T_b	0.125 ms
Path loss model, $10\log_{10}(\alpha)$	$35.3 + 37.6\log_{10}(d)$
Single-sided noise spectral density, N_0	-173 dBm/Hz
Learning rate, $\phi^{(t)}$	0.001
Number of hidden layers	4
Number of neurons in 1st, 2nd, 3rd, and 4th hidden layer	10/10/4/2
Batch size for each iteration, N	100
Activation function	ReLU

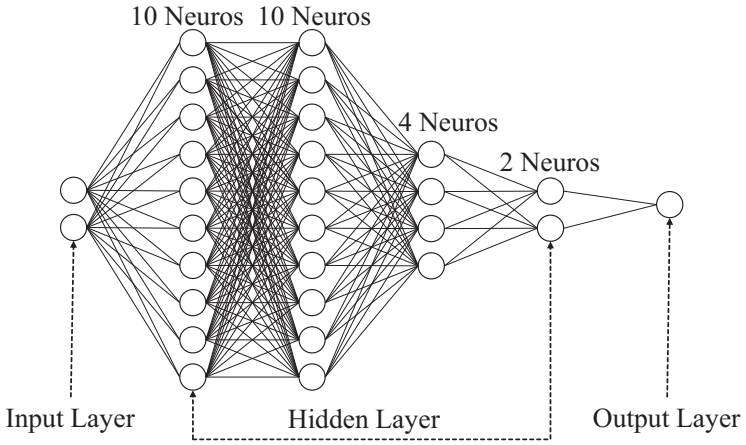

Figure 5.2: Illustration of our DNN model with one input layer, four hidden layers, and one output layer.

5.7.1 System Parameters

Specifically, we build a DNN model in Fig. 5.2, which consists of one input layer, four hidden layers, and one output layer. The input and output of the DNN are the small-scale channel gains (based on the assumptions of available CSI in different scenarios) and the corresponding normalized transmit power, respectively. The initial weights of the DNN are Gaussian random variables with zero mean and unit variance, and the initial bias are fixed at 0.1. The initial value of the Lagrangian multiplier is set as 0. In each iteration, we generate 100 channel realizations to update the Lagrangian multiplier and the parameters of the DNN according to the primal-

dual method. The final power control policy is obtained after 10^4 iterations, where the Adam optimizer is used to minimize the loss function. To show the performance of our method in low and high SNR regimes, we adjust the distance between the AP and the intended user, denoted by d. Other simulation parameters and hyper-parameters of the DNN are summarized in Table 5.1.

5.7.2 Performance Evaluation

In Fig. 5.3, we illustrate the convergence behaviors of the unsupervised learning method by comparing it with the closed-form optimal power control policy. We take the full CSI scenario as an example, and provide the normalized effective secrecy throughput, $\mathrm{E_{SC}}$, and the right-hand side of the average power constraint, $\mathbb{E}\left[\mu\left(g_b, g_e\right)\right] - 1 \leq 0$, against the iteration number in Fig. 5.3(a) and Fig. 5.3(b), respectively. The expectations in normalized effective secrecy throughput and transmit power constraints are taken over 100 successive iterations. The results in Fig. 5.3 show that the unsupervised learning method converges after 2000 iterations, i.e., the normalized effective secrecy throughput approaches the optimal values obtained from the closed-form method and the right-hand side of the average power constraint approaches zero. The results indicate that the learning-based method converges rapidly and can satisfy the constraint. From the path loss model in Table 5.1, we can obtain that $\varphi_b = \varphi_e \approx 6.16$ dB when $d = 300$ m and $\varphi_b = \varphi_e \approx 12.78$ dB when $d = 200$ m. As can be seen from the figure, when $d = 200$ m, the average SNR is larger than 10 dB, and the normalized effective secrecy throughput via the learning-based method in the general case converges to the one in the special case as the iteration number increases. These results confirm that the approximation of $V_x \approx 1$ is accurate in the high SNR regime. However, when $d = 300$ m, the average SNR is smaller than 10 dB. As such, the channel dispersion is smaller than 1. By substituting $V_x < 1$ into (5.2), we obtain a larger value of the achievable secrecy rate when comparing the case of $V_x < 1$ to the case of $V_x \approx 1$. It will eventually lead to the normalized effective secrecy throughput achieved by the learning-based method in the general case being larger than that in the special case. Therefore, the observation from the figure is not surprising. It confirms that, when $d = 300$, the normalized effective secrecy throughput via the learning-based method in the general case is larger than the one in the special case.

In Fig. 5.4, we show the performance comparison of the unsupervised learning method in the full CSI scenario against two different power control policies with different values of d. It is clear that the learning-based power control policy outperforms the two baselines, and the performance gain in the low SNR regime is larger than that in the high SNR regime (i.e., 30 % gain when $d = 300$ m versus 10 % gain when $d = 200$ m).

In Fig. 5.5, we show the normalized effective secrecy throughput in the special cases with or without the instantaneous CSI of the eavesdropper. Specifically, the normalized optimal

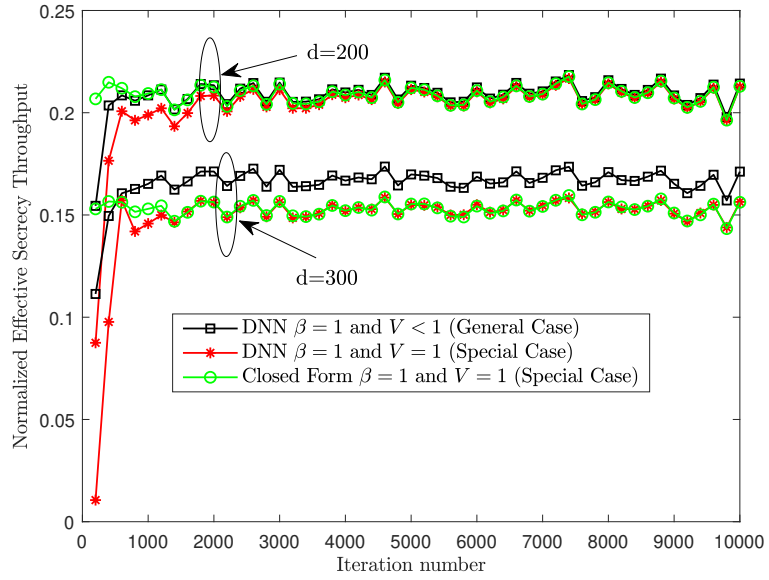

(a)

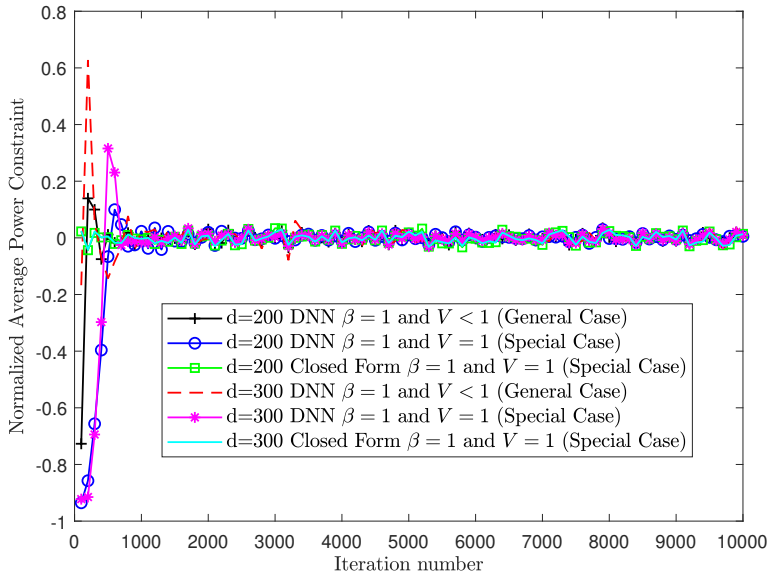

(b)

Figure 5.3: Convergence of the proposed unsupervised learning method in full CSI scenario in terms of (a) the normalized effective secrecy throughput and (b) the normalized average power constraint versus the iteration number for different value of d, where $\bar{P} = 20$ dBm, $\varphi_b = \varphi_e$, $\theta = 10^{-3}$, $\beta = 1$, $\varepsilon_c = 10^{-5}$, and $\delta = 10^{-2}$.

power control policies in the special case for both of the full and partial CSI scenarios are obtained from (5.29) and (5.38), respectively. It can be seen from the figure that knowing the instantaneous CSI of the eavesdropper's channel for power control does not provide significant performance improvement when the average SNR is larger than 25 dB.

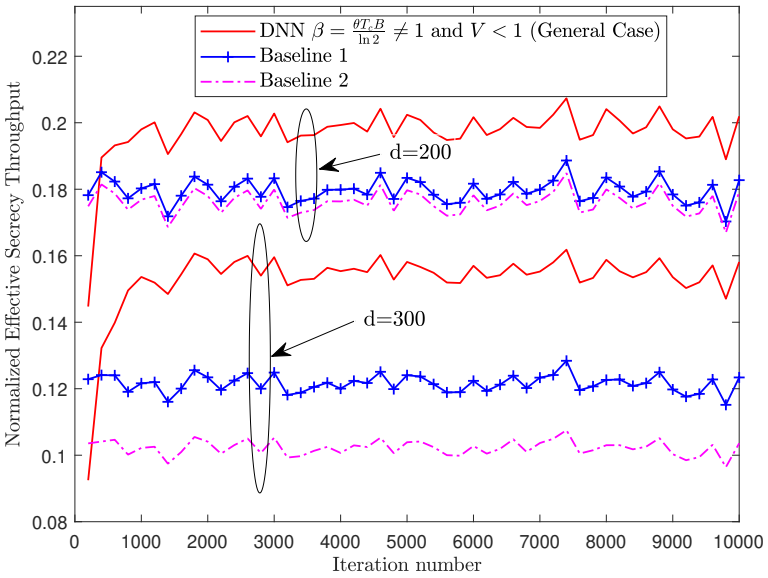

Figure 5.4: Performance comparison of unsupervised learning in full CSI scenario with different power control policies for different value of d, where $\bar{P} = 20$ dBm, $\varphi_b = \varphi_e$, $\theta = 10^{-3}$, $B = 1$ MHz, $\beta = \frac{\theta T_c B}{\ln 2} \neq 1$, $\varepsilon_c = 10^{-5}$, and $\delta = 10^{-2}$.

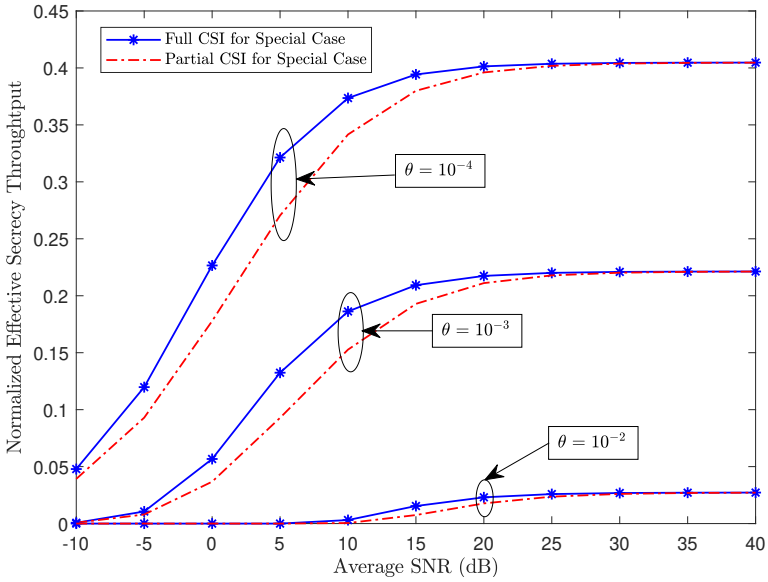

Figure 5.5: Normalized effective secrecy throughput versus the average SNR at the intended user with different QoS requirements, where $V_b = V_e = 1$, $\beta = 1$, $\varphi_b = \varphi_e$, $\varepsilon_c = 10^{-5}$, $\delta = 10^{-2}$, and $d = 300$ m.

In Fig. 5.6, we plot the normalized effective secrecy throughput, $\mathrm{E_{SC}}$, and the right-hand side of the normalized average power constraint, $\mathbb{E}\left[\mu\left(g_b, g_e\right)\right] - 1 \leq 0$, against the variance of channel estimation errors. The results are generated in the full CSI scenario via the unsupervised learning method and the closed-form power control policy. To illustrate the impact of

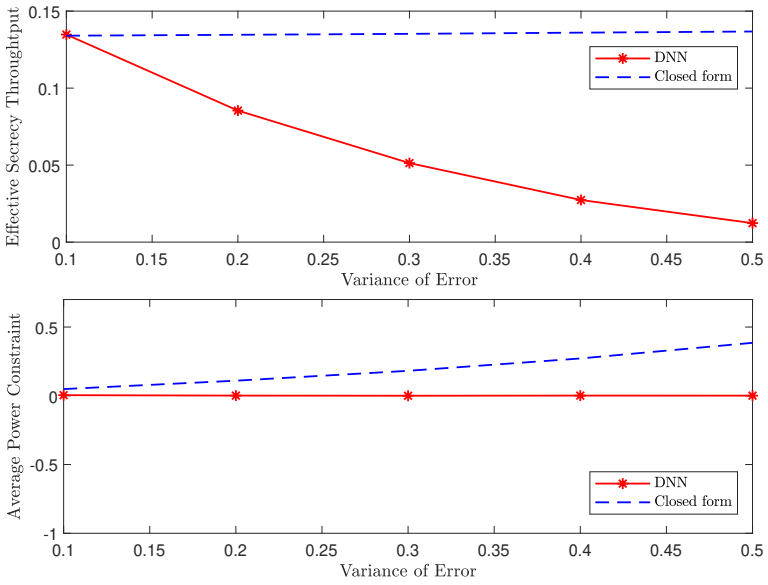

Figure 5.6: Normalized effective secrecy throughput and normalized average power constraint in full CSI scenario versus the variance of channel estimation errors, where $\bar{P} = 20$ dBm, $\theta = 10^{-3}$, $\beta = 1$, $\varphi_b = \varphi_e$, $\varepsilon_c = 10^{-5}$, $\delta = 10^{-2}$, and $d = 200$ m.

model mismatch on the average power constraint, we substitute $\hat{g}_b$ and $\hat{g}_e$ into the closed-form solution in (5.29) by assuming that the distributions of $\hat{g}_b$ and $\hat{g}_e$ are the same as that of g_b and g_e (e.g., Rayleigh fading is considered in this work). The results in Fig. 5.6 show that the effective secrecy throughput of the learning-based method degrades as the variance of estimation errors increases, but the average power constraint can be guaranteed. This is because that the learning-based method is trained by the estimated channels. The average power constraint can be satisfied as we estimate the average power consumption according to the batch of training samples, where the samples are obtained from the estimated CSI. However, the closed-form method assumes that the estimated CSI and the actual CSI follow the same distribution. Due to the model mismatch, the average power constraint cannot be satisfied.

5.8 Summary

In this chapter, we carried out a comprehensive study of secure short-packet transmissions with different assumptions on the CSI. We derived closed-form solutions of optimal power control policies in the special case and used the unsupervised deep learning algorithm to solve the optimization problem numerically in general cases. Our numerical results showed that the unsupervised deep learning algorithm converges to the closed-form solution after a small number of iterations in the special case. In general cases, the unsupervised deep learning algorithm also converges fast and outperforms two existing power control policies. The results

also indicated that knowing the instantaneous CSI of the eavesdropper only provides marginal performance gains in terms of the effective secrecy throughput. Moreover, we found that the learning-based policy can guarantee the average transmit power constraint with channel estimation errors. Due to the mismatch between the channel model and the estimated channel, the closed-form policy for the special case cannot guarantee the constraint. Given that the effective secrecy throughput decreases rapidly with the variance of channel estimation errors, how to design power control policies that are robust to the channel estimation errors deserves further study. Furthermore, when the number of samples is limited and insufficient, generative adversarial networks (GANs) may be used to generate some synthetic samples. [110, 111, 112, 113] showed that a synthetic dataset with a large number of training samples can be obtained from a GAN model trained with limited real-world data samples. In addition, how to train GANs and whether the GAN-aided power control policy can guarantee the statistical QoS requirements or not need to be comprehensively investigated in future studies.

Chapter 6

Conclusions

In this chapter, we first summarize the general conclusions drawn from the thesis, and then outline some future research directions arising from this thesis.

6.1 Thesis Conclusions

This thesis focused on the transmission strategies and power control policies design of SPC to exploit the benefits of SPC for supporting URLLC applications. In particular, we focused on the channel training strategies of SPC in Chapter 2, the optimal resource allocation of SPC in Chapter 3, the reduction of communication latency and signalling overhead in Chapter 4, and the physical layer security of SPC in Chapter 5. The detailed contributions and directly related future works are given as follows.

Channel training strategies in SPC: In Chapter 2, the performance of dowlink and uplink channel training strategies in SPC was studied. We derived closed-form expressions for the lower bounds on the data rates achieved by these two strategies, in which the impact of finite blocklength was considered. Aided by these expressions, we analytically determined an expression to approximate the minimum channel reciprocity coefficient which enables the uplink channel training, instead of downlink channel training, to achieve a higher data rate for the downlink transmission in the MISO system. Our examination demonstrated that this minimum channel reciprocity coefficient decreases as the blocklength decreases or the number of transmit antennas increases, revealing the benefits of the uplink channel training in SPC with multiple transmit antennas.

The presented work serves as the first step to explore the fundamental benefits of the uplink channel training in SPC with multiple transmit antennas, which shows the potential to improve the reliability performance of SPC and support future URLLC applications. For future work, it is interesting to investigate the signalling overhead of two different channel training strategies in SPC when the multi-user scenarios with single and multiple receiver antennas are considered.

Optimal resource allocation for SPC: In Chapter 3, we studied the optimal transmission

strategy of SPC for the downlink transmission in the MISO system. We investigated the optimal resource allocation (e.g., the total transmit power and a finite number of symbol periods) for downlink training, uplink feedback, and data transmission to maximize the average data rate. Specifically, we proved that the optimal number of symbol periods allocated to downlink training is equal to the number of transmit antennas at the AP. We also derived an approximate closed-form lower bound on the average data rate, an easy-to-implement method to find the optimal number of symbol periods for uplink feedback, and a simple expression for the optimal power allocation between data transmission and downlink training. Through numerical results, we examined the impact of various system parameters, e.g., the number of antennas at the AP and the blocklength, on the optimal solutions.

The presented work serves as the first step to provide a guideline to assist URLLC designers with the fundamental problem of transmit power and symbol period allocation to guarantee the advantage of SPC in practice. For future work, the impact of feedback error needs to be investigated. The considered MISO system can be also extended to a MIMO system for improving the reliability. However, the signalling overhead is high when more receive antennas are used. Therefore, the system parameters (e.g., the number of receive and transmit antennas and the blocklength) in SPC need to be well designed to meet the URLLC requirement.

Channel inversion power control for one-way URLLC: In Chapter 4, we studied the feasibility and optimal design of using CIPC in SPC to reduce the channel estimation overhead for achieving one-way URLLC and establish the fundamental limit of one-way URLLC achieved by CIPC. With the aid of channel reciprocity in TDD systems, our proposed CIPC schemes guarantee the power of received signal that is used to decode the information to be a constant value Q, by varying the transmit signal and power, which relaxes the assumption of knowing CSI at the user. Thus, the CIPC schemes eliminate the overhead of CSI feedback, reduce communication latency, and explore the benefits of multiple antennas to significantly improve transmission reliability. Specifically, we first derived expressions for the packet loss probabilities of the truncated and traditional CIPC schemes with imperfect channel reciprocity. Using these expressions, we determined a closed interval for the optimal value of the received signal power Q, which significantly facilitates the optimal design of the CIPC schemes. Then, we analyzed the performance of the truncated CIPC scheme with perfect channel reciprocity, which provides an upper bound on the performance of truncated CIPC in practical scenarios. Based on this analysis, we proved that the optimal Q lies in a convex set in the case with perfect channel reciprocity. Our results showed that CIPC is an effective means to achieve one-way URLLC.

The presented work serves as the first step to determine the trade-off among reliability, latency, and required communication resources (e.g., transmit antennas and transmit power) for one-way URLLC with CIPC schemes. For future work, the multi-user scenario needs to be analyzed to implement the proposed scheme in URLLC applications, e.g., industrial factory.

Secure transmission rate of short packets: In Chapter 5, we conducted a comprehensive study of secure SPC via PLS techniques with different assumptions on CSI. We investigated how much CSI is needed to realize secure SPC under the average power constraint and the queueing delay requirement by comparing the secure transmission rates of short packets in different scenarios (i.e., with/without eavesdropper's instantaneous CSI). We also derived closed-form solutions of optimal power control policies in the special case and used the unsupervised deep learning algorithm to solve the optimization problem numerically in general cases. Our numerical results showed that: 1) The learning-based power control policy approaches the closed-form optimal policy in the special case and outperforms two existing power control policies in general cases, 2) Knowing the instantaneous CSI of the eavesdropper only provides a marginal gain of the secure data rate in the high signal-to-noise ratio regime, and 3) In the presence of channel estimation errors, the learning-based policy trained by the estimated channels can guarantee the average transmit power constraint, while the closed-form optimal policy cannot.

The presented work serves as the first step to explore the fundamental benefits of using PLS techniques with deep learning to achieve security in SPC, which shows the potentials and benefits of applying deep learning to support URLLC applications in the near future. For future work, it is meaningful to analyze the property of the learning-based algorithm, e.g., the stability and the convergence speed with proper initialization. Besides, how to design power control policies that are robust to the channel estimation errors deserves further study.

6.2 Future Research Directions

The optimal design of SPC plays a crucial role in supporting URLLC applications. While the state-of-the-art wireless communication systems cannot support SPC to satisfy the stringent requirements of latency and reliability in URLLC. Besides, due to the non-stationary property of wireless networks and non-convex constraints involved in SPC, the acquisition of optimal solutions to optimization problems normally results in large processing delays. It is noted that the processing delay caused by finding the optimal solutions to optimization problems in Chapter 2, Chapter 3, and Chapter 4 are assumed to be negligible. However, the corresponding signal processing time may dominate the overall end-to-end latency when conducting searching algorithms iteratively, which definitely violates the latency requirement of URLLC.

Fortunately, with the advancement of deep learning and their breakthroughs especially in computer vision for real-time image processing, researchers have started to investigate the use of deep learning in optimizing wireless networks [75, 84, 114, 115, 116, 117, 118]. The existing research contributions have shown that the deep learning algorithm is a promising method in solving complicated non-convex optimization problems in wireless networks. Therefore, by applying deep learning into optimization problems in wireless networks, the processing time

could be significantly reduced by applying well-trained deep neural networks. For example, the processing task could be completed within one TTI (1 ms) in 5G NR [57]. More specifically, a traditional method to find the optimal power control policy in SPC is to execute optimization algorithms [65], which is in general of high computational complexity and hence can hardly be implemented in real time. To avoid the time-consuming optimization algorithms, learning-based power control algorithms have been developed for wireless networks [56, 83, 119, 120]. Specifically, the transmitter can obtain the optimal power control policy from a well-trained DNN, after offline training. Here, the forward-propagation algorithm has great potential to compute the output of a DNN in a real-time manner, due to its lower computational complexity rather than iterative optimization algorithms.

Motivated by the aforementioned potentials of deep learning, it is promising to use it in SPC to achieve real-time radio resource management in one TTI in 5G NR to support URLLC applications. A fundamental tutorial of applying deep learning for URLLC was recently presented in [75], which illustrates how to jointly utilize the model-based and knowledge-based deep learning algorithms to support URLLC applications. However, the optimal design of SPC with deep learning to fully unlock diverse URLLC applications is still at the very early stage, which triggers many challenges that are needed to be addressed in future research. Some of future research problems on this topic are listed as follows:

- **Model mismatch:** In Chapter 5, we assume that the DNN trained in off-line could always match the real communication system when analyzing the secure transmission rate in SPC. However, wireless networks are in general non-stationary. As such, some practical QoS constraints might cannot be guaranteed, which refers to a issue of model mismatch. Therefore, an adaptive learning-based framework is needed for practical wireless networks to dynamically perform the fine-tuning. Only few early works [40, 57] proposed to use deep reinforcement learning with transfer learning to solve the issue. However, some ideal assumptions are made to model the problem using theoretical model-based knowledge, which eventually leads to conservative strategy in term of resource allocation for URLLC applications. Therefore, the impact of model mismatch in URLLC applications is unclear, which is worth being well studied and verified.

- **Scalability:** As mentioned in Chapter 5, there are some major issues when using deep learning to optimize wireless networks: 1) lack of labeled training samples, 2) no QoS guarantee. Apart from that, scalability is another challenging issue in URLLC with massive connections (e.g., factory automation and autonomous vehicles). With the increasing number of devices in 5G and beyond wireless networks, the increasing optimization variables and related constraints would significantly degrade the performance of deep learning-based algorithm. The main reason is that most of well-established optimization algorithms only work well for small and medium scale problems. Recently, GNN

is proposed to address the scalability issue for wireless networks [119, 121, 122] due to the property of GNNs that the number of parameters of a GNN does not increase with the dimension of the input. It will be very interesting to investigate how to utilize a GNN to address the scalability in URLLC applications while satisfying the stringent requirements on latency and reliability.

Appendix A

A.1 Proof of Theorem 2.1

In order to prove Theorem 2.1, we have to solve two integrals in the following:

$$\Phi\left(\gamma_{\text{eff}}^{\text{u}}, N_{\text{B}}\right) = \mathbb{E}_{\left\|\bar{\mathbf{h}}_{\text{u}}\right\|^2}\left[C\left(\gamma_{\text{eff}}^{\text{u}}\left\|\bar{\mathbf{h}}_{\text{u}}\right\|^2\right)\right] = \int_0^{\infty} \log_2(1+\gamma_{\text{eff}}^{\text{u}} x) f_X(x) dx \tag{A.1}$$

and

$$\begin{aligned}\Psi\left(\gamma_{\text{eff}}^{\text{u}}, N_{\text{B}}, T\right) &= \mathbb{E}_{\left\|\bar{\mathbf{h}}_{\text{u}}\right\|^2}\left[\sqrt{\frac{1}{T}} f_Q^{-1}(\varepsilon)\sqrt{V\left(\gamma_{\text{eff}}^{\text{u}}\left\|\bar{\mathbf{h}}_{\text{u}}\right\|^2\right)}\right] \\ &= \int_0^{\infty} \sqrt{\frac{1}{T}} f_Q^{-1}(\varepsilon)\sqrt{V\left(\gamma_{\text{eff}}^{\text{u}} x\right)} f_X(x) dx,\end{aligned} \tag{A.2}$$

where $f_X(x) = x^{N_{\text{B}}-1}e^{-x}/\Gamma(N_{\text{B}})$ is the PDF of $\|\bar{\mathbf{h}}_{\text{u}}\|^2$, since $\bar{\mathbf{h}}_{\text{u}} \sim \mathcal{CN}(0, \mathbf{I}_{N_{\text{B}}})$.

We first tackle the integral in (A.1). Substituting $f_X(x)$ into (A.1), setting $y = 1+\gamma_{\text{eff}}^{\text{u}} x$, and using the binomial expansion given in [96, Eq. (1.111)], we rewrite $\Phi\left(\gamma_{\text{eff}}^{\text{u}}, N_{\text{B}}\right)$ as

$$\begin{aligned}\Phi(\gamma_{\text{eff}}^{\text{u}}, N_{\text{B}}) &= \frac{e^{\frac{1}{\gamma_{\text{eff}}^{\text{u}}}}\left(\gamma_{\text{eff}}^{\text{u}}\right)^{-N_{\text{B}}}}{\Gamma(N_{\text{B}})\,\ln 2}\int_1^{\infty}(y-1)^{N_{\text{B}}-1}\ln(y)e^{-\frac{y}{\gamma_{\text{eff}}^{\text{u}}}}dy \\ &= \frac{e^{\frac{1}{\gamma_{\text{eff}}^{\text{u}}}}\left(\gamma_{\text{eff}}^{\text{u}}\right)^{-N_{\text{B}}}}{\Gamma(N_{\text{B}})\,\ln 2}\sum_{i=0}^{N_{\text{B}}-1}\binom{N_{\text{B}}-1}{i}(-1)^{N_{\text{B}}-1-i}\int_1^{\infty} y^i \ln(y)e^{-\frac{y}{\gamma_{\text{eff}}^{\text{u}}}}dy.\end{aligned} \tag{A.3}$$

Using the Meijer's G-Function [96, Eq. (9.301)], we obtain

$$\int_1^{\infty} y^i \ln(y)e^{-\frac{y}{\gamma_{\text{eff}}^{\text{u}}}}dy = \mathbf{G}_{2,3}^{3,0}\left(\begin{array}{c|c} -i,-i & \\ 0,-1-i,-1-i & \dfrac{1}{\gamma_{\text{eff}}^{\text{u}}}\end{array}\right). \tag{A.4}$$

Substituting (A.4) into (A.3) we obtain $\Phi\left(\gamma_{\text{eff}}, N_{\text{B}}\right)$ in (2.10). We now solve the integral in (A.2). Substituting $f_X(x)$ into (A.1) and setting $t = x/\left(N_{\text{B}}-1\right)$, $\Psi\left(\gamma_{\text{eff}}^{\text{u}}, N_{\text{B}}, T\right)$ in (A.2) can be

rewritten as

$$\begin{aligned}\Psi\left(\gamma_{\text{eff}}^{\text{u}},N_{\text{B}},T\right) &= \frac{f_Q^{-1}(\varepsilon)}{\Gamma(N_{\text{B}})}\sqrt{\frac{1}{T}}\int_0^{\infty}\sqrt{V\left(\gamma_{\text{eff}}^{\text{u}}\,x\right)}e^{(N_{\text{B}}-1)\left(\ln x-\frac{x}{N_{\text{B}}-1}\right)}dx \\ &= \frac{f_Q^{-1}(\varepsilon)}{\Gamma(N_{\text{B}})}\sqrt{\frac{1}{T}}(N_{\text{B}}-1)^{N_{\text{B}}}\int_0^{\infty}e^{(N_{\text{B}}-1)(\ln t-t)}\sqrt{V\left(\gamma_{\text{eff}}^{\text{u}}\,t\,(N_{\text{B}}-1)\right)}\,dt \\ &= \frac{f_Q^{-1}(\varepsilon)}{\Gamma(\eta+1)}\sqrt{\frac{1}{T}}\eta^{\eta+1}\int_0^{\infty}e^{\eta g(t)}\varphi(t)\,dt, \end{aligned} \tag{A.5}$$

where $g(t)=\ln t-t$, $\eta=N_{\text{B}}-1$, and $\varphi(t)=\sqrt{V\left(\gamma_{\text{eff}}^{\text{u}}t\eta\right)}$.

Then, it is noted that Laplace's method [123] is a technique used to approximate integrals of the form $\int_a^b e^{Mf(x)}dx$, where $f(x)$ is a twice-differentiable function, M is a large number, and the endpoints a and b could possibly be infinite. Therefore, we can approximate the integral in (A.5) via the Laplace method as

$$\int_0^{\infty}e^{\eta g(t)}\varphi(t)dt\approx e^{\eta g(t_0)}\varphi(t_0)\sqrt{\frac{2\pi}{\eta\left|g^{''}(t_0)\right|}}, \tag{A.6}$$

where $g^{''}(t)=-1/t^2$ and $t_0=1$, which is obtained by solving $g^{'}(t)=1/t-1=0$. Finally, substituting $t_0=1$ and (A.6) into (A.5), we obtain the desired result in (2.11) by performing some algebra manipulations, which completes the proof.

A.2 Proof of Proposition 2.1

According to its definition, ϕ^* can guarantee $R_{\text{u}}=R_{\text{d}}$. Following (2.9) and (2.15), we find that in order to guarantee $R_{\text{u}}=R_{\text{d}}$ we need

$$\Phi\left(\gamma_{\text{eff}}^{\text{u}},N_{\text{B}}\right)-\Psi\left(\gamma_{\text{eff}}^{\text{u}},N_{\text{B}},T\right)=\left(1-\frac{T_{\text{tr}}^*}{T}\right)\left[\Phi\left(\gamma_{\text{eff}}^{\text{d}},N_{\text{B}}\right)-\Psi\left(\gamma_{\text{eff}}^{\text{d}},N_{\text{B}},T\right)\right]. \tag{A.7}$$

We find that it is difficult to obtain an expression for ϕ^* from (A.7) directly. To tackle this, we find that the rate loss (i.e., $\Psi\left(\gamma_{\text{eff}}^{\text{u}},N_{\text{B}},T\right)$ or $\Psi\left(\gamma_{\text{eff}}^{\text{d}},N_{\text{B}},T\right)$) is negligible comparing to the channel capacity. Then, we approximate (A.7) as

$$\Phi\left(\gamma_{\text{eff}}^{\text{u}},N_{\text{B}}\right)=\left(1-\frac{T_{\text{tr}}^*}{T}\right)\Phi\left(\gamma_{\text{eff}}^{\text{d}},N_{\text{B}}\right). \tag{A.8}$$

Although a closed-form solution for ϕ^* is still mathematically intractable, we present an accurate approximation based on the Jensen's inequality. That is, when χ is a concave function, we

have $\mathbb{E}[\chi(x)] \leq \chi(\mathbb{E}[x])$. We then approximate (A.8) as

$$\log_2\left(1+\gamma_{\text{eff}}^{\text{u}}\mathbb{E}\left[\left\|\bar{\mathbf{h}}_{\text{u}}\right\|^2\right]\right)=\left(1-\frac{T_{\text{tr}}^*}{T}\right)\log\left(1+\gamma_{\text{eff}}^{\text{d}}\mathbb{E}\left[\left\|\bar{\mathbf{h}}_{\text{d}}\right\|^2\right]\right),$$

which leads to

$$\log_2\left(1+\gamma_{\text{eff}}^{\text{u}}N_{\text{B}}\right)\overset{(a)}{=}\left(1-\frac{T_{\text{tr}}^*}{T}\right)\log_2\left(1+\gamma_{\text{eff}}^{\text{d}}N_{\text{B}}\right), \tag{A.9}$$

where (a) holds since $\mathbb{E}\left[\left\|\bar{\mathbf{h}}_{\text{u}}\right\|^2\right]=\mathbb{E}\left[\left\|\bar{\mathbf{h}}_{\text{d}}\right\|^2\right]=N_{\text{B}}$.

After performing some algebraic manipulations, we reach the desired result given in (2.16) following (A.9), which completes the proof.

Appendix B

B.1 Proof of Theorem 3.1

With the aid of the Jensen's inequality and the approximation of quantization errors given in [124], the average data rate in (3.4) can be approximated as

$$R \approx \tau \mathbb{E}_{\hbar}\left[C\left(\tilde{\rho}_e \hbar\right) - \sqrt{V\left(\tilde{\rho}_e \hbar\right)} f_Q^{-1}\left(\varepsilon\right)/\sqrt{T}\right], \tag{B.1}$$

where, $\hbar = \left\|\bar{\mathbf{h}}_d\right\|^2$. Then we obtain (3.5) by following the procedure similar to [86, Appendix A].

B.2 Proof of Theorem 3.2

The first derivative of $R\left(T_t, T_f, \eta\right)$, given in (B.1), with respect to T_d is derived as

$$\begin{aligned}\frac{\partial R\left(T_t, T_f, \eta\right)}{\partial T_d} = & \frac{1}{T}\mathbb{E}_{\hbar}\left[\log_2\left(1+\omega\right) - \frac{\alpha_1\sqrt{\omega\left(2+\omega\right)}}{1+\omega}\right] \\ & + \frac{1}{T}\mathbb{E}_{\hbar}\left[\frac{\alpha_1\alpha_2\omega}{\left(1+\omega\right)^2\sqrt{\omega\left(2+\omega\right)}} - \frac{\alpha_2\omega}{\left(1+\omega\right)\ln 2}\right],\end{aligned} \tag{B.2}$$

where $\hbar = \left\|\bar{\mathbf{h}}_d\right\|^2$, $\omega = \tilde{\rho}_e\hbar$, $\alpha_1 = f_Q^{-1}(\varepsilon)/(\sqrt{T}\ln 2)$, and $\alpha_2 = \frac{T_d}{T_d - N_A}\left(1 - \sqrt{\frac{N_A(N_A+\rho T)}{T_d(T_d+\rho T)}}\right)$.

We find that $\alpha_1 < 1$ and $\alpha_2 < 1$ due to $T_d > N_A$. Then, we need to show that $\Omega\left(\omega\right) = \log_2\left(1+\omega\right) - \frac{\sqrt{\omega(2+\omega)}}{1+\omega} - \frac{\omega}{(1+\omega)\ln 2} \geq 0$ for all $\omega \geq \omega_0$, where ω_0 is the solution to $\Omega\left(\omega\right) = 0$. It is noted that $\Omega\left(\omega\right) = 0$ at $\omega = \omega_0$ and for all $\omega \geq \omega_0$ its first derivative is given by

$$d\Omega\left(\omega\right)/d\omega = \left(\frac{\omega}{\ln 2} - \frac{1}{\sqrt{\omega(2+\omega)}}\right)\frac{1}{(1+\omega)^2} > 0. \tag{B.3}$$

We also find that $d\Omega\left(\omega\right)/d\omega$ is a monotonically increasing function of ω for all $\omega \geq \omega_0$,

where the value of ω_0 is relatively small compared to the required value of SNR in URLLC scenarios (e.g., the SNR $>$ 10 dB [37, 54, 64]). Therefore, we conclude that the optimal value of T_t is the minimum value of T_t for given ρT in the case of $T_t \geq N_A$ and $T_d > N_A$. This is due to the fact that (3.4) is a monotonically increasing function of T_d and keeping the minimum value of T_t maximizes $R\left(T_t, T_f, \eta\right)$ for given T_f.

Appendix C

C.1 Proof of Lemma 4.1

The conditional CDF of the SINR with the maximum transmit power constraint is rewritten as

$$F_\gamma\left(\gamma\middle|\|\mathbf{h}_\mathrm{u}\|^2 \geq \frac{Q}{P_\mathrm{max}}\right) = \Pr\left\{\frac{Q\phi}{Q(1-\phi)\frac{Y}{X}+\sigma_w^2} \leq \gamma\middle| X \geq \frac{Q}{P_\mathrm{max}}\right\}$$
$$= 1 - \Pr\left\{Y \leq X\xi(\gamma)\middle| X \geq \frac{Q}{P_\mathrm{max}}\right\}, \tag{C.1}$$

where $\xi(\gamma)$ is defined below (4.17). Then, we write $\Pr\left\{Y \leq X\xi(\gamma)\middle| X \geq \frac{Q}{P_\mathrm{max}}\right\}$ as

$$\Pr\left\{Y \leq X\xi(\gamma)\middle| X \geq \frac{Q}{P_\mathrm{max}}\right\} = \frac{\Pr\left\{Y \leq X\xi(\gamma), X \geq \frac{Q}{P_\mathrm{max}}\right\}}{\Pr\left\{X \geq \frac{Q}{P_\mathrm{max}}\right\}}$$
$$= \frac{\int_{\frac{Q}{P_\mathrm{max}}}^{\infty} F_Y\left(x\xi(\gamma)\right) f_X(x)dx}{\Pr\left\{X \geq \frac{Q}{P_\mathrm{max}}\right\}}$$
$$= \frac{\int_{\frac{Q}{P_\mathrm{max}}}^{\infty} \left(1-e^{-(x\xi(\gamma))}\right)\frac{x^{N_\mathrm{t}-1}}{\Gamma(N_\mathrm{t})}e^{-x}dx}{\left(\frac{\gamma_\mathrm{up}\left(N_\mathrm{t},\frac{Q}{P_\mathrm{max}}\right)}{\Gamma(N_\mathrm{t})}\right)}$$
$$= \frac{\frac{1}{\Gamma(N_\mathrm{t})}\left(\gamma_\mathrm{up}\left(N_\mathrm{t},\frac{Q}{P_\mathrm{max}}\right) - \frac{\gamma_\mathrm{up}\left(N_\mathrm{t},\frac{Q(1+\xi(\gamma))}{P_\mathrm{max}}\right)}{(1+\xi(\gamma))^{N_\mathrm{t}}}\right)}{\left(\frac{\Gamma(N_\mathrm{t})}{\gamma_\mathrm{up}\left(N_\mathrm{t},\frac{Q}{P_\mathrm{max}}\right)}\right)}$$
$$= 1 - \frac{\gamma_\mathrm{up}\left(N_\mathrm{t},\frac{Q(1+\xi(\gamma))}{P_\mathrm{max}}\right)}{\gamma_\mathrm{up}\left(N_\mathrm{t},\frac{Q}{P_\mathrm{max}}\right)(1+\xi(\gamma))^{N_\mathrm{t}}}, \tag{C.2}$$

where $f_{\mathrm{X}}(x)=\frac{x^{N_{\mathrm{t}}-1}}{\Gamma(N_{\mathrm{t}})}e^{-x}$, $F_{\mathrm{Y}}(y)=1-e^{-y}$, and $\gamma_{\mathrm{up}}(s,x)$ is defined below (4.17). By substituting (C.2) into (C.1), we obtain the result in (4.17), which completes the proof.

C.2 Proof of Corollary 4.1

Following Theorem 4.1 and considering $P_{\max}\to\infty$, the packet loss probability of the conventional CIPC scheme, $P_{\varepsilon}^{\infty}(Q)$, is given by

$$\begin{aligned}P_{\varepsilon}^{\infty}(Q)=&\left[\left(\frac{1}{2}-\delta\gamma_0+\delta\alpha\right)F_{\gamma}\left(\alpha\middle|\|\mathbf{h}_{\mathrm{u}}\|^2\geq 0\right)+\left(\frac{1}{2}+\delta\gamma_0-\delta\beta\right)F_{\gamma}\left(\beta\middle|\|\mathbf{h}_{\mathrm{u}}\|^2\geq 0\right)\right.\\&\left.+\delta\int_{\alpha}^{\beta}F_{\gamma}\left(\gamma\middle|\|\mathbf{h}_{\mathrm{u}}\|^2\geq 0\right)d\gamma\right]\left(1-\frac{\gamma_{\mathrm{lw}}\left(N_{\mathrm{t}},0\right)}{\Gamma(N_{\mathrm{t}})}\right)+\frac{\gamma_{\mathrm{lw}}\left(N_{\mathrm{t}},0\right)}{\Gamma(N_{\mathrm{t}})}\\=&\delta\int_{\alpha}^{\beta}F_{\gamma}\left(\gamma\middle|\|\mathbf{h}_{\mathrm{u}}\|^2\geq 0\right)d\gamma+\left(\frac{1}{2}-\delta\gamma_0+\delta\alpha\right)F_{\gamma}\left(\alpha\middle|\|\mathbf{h}_{\mathrm{u}}\|^2\geq 0\right)\\&+\left(\frac{1}{2}+\delta\gamma_0-\delta\beta\right)F_{\gamma}\left(\beta\middle|\|\mathbf{h}_{\mathrm{u}}\|^2\geq 0\right),\end{aligned}\tag{C.3}$$

where $\frac{\gamma_{\mathrm{lw}}\left(N_{\mathrm{t}},\frac{Q}{P_{\max}}\right)}{\Gamma(N_{\mathrm{t}})}=\frac{\gamma_{\mathrm{lw}}(N_{\mathrm{t}},0)}{\Gamma(N_{\mathrm{t}})}=0$ as $P_{\max}\to\infty$.

Then, we need to derive the CDF of the SINR to solve the integration in (C.3). According to Lemma 4.1, we obtain $F_{\gamma}\left(\gamma\middle|\|\mathbf{h}_{\mathrm{u}}\|^2\geq 0\right)$ by substituting $\frac{Q}{P_{\max}}=0$ into (4.17), which leads to

$$F_{\gamma}\left(\gamma\middle|\|\mathbf{h}_{\mathrm{u}}\|^2\geq 0\right)=\frac{\gamma_{\mathrm{up}}\left(N_{\mathrm{t}},0\right)}{\gamma_{\mathrm{up}}\left(N_{\mathrm{t}},0\right)\left(1+\xi\left(\gamma\right)\right)^{N_{\mathrm{t}}}}=\left(\frac{1}{1+\xi\left(\gamma\right)}\right)^{N_{\mathrm{t}}},\tag{C.4}$$

where $\gamma_{\mathrm{up}}\left(N_{\mathrm{t}},0\right)=\Gamma(N_{\mathrm{t}})$. As such, $\int_{\alpha}^{\beta}F_{\gamma}\left(\gamma\middle|\|\mathbf{h}_{\mathrm{u}}\|^2\geq 0\right)d\gamma$ can be obtained as

$$\begin{aligned}\int_{\alpha}^{\beta}F_{\gamma}\left(\gamma\middle|\|\mathbf{h}_{\mathrm{u}}\|^2\geq 0\right)d\gamma=&\int_{\alpha}^{\beta}\left(\frac{1}{1+\xi\left(\gamma\right)}\right)^{N_{\mathrm{t}}}d\gamma\overset{(e)}{=}\int_{\alpha}^{\beta}\left(\frac{M_1\gamma}{\gamma+M_2}\right)^{N_{\mathrm{t}}}d\gamma=\int_{\alpha}^{\beta}M_1^{N_{\mathrm{t}}}\left(\frac{\gamma}{\gamma+M_2}\right)^{N_{\mathrm{t}}}d\gamma\\=&M_1^{N_{\mathrm{t}}}\left((-1)^{-N_{\mathrm{t}}}M_2\left(B_{-\frac{\alpha}{M_2}}\left(1+N_{\mathrm{t}},1-N_{\mathrm{t}}\right)-B_{-\frac{\beta}{M_2}}\left(1+N_{\mathrm{t}},1-N_{\mathrm{t}}\right)\right)\right),\end{aligned}\tag{C.5}$$

where step (e) is achieved by using $\frac{1}{1+\xi(\gamma)}=\frac{M_1\gamma}{\gamma+M_2}$, while $\xi(x)$, M_1, M_2, and $B_x(a,b)$ are defined below (4.26). Then, we obtain (4.26) by substituting (C.4) and (C.5) into (C.3), which completes the proof.

C.3 Proof of Proposition 4.1

In order to find the optimal Q to minimize the packet loss probability, $P_{\varepsilon}^{\phi=1}(Q)$, we need to find the monotonicity and convexity of $P_{\varepsilon}^{\phi=1}(Q)$ w.r.t. Q. To this end, we first derive the first-order

derivative of $P_{\varepsilon}^{\phi=1}(Q)$ w.r.t. Q, which is given by

$$\frac{\partial\{P_{\varepsilon}^{\phi=1}(Q)\}}{\partial Q} = \frac{\partial\{p_t(Q)\}}{\partial Q}\Big(\varepsilon(Q)-1\Big) + p_t(Q)\frac{\partial\{\varepsilon(Q)\}}{\partial Q}. \tag{C.6}$$

Then, the second-order derivative of $P_{\varepsilon}^{\phi=1}(Q)$ w.r.t. Q is obtained as

$$\frac{\partial^2\{P_{\varepsilon}^{\phi=1}(Q)\}}{\partial Q^2} = \frac{\partial^2\{p_t(Q)\}}{\partial Q^2}\Big(\varepsilon(Q)-1\Big) + 2\frac{\partial\{p_t(Q)\}}{\partial Q}\frac{\partial\{\varepsilon(Q)\}}{\partial Q} + p_t(Q)\frac{\partial^2\{\varepsilon(Q)\}}{\partial Q^2}. \tag{C.7}$$

In order to determine the sign of $\frac{\partial^2\{P_{\varepsilon}^{\phi=1}(Q)\}}{\partial Q^2}$, we first need to tackle $\frac{\partial\{p_t(Q)\}}{\partial Q}$ and $\frac{\partial^2\{p_t(Q)\}}{\partial Q^2}$. Recall that $\frac{\partial\{p_t(Q)\}}{\partial Q} < 0$ and $\frac{\partial^2\{p_t(Q)\}}{\partial Q^2}$ have been derived in (4.22) and (4.23), respectively. As such, we find that $p_t(Q)$ is a monotonically decreasing function of Q due to $\frac{\partial\{p_t(Q)\}}{\partial Q} < 0$. Besides, with the aid of the proof in Lemma 4.2, we can obtain that $\frac{\partial\{p_t(Q)\}}{\partial Q} < 0$ and $\frac{\partial^2\{p_t(Q)\}}{\partial Q^2} < 0$ for $0 < Q < P_{\max}(N_{\mathrm{t}}-1)$. Then, we detail the signs of $\frac{\partial\{\varepsilon(Q)\}}{\partial Q}$ and $\frac{\partial^2\{\varepsilon(Q)\}}{\partial Q^2}$ as follows.

We first find the sign of $\frac{\partial\varepsilon(Q)}{\partial Q}$. To this end, we rewrite the decoding error probability in (4.10) as $\varepsilon(\gamma_{\phi=1}) = f(A(\gamma_{\phi=1}))$, where $A(\gamma_{\phi=1}) = \frac{\sqrt{T}\left(\ln(1+\gamma_{\phi=1})-R\ln 2\right)}{\sqrt{1-\left(1+\gamma_{\phi=1}\right)^{-2}}}$. As such, the first-order partial derivative of $\varepsilon(Q)$ w.r.t. Q is derived as

$$\frac{\partial\{\varepsilon(Q)\}}{\partial Q} = \frac{\partial\{f(A(\gamma_{\phi=1}))\}}{\partial Q} = \frac{\partial\left\{f(A(\gamma_{\phi=1}))\right\}}{\partial\{A(\gamma_{\phi=1})\}}\frac{\partial\{A(\gamma_{\phi=1})\}}{\partial\gamma_{\phi=1}}\frac{\partial\gamma_{\phi=1}}{\partial Q}. \tag{C.8}$$

We note that the sign of $\frac{\partial\{\varepsilon(Q)\}}{\partial Q}$ is determined by the signs of $\frac{\partial\left\{f(A(\gamma_{\phi=1}))\right\}}{\partial\{A(\gamma_{\phi=1})\}}$, $\frac{\partial\{A(\gamma_{\phi=1})\}}{\partial\gamma_{\phi=1}}$, and $\frac{\partial\gamma_{\phi=1}}{\partial Q}$. As such, we can conclude that $\varepsilon(Q)$ is a decreasing function of Q if we can prove $\frac{\partial\left\{f(A(\gamma_{\phi=1}))\right\}}{\partial\{A(\gamma_{\phi=1})\}}\frac{\partial\{A(\gamma_{\phi=1})\}}{\partial\gamma_{\phi=1}}\frac{\partial\gamma_{\phi=1}}{\partial Q} < 0$. In order to prove this, we present the following three results given by

$$\frac{\partial\left\{f(A(\gamma_{\phi=1}))\right\}}{\partial\{A(\gamma_{\phi=1})\}} = -\frac{1}{\sqrt{2\pi}}\exp\left(-\frac{A^2(\gamma_{\phi=1})}{2}\right) < 0, \tag{C.9}$$

$$\frac{\partial\{A(\gamma_{\phi=1})\}}{\partial\gamma_{\phi=1}} = \frac{\sqrt{T}\left(1-\frac{\ln(1+\gamma_{\phi=1})-R\ln 2}{(1+\gamma_{\phi=1})^2-1}\right)}{\sqrt{(1+\gamma_{\phi=1})^2-1}} > 0, \tag{C.10}$$

$$\frac{\partial\gamma_{\phi=1}}{\partial Q} = \frac{1}{\sigma_w^2} > 0. \tag{C.11}$$

We note that (C.9) is obtained due to the properties of the Q-function and (C.10) is obtained due to the proof in [86, Appendix A]. According to (C.9), (C.10), and (C.11), we obtain $\frac{\partial\{f(A(\gamma_{\phi=1}))\}}{\partial Q} = \frac{\partial\left\{f(A(\gamma_{\phi=1}))\right\}}{\partial\{A(\gamma_{\phi=1})\}}\frac{\partial\{A(\gamma_{\phi=1})\}}{\partial\gamma_{\phi=1}}\frac{\partial\gamma_{\phi=1}}{\partial Q} < 0$, which results in $\frac{\partial\{\varepsilon(Q)\}}{\partial Q} < 0$. We then find

the sign of $\frac{\partial^2\{\varepsilon(Q)\}}{\partial Q^2}$. To this end, we express $\frac{\partial^2\{\varepsilon(Q)\}}{\partial Q^2}$ as

$$\frac{\partial^2\{\varepsilon(Q)\}}{\partial Q^2} = \frac{\partial^2\{f(A(\gamma_{\phi=1}))\}}{\partial Q^2}. \tag{C.12}$$

In order to obtain the sign of $\frac{\partial^2\left\{f(A(\gamma_{\phi=1}))\right\}}{\partial Q^2}$, we rewrite $\frac{\partial^2\left\{f(A(\gamma_{\phi=1}))\right\}}{\partial Q^2}$ as

$$\begin{aligned}
\frac{\partial^2\left\{f(A(\gamma_{\phi=1}))\right\}}{\partial Q^2} &= \frac{\partial^2\left\{f(A(\gamma_{\phi=1}))\right\}}{\partial\{A(\gamma_{\phi=1})\}\partial Q}\frac{\partial\{A(\gamma_{\phi=1})\}}{\partial\gamma_{\phi=1}}\frac{\partial\gamma_{\phi=1}}{\partial Q} \\
&\quad + \frac{\partial\left\{f(A(\gamma_{\phi=1}))\right\}}{\partial\{A(\gamma_{\phi=1})\}}\frac{\partial^2\{A(\gamma_{\phi=1})\}}{\partial\gamma_{\phi=1}\partial Q}\frac{\partial\gamma_{\phi=1}}{\partial Q} \\
&\quad + \frac{\partial\left\{f(A(\gamma_{\phi=1}))\right\}}{\partial\{A(\gamma_{\phi=1})\}}\frac{\partial\{A(\gamma_{\phi=1})\}}{\partial\gamma_{\phi=1}}\frac{\partial^2\gamma_{\phi=1}}{\partial Q^2} \\
&= \frac{\partial^2\left\{f(A(\gamma_{\phi=1}))\right\}}{\partial\{A^2(\gamma_{\phi=1})\}}\left\{\frac{\partial\{A(\gamma_{\phi=1})\}}{\partial\gamma_{\phi=1}}\right\}^2\left\{\frac{\partial\gamma_{\phi=1}}{\partial Q}\right\}^2 \\
&\quad + \frac{\partial\left\{f(A(\gamma_{\phi=1}))\right\}}{\partial\{A(\gamma_{\phi=1})\}}\frac{\partial^2\{A(\gamma_{\phi=1})\}}{\partial\gamma_{\phi=1}^2}\left\{\frac{\partial\gamma_{\phi=1}}{\partial Q}\right\}^2 \\
&\quad + \frac{\partial\left\{f(A(\gamma_{\phi=1}))\right\}}{\partial\{A(\gamma_{\phi=1})\}}\frac{\partial\{A(\gamma_{\phi=1})\}}{\partial\gamma_{\phi=1}}\frac{\partial^2\gamma_{\phi=1}}{\partial Q^2},
\end{aligned} \tag{C.13}$$

where $\frac{\partial^2\gamma_{\phi=1}}{\partial Q^2} = 0$. Based on the properties of the Q-function, we express $\frac{\partial^2\left\{f(A(\gamma_{\phi=1}))\right\}}{\partial\{A^2(\gamma_{\phi=1})\}}$ as

$$\frac{\partial^2\left\{f(A(\gamma_{\phi=1}))\right\}}{\partial\{A^2(\gamma_{\phi=1})\}} = \frac{A(\gamma_{\phi=1})}{\sqrt{2\pi}}\exp\left(-\frac{A^2(\gamma_{\phi=1})}{2}\right) > 0. \tag{C.14}$$

For now, we have $\frac{\partial^2\left\{f(A(\gamma_{\phi=1}))\right\}}{\partial\{A^2(\gamma_{\phi=1})\}} > 0$ in (C.14), $\frac{\partial\left\{f(A(\gamma_{\phi=1}))\right\}}{\partial\{A(\gamma_{\phi=1})\}} < 0$ in (C.9), $\frac{\partial\{A(\gamma_{\phi=1})\}}{\partial\gamma_{\phi=1}} > 0$ in (C.10), $\frac{\partial\gamma_{\phi=1}}{\partial Q} > 0$ in (C.11), and $\frac{\partial^2\gamma_{\phi=1}}{\partial Q^2} = 0$. Thus, determining the sign of $\frac{\partial^2\left\{f(A(\gamma_{\phi=1}))\right\}}{\partial Q^2}$ is equivalent to identifying the sign of $\frac{\partial^2\{A(\gamma_{\phi=1})\}}{\partial\gamma_{\phi=1}^2}$. As per the proof given in [87, Appendix A], we prove that $\frac{\partial^2\{A(\gamma_{\phi=1})\}}{\partial\gamma_{\phi=1}^2} < 0$ for $\gamma_{\phi=1} > \gamma_a$, where γ_a is the solution to

$$\frac{\ln(1+\gamma_a)}{(1+\gamma_a)^2-1} = \frac{1}{3}. \tag{C.15}$$

Following (5.1), $\gamma_{\phi=1} > \gamma_a$ leads to

$$\gamma_{\phi=1} > \gamma_a \Longrightarrow \frac{Q}{\sigma_w^2} > \gamma_a \Longrightarrow Q > Q_0, \tag{C.16}$$

where $Q_0 = \sigma_w^2 \gamma_a$ As such, for $Q > Q_0$, we have $\frac{\partial^2\{f(A(\gamma_{\phi=1}))\}}{\partial Q^2} > 0$, due to

$$\begin{aligned}\frac{\partial^2\{f(A(\gamma_{\phi=1}))\}}{\partial Q^2} = &\underbrace{\frac{\partial^2\{f(A(\gamma_{\phi=1}))\}}{\partial\{A^2(\gamma_{\phi=1})\}}}_{>0}\underbrace{\left\{\frac{\partial\{A(\gamma_{\phi=1})\}}{\partial\gamma_{\phi=1}}\right\}^2}_{>0}\underbrace{\left\{\frac{\partial\gamma_{\phi=1}}{\partial Q}\right\}^2}_{>0}\\ &+\underbrace{\frac{\partial\{f(A(\gamma_{\phi=1}))\}}{\partial\{A(\gamma_{\phi=1})\}}}_{<0}\underbrace{\frac{\partial^2\{A(\gamma_{\phi=1})\}}{\partial\gamma_{\phi=1}^2}}_{<0}\underbrace{\left\{\frac{\partial\gamma_{\phi=1}}{\partial Q}\right\}^2}_{>0}\\ &+\underbrace{\frac{\partial\{f(A(\gamma_{\phi=1}))\}}{\partial\{A(\gamma_{\phi=1})\}}}_{<0}\underbrace{\frac{\partial\{A(\gamma_{\phi=1})\}}{\partial\gamma_{\phi=1}}}_{>0}\underbrace{\frac{\partial^2\gamma_{\phi=1}}{\partial Q^2}}_{=0} > 0. \end{aligned} \tag{C.17}$$

Then, following (C.17), we find that $\frac{\partial^2\{\varepsilon(Q)\}}{\partial Q^2} > 0$ for $Q > Q_0$, due to $\frac{\partial^2\{f(A(\gamma_{\phi=1}))\}}{\partial Q^2} > 0$.

Based on the analysis above, the sign of $\frac{\partial^2\{P_\varepsilon(Q)\}}{\partial Q^2}$ in (C.7) is determined as

$$\begin{aligned}\frac{\partial^2\{P_\varepsilon^{\phi=1}(Q)\}}{\partial Q^2} = &\underbrace{\frac{\partial^2\{p_t(Q)\}}{\partial Q^2}}_{<0 \text{ for } 0<Q<P_{\max}(N_t-1)}\underbrace{\Big(\varepsilon(Q)-1\Big)}_{\leq 0}+2\underbrace{\frac{\partial\{p_t(Q)\}}{\partial Q}}_{<0}\underbrace{\frac{\partial\{\varepsilon(Q)\}}{\partial Q}}_{<0}\\ &+\underbrace{p_t(Q)}_{>0}\underbrace{\frac{\partial^2\{\varepsilon(Q)\}}{\partial Q^2}}_{>0 \text{ for } Q>Q_0} > 0. \end{aligned} \tag{C.18}$$

To summarize, we prove that $\frac{\partial^2\{P_\varepsilon^{\phi=1}(Q)\}}{\partial Q^2} > 0$ for $Q_0 < Q < P_{\max}(N_t - 1)$, which completes the proof.

Bibliography

[1] 3GPP, "Study on physical layer enhancements for NR ultra-reliable and low latency case (URLLC)," 3rd Generation Partnership Project (3GPP), TR 38.824, Mar. 2019, Rel. 16. (cited on pages xxi and 2)

[2] ITU-R, "IMT vision – framework and overall objectives of the future development of IMT for 2020 and beyond," ITU, M. 2083-0, Sept. 2015. (cited on pages 1 and 2)

[3] E. D. et al., "5G radio access," *Ericsson Rev.*, no. 6, Jun. 2014. (cited on page 1)

[4] Ericsson, "Overview of URLLC," 3rd Generation Partnership Project (3GPP), Tdoc R2-1700393, Jan. 2017, R2-1700393. (cited on page 1)

[5] ITU-R, "Minimum requirements related to technical performance for IMT-2020 radio interface(s)," ITU-R, IMT-2020.TECH PERF REQ, Feb. 2017. (cited on pages 1 and 2)

[6] P. Popovski, "Ultra-reliable communication in 5G wireless systems," in *Proc. 1st Int. Conf. 5G for Ubiquitous Connectivity*, Nov. 2014, pp. 146–151. (cited on page 1)

[7] J. G. Andrews, S. Buzzi, W. Choi, S. V. Hanly, A. Lozano, A. C. K. Soong, and J. C. Zhang, "What will 5G be?" *IEEE J. Sel. Areas Commun.*, vol. 32, no. 6, pp. 1065–1082, Jun. 2014. (cited on page 1)

[8] 3GPP, "Study on scenarios and requirements for next generation access technologies," 3rd Generation Partnership Project (3GPP), TR 38.913, Jul. 2020, Rel. 16. (cited on pages 1 and 2)

[9] C. Li, C. Li, K. Hosseini, S. B. Lee, J. Jiang, W. Chen, G. Horn, T. Ji, J. E. Smee, and J. Li, "5G-based systems design for Tactile Internet," *Proc. IEEE*, pp. 1–18, Aug. 2018. (cited on pages 2 and 4)

[10] 3GPP, "Study on latency reduction techniques for LTE," 3rd Generation Partnership Project (3GPP), TR 36.881, Jun. 2016, Rel. 14.0. (cited on pages 2 and 3)

[11] B. Holfeld, D. Wieruch, T. Wirth, L. Thiele, S. A. Ashraf, J. Huschke, I. Aktas, and J. Ansari, "Wireless communication for factory automation: An opportunity for LTE and 5G systems," *IEEE Commun. Mag.*, vol. 54, no. 6, pp. 36–43, Jun. 2016. (cited on pages 2 and 3)

[12] P. Schulz, M. Matthe, H. Klessig, M. Simsek, G. Fettweis, J. Ansari, S. A. Ashraf, B. Almeroth, J. Voigt, I. Riedel, A. Puschmann, A. Mitschele-Thiel, M. Muller, T. Elste, and M. Windisch, "Latency critical IoT applications in 5G: Perspective on the design of radio interface and network architecture," *IEEE Commun. Mag.*, vol. 55, no. 2, pp. 70–78, Feb. 2017. (cited on page 2)

[13] H. Chen, R. Abbas, P. Cheng, M. Shirvanimoghaddam, W. Hardjawana, W. Bao, Y. Li, and B. Vucetic, "Ultra-reliable low latency cellular networks: Use cases, challenges and approaches," *IEEE Commun. Mag.*, vol. 56, no. 12, pp. 119–125, Dec. 2018. (cited on pages 2 and 3)

[14] H. Holma and A. Toskala, *LTE for UMTS: Evolution to LTE-Advanced*, 2nd ed. Wiley, 2011. (cited on page 2)

[15] M. Lauridsen, L. C. Gimenez, I. Rodriguez, T. B. Sorensen, and P. Mogensen, "From LTE to 5G for connected mobility," *IEEE Commun. Mag.*, vol. 55, no. 3, pp. 156–162, Mar. 2017. (cited on page 3)

[16] C. She, C. Yang, and T. Q. S. Quek, "Radio resource management for ultra-reliable and low-latency communications," *IEEE Commun. Mag.*, vol. 55, no. 6, pp. 72–78, Jun. 2017. (cited on pages 3 and 8)

[17] 3GPP, "Study on New Radio Access Technology Physical Layer Aspects," 3rd Generation Partnership Project (3GPP), TR 38.802, Sept. 2017, Rel. 14.2. (cited on page 3)

[18] P. Kela, M. Costa, J. Salmi, K. Leppanen, J. Turkka, T. Hiltunen, and M. Hronec, "A novel radio frame structure for 5G dense outdoor radio access networks," in *Proc. IEEE Veh. Technol. Conf. (VTC Spring)*, May 2015, pp. 1–6. (cited on page 3)

[19] S. A. Ashraf, I. Aktas, E. Eriksson, K. W. Helmersson, and J. Ansari, "Ultra-reliable and low-latency communication for wireless factory automation: From LTE to 5G," in *Proc. IEEE 21st Int. Conf. Emerging Technol. Factory Automation (ETFA)*, Berlin, Germany, Sept. 2016, pp. 1–8. (cited on page 3)

[20] F. Capozzi, G. Piro, L. A. Grieco, G. Boggia, and P. Camarda, "Downlink packet scheduling in LTE cellular networks: Key design issues and a survey," *IEEE Commun. Surveys Tuts.*, vol. 15, no. 2, pp. 678–700, 2nd Quart. 2013. (cited on page 3)

[21] G. Durisi, T. Koch, and P. Popovski, "Toward massive, ultrareliable, and low-latency wireless communication with short packets," *Proc. IEEE*, vol. 104, no. 9, pp. 1711–1726, Sept. 2016. (cited on pages 3, 4, 6, and 8)

[22] N. A. Johansson, Y. P. E. Wang, E. Eriksson, and M. Hessler, "Radio access for ultra-reliable and low-latency 5G communications," in *Proc. IEEE Int. Conf. Commun. (ICC) Workshop*, Jun. 2015, pp. 1184–1189. (cited on pages 3 and 9)

[23] O. N. C. Yilmaz, Y. P. E. Wang, N. A. Johansson, N. Brahmi, S. A. Ashraf, and J. Sachs, "Analysis of ultra-reliable and low-latency 5G communication for a factory automation use case," in *Proc. IEEE Int. Conf. Commun. (ICC) Workshop*, Jun. 2015, pp. 1190–1195. (cited on pages 3 and 9)

[24] K. I. Pedersen, G. Berardinelli, F. Frederiksen, P. Mogensen, and A. Szufarska, "A flexible 5G frame structure design for frequency-division duplex cases," *IEEE Commun. Mag.*, vol. 54, no. 3, pp. 53–59, Mar. 2016. (cited on page 3)

[25] G. Durisi, T. Koch, J. Östman, Y. Polyanskiy, and W. Yang, "Short-packet communications over multiple-antenna Rayleigh-fading channels," *IEEE Trans. Commun.*, vol. 64, no. 2, pp. 618–629, Feb. 2016. (cited on pages 4, 6, 7, 8, 9, 19, 28, and 45)

[26] C. E. Shannon, "A mathematical theory of communication," *Bell Syst. Tech. J.*, vol. 27, no. 3, pp. 379–423, Jul. 1948. (cited on pages 4 and 6)

[27] Y. Polyanskiy, H. V. Poor, and S. Verdu, "Channel coding rate in the finite blocklength regime," *IEEE Trans. Inf. Theory*, vol. 56, no. 5, pp. 2307–2359, May 2010. (cited on pages 4, 6, 7, 19, 21, 28, 41, and 45)

[28] C. Kolias, G. Kambourakis, and S. Gritzalis, "Attacks and countermeasures on 802.16: Analysis and assessment," *IEEE Commun. Surveys Tuts.*, vol. 15, no. 1, pp. 487–514, 1th Quart. 2013. (cited on page 4)

[29] Y. Zou, J. Zhu, X. Wang, and L. Hanzo, "A survey on wireless security: Technical challenges, recent advances, and future trends," *Proc. IEEE*, vol. 104, no. 9, pp. 1727–1765, Sept. 2016. (cited on pages 4 and 10)

[30] R. Khan, P. Kumar, D. N. K. Jayakody, and M. Liyanage, "A survey on security and privacy of 5G technologies: Potential solutions, recent advancements, and future directions," *IEEE Commun. Surveys Tuts.*, vol. 22, no. 1, pp. 196–248, 1st Quart. 2020. (cited on page 4)

[31] N. Yang, L. Wang, G. Geraci, M. Elkashlan, J. Yuan, and M. D. Renzo, "Safeguarding 5G wireless communication networks using physical layer security," *IEEE Commun. Mag.*, vol. 53, no. 4, pp. 20–27, Apr. 2015. (cited on pages 4 and 5)

[32] Y. Wu, A. Khisti, C. Xiao, G. Caire, K. Wong, and X. Gao, "A survey of physical layer security techniques for 5G wireless networks and challenges ahead," *IEEE J. Sel. Areas Commun.*, vol. 36, no. 4, pp. 679–695, April 2018. (cited on pages 4, 5, and 10)

[33] R. Chen, C. Li, S. Yan, R. Malaney, and J. Yuan, "Physical layer security for ultra-reliable and low-latency communications," *IEEE Wireless Commun.*, vol. 26, no. 5, pp. 6–11, Oct. 2019. (cited on page 4)

[34] H. Ren, C. Pan, Y. Deng, M. Elkashlan, and A. Nallanathan, "Resource allocation for secure URLLC in mission-critical IoT scenarios," *IEEE Trans. Commun.*, vol. 68, no. 9, pp. 5793–5807, Sept. 2020. (cited on pages 4, 5, and 11)

[35] S. Xu, T. Chang, S. Lin, C. Shen, and G. Zhu, "Energy-efficient packet scheduling with finite blocklength codes: Convexity analysis and efficient algorithms," *IEEE Trans. Wireless Commun.*, vol. 15, no. 8, pp. 5527–5540, Aug. 2016. (cited on page 5)

[36] C. Sun, C. She, C. Yang, T. Q. S. Quek, Y. Li, and B. Vucetic, "Optimizing resource allocation in the short blocklength regime for ultra-reliable and low-latency communications," *IEEE Trans. Wireless Commun.*, vol. 18, no. 1, pp. 402–415, Jan. 2019. (cited on pages 5 and 64)

[37] S. Schiessl, J. Gross, and H. Al-Zubaidy, "Delay analysis for wireless fading channels with finite blocklength channel coding," in *Proc. 18th ACM Int. Conf. Model., Anal. Simul. Wireless Mobile Syst (MSWiM).*, Cancun, Mexico, Nov. 2015, pp. 13–22. (cited on pages 5, 31, 64, and 96)

[38] A. Goldsmith, *Wireless communications*. Cambridge University Press, 2005. (cited on pages 6, 7, 15, and 78)

[39] L. H. Ozarow, S. Shamai, and A. D. Wyner, "Information theoretic considerations for cellular mobile radio," *IEEE Trans. Veh. Technol.*, vol. 43, no. 2, pp. 359–378, May 1994. (cited on pages 6 and 7)

[40] R. Dong, C. She, W. Hardjawana, Y. Li, and B. Vucetic, "Deep learning for hybrid 5G services in mobile edge computing systems: Learn from a digital wwin," *IEEE Trans. Wireless Commun.*, vol. 18, no. 10, pp. 4692–4707, Oct. 2019. (cited on pages 8, 78, and 88)

[41] Y. Yu, H. Chen, Y. Li, Z. Ding, and B. Vucetic, "On the performance of non-orthogonal multiple access in short-packet communications," *IEEE Commun. Lett.*, vol. 22, no. 3, pp. 590–593, Mar. 2018. (cited on page 8)

[42] X. Sun, S. Yan, N. Yang, Z. Ding, C. Shen, and Z. Zhong, "Short-packet downlink transmission with non-orthogonal multiple access," *IEEE Trans. Wireless Commun.*, vol. 17, no. 7, pp. 4550–4564, Jul. 2018. (cited on page 8)

[43] R. Chen, C. Li, S. Yan, R. A. Malaney, and J. Yuan, "Physical layer security for ultra-reliable and low-latency communications," *IEEE Wireless Commun.*, vol. 26, no. 5, pp. 6–11, Oct. 2019. (cited on page 8)

[44] H. Wang, Q. Yang, Z. Ding, and H. V. Poor, "Secure short-packet communications for mission-critical IoT applications," *IEEE Trans. Wireless Commun.*, vol. 18, no. 5, pp. 2565–2578, May 2019. (cited on pages 8, 11, and 58)

[45] Y. Hu, M. C. Gursoy, and A. Schmeink, "Relaying-enabled ultra-reliable low-latency communications in 5G," *IEEE Netw.*, vol. 32, no. 2, pp. 62–68, Mar. 2018. (cited on page 8)

[46] Y. Gu, H. Chen, Y. Li, L. Song, and B. Vucetic, "Short-packet two-way amplify-and-forward relaying," *IEEE Signal Process. Lett.*, vol. 25, no. 2, pp. 263–267, Feb. 2018. (cited on page 8)

[47] Y. Gu, H. Chen, Y. Li, and B. Vucetic, "Ultra-reliable short-packet communications: Half-duplex or full-duplex relaying?" *IEEE Wireless Commun. Lett.*, vol. 7, no. 3, pp. 348–351, Jun. 2018. (cited on page 8)

[48] Y. Hu, Y. Zhu, M. C. Gursoy, and A. Schmeink, "SWIPT-enabled relaying in IoT networks operating with finite blocklength codes," *IEEE J. Sel. Areas Commun.*, vol. 37, no. 1, pp. 74–88, Jan. 2019. (cited on page 8)

[49] L. Zhang and Y. Liang, "Average throughput analysis and optimization in cooperative IoT networks with short packet communication," *IEEE Trans. Veh. Technol.*, vol. 67, no. 12, pp. 11 549–11 562, Dec. 2018. (cited on pages 8 and 30)

[50] H. Ren, C. Pan, Y. Deng, M. Elkashlan, and A. Nallanathan, "Joint power and blocklength optimization for URLLC in a factory automation scenario," *IEEE Trans. Wireless Commun.*, vol. 19, no. 3, pp. 1786–1801, Mar. 2020. (cited on page 8)

[51] H. Ren, C. Pan, K. Wang, Y. Deng, M. Elkashlan, and A. Nallanathan, "Achievable data rate for URLLC-enabled UAV systems with 3-D channel model," *IEEE Wireless Commun. Lett.*, vol. 8, no. 6, pp. 1587–1590, Dec. 2019. (cited on page 8)

[52] C. She, C. Liu, T. Q. S. Quek, C. Yang, and Y. Li, "Ultra-reliable and low-latency communications in unmanned aerial vehicle communication systems," *IEEE Trans. Commun.*, vol. 67, no. 5, pp. 3768–3781, May 2019. (cited on page 8)

[53] O. L. A. López, E. M. G. Fernández, R. D. Souza, and H. Alves, "Ultra-reliable cooperative short-packet communications with wireless energy transfer," *IEEE Sensors J.*, vol. 18, no. 5, pp. 2161–2177, Mar. 2018. (cited on page 8)

[54] C. She, C. Yang, and T. Q. S. Quek, "Cross-layer optimization for ultra-reliable and low-latency radio access networks," *IEEE Trans. Wireless Commun.*, vol. 17, no. 1, pp. 127–141, Jan. 2018. (cited on pages 8, 9, 31, 59, 60, and 96)

[55] H. Ren, C. Pan, Y. Deng, M. Elkashlan, and A. Nallanathan, "Joint pilot and payload power allocation for massive-MIMO-enabled URLLC IIoT networks," *IEEE J. Sel. Areas Commun.*, vol. 38, no. 5, pp. 816–830, May 2020. (cited on page 8)

[56] C. She, R. Dong, Z. Gu, Z. Hou, Y. Li, W. Hardjawana, C. Yang, L. Song, and B. Vucetic, "Deep learning for ultra-reliable and low-latency communications in 6G networks," *IEEE Netw.*, vol. 34, no. 5, pp. 219–225, Sept. 2020. (cited on pages 8, 12, and 88)

[57] Z. Gu, C. She, W. Hardjawana, S. Lumb, D. McKechnie, T. Essery, and B. Vucetic, "Knowledge-assisted deep reinforcement learning in 5G scheduler design: From theoretical framework to implementation," *IEEE J. Sel. Areas Commun.*, vol. 39, no. 7, pp. 2014–2028, Jul. 2021. (cited on pages 8, 38, and 88)

[58] C. She, C. Sun, Z. Gu, Y. Li, C. Yang, H. V. Poor, and B. Vucetic, "A tutorial on ultrareliable and low-latency communications in 6G: Integrating domain knowledge into deep learning," *Proc. IEEE*, vol. 109, no. 3, pp. 204–246, Mar. 2021. (cited on page 8)

[59] A. Lozano and N. Jindal, "Transmit diversity vs. spatial multiplexing in modern MIMO systems," *IEEE Trans. Wireless Commun.*, vol. 9, no. 1, pp. 186–197, Jan. 2010. (cited on page 8)

[60] B. Hassibi and B. M. Hochwald, "How much training is needed in multiple-antenna wireless links?" *IEEE Trans. Inf. Theory*, vol. 49, no. 4, pp. 951–963, Apr. 2003. (cited on pages 8, 19, 20, 28, 29, 31, 72, and 73)

[61] J. Jose, A. Ashikhmin, T. L. Marzetta, and S. Vishwanath, "Pilot contamination and precoding in multi-cell TDD systems," *IEEE Trans. Wireless Commun.*, vol. 10, no. 8, pp. 2640–2651, Aug. 2011. (cited on page 9)

[62] T. L. Marzetta, "Noncooperative cellular wireless with unlimited numbers of base station antennas," *IEEE Trans. Wireless Commun.*, vol. 9, no. 11, pp. 3590–3600, Nov. 2010. (cited on page 9)

[63] F. Kaltenberger, H. Jiang, M. Guillaud, and R. Knopp, "Relative channel reciprocity calibration in MIMO/TDD systems," in *Proc. Future Network Mobile Summit*, Jun. 2010, pp. 1–10. (cited on pages 9 and 39)

[64] C. She, C. Yang, and T. Q. S. Quek, "Joint uplink and downlink resource configuration for ultra-reliable and low-latency communications," *IEEE Trans. Commun.*, vol. 66, no. 5, pp. 2266–2280, May 2018. (cited on pages 9, 29, 31, and 96)

[65] Y. Hu, M. Ozmen, M. C. Gursoy, and A. Schmeink, "Optimal power allocation for QoS-constrained downlink multi-user networks in the finite blocklength regime," *IEEE Trans. Wireless Commun.*, vol. 17, no. 9, pp. 5827–5840, Sept. 2018. (cited on pages 9, 12, 59, and 88)

[66] C. Li, N. Yang, and S. Yan, "Optimal transmission of short-packet communications in multiple-input single-output systems," *IEEE Trans. Veh. Technol.*, vol. 68, no. 7, pp. 7199–7203, Jul. 2019. (cited on pages 9 and 13)

[67] H. ElSawy, E. Hossain, and M. Alouini, "Analytical modeling of mode selection and power control for underlay D2D communication in cellular networks," *IEEE Trans. Commun.*, vol. 62, no. 11, pp. 4147–4161, Nov. 2014. (cited on page 10)

[68] H. ElSawy and E. Hossain, "On stochastic geometry modeling of cellular uplink transmission with truncated channel inversion power control," *IEEE Trans. Wireless Commun.*, vol. 13, no. 8, pp. 4454–4469, Aug. 2014. (cited on pages 10 and 40)

[69] J. Hu, S. Yan, X. Zhou, F. Shu, and J. Li, "Covert wireless communications with channel inversion power control in rayleigh fading," *IEEE Trans. Veh. Technol.*, vol. 68, no. 12, pp. 12 135–12 149, Dec. 2019. (cited on page 10)

[70] Z. Chen and E. Björnson, "Channel Hardening and Favorable Propagation in Cell-Free Massive MIMO With Stochastic Geometry," *IEEE Trans. Commun.*, vol. 66, no. 11, pp. 5205–5219, Nov. 2018. (cited on page 10)

[71] H. Q. Ngo and E. G. Larsson, "No downlink pilots are needed in TDD massive MIMO," *IEEE Trans. Wireless Commun.*, vol. 16, no. 5, pp. 2921–2935, May 2017. (cited on page 10)

[72] D. Mi, M. Dianati, L. Zhang, S. Muhaidat, and R. Tafazolli, "Massive MIMO performance with imperfect channel reciprocity and channel estimation error," *IEEE Trans. Commun.*, vol. 65, no. 9, pp. 3734–3749, Sept. 2017. (cited on pages 10, 18, and 39)

[73] Y. Liu, H. Chen, and L. Wang, "Physical layer security for next generation wireless networks: Theories, technologies, and challenges," *IEEE Commun. Surveys Tuts.*, vol. 19, no. 1, pp. 347–376, 1th Quart. 2017. (cited on page 10)

[74] F. Jameel, S. Wyne, G. Kaddoum, and T. Q. Duong, "A comprehensive survey on cooperative relaying and jamming strategies for physical layer security," *IEEE Commun. Surveys Tuts.*, vol. 21, no. 3, pp. 2734–2771, 3rd Quart. 2019. (cited on page 10)

[75] C. She, C. Sun, Z. Gu, Y. Li, C. Yang, H. V. Poor, and B. Vucetic, "A tutorial of ultra-reliable and low-latency communications in 6G: Integrating theoretical knowledge into deep learning," *arXiv preprint arXiv:2009.06010*, 2020. (cited on pages 11, 12, 78, 87, and 88)

[76] W. Yang, R. F. Schaefer, and H. V. Poor, "Wiretap channels: Nonasymptotic fundamental limits," *IEEE Trans. Inf. Theory*, vol. 65, no. 7, pp. 4069–4093, Jul. 2019. (cited on pages 11 and 58)

[77] W. R. Ghanem, V. Jamali, and R. Schober, "Resource allocation for secure multi-user downlink MISO-URLLC systems," in *Proc. IEEE Int. Conf. Commun. (ICC)*, Dublin, Ireland, Jun. 2020, pp. 1–7. (cited on page 11)

[78] D. Qiao, M. C. Gursoy, and S. Velipasalar, "Secure wireless communication and optimal power control under statistical queueing constraints," *IEEE Trans. Inf. Forensics Security*, vol. 6, no. 3, pp. 628–639, Sept. 2011. (cited on pages 11, 15, 58, 65, 66, 67, and 68)

[79] M. Ozmen and M. C. Gursoy, "Secure transmission of delay-sensitive data over wireless fading channels," *IEEE Trans. Inf. Forensics Security*, vol. 12, no. 9, pp. 2036–2051, Sept. 2017. (cited on pages 11 and 68)

[80] J. Wan, D. Qiao, H. Wang, and H. Qian, "Buffer-aided two-hop secure communications with power control and link selection," *IEEE Trans. Wireless Commun.*, vol. 17, no. 11, pp. 7635–7647, Nov. 2018. (cited on page 11)

[81] S. Lv, X. Xu, S. Han, and X. Tao, "Secure transmission in NOMA-based mMTC networks under statistical delay QoS guarantees," in *Proc. IEEE/CIC Int. Conf. Commun. in China (ICCC)*, Changchun, China, Aug. 2019, pp. 1000–1005. (cited on pages 11 and 68)

[82] Z. Bai, L. Ma, Y. Dong, P. Ma, and Y. Ma, "Energy-efficient resource allocation for secure cognitive radio network with delay QoS guarantee," *IEEE Syst. J.*, vol. 13, no. 3, pp. 2795–2805, Sept. 2019. (cited on page 11)

[83] F. Liang, C. Shen, W. Yu, and F. Wu, "Towards optimal power control via ensembling deep neural networks," *IEEE Trans. Commun.*, vol. 68, no. 3, pp. 1760–1776, Mar. 2020. (cited on pages 12 and 88)

[84] M. Eisen, C. Zhang, L. F. O. Chamon, D. D. Lee, and A. Ribeiro, "Learning optimal resource allocations in wireless systems," *IEEE Trans. Signal Process.*, vol. 67, no. 10, pp. 2775–2790, May 2019. (cited on pages 12, 68, 69, 70, and 87)

[85] C. Sun, C. She, and C. Yang, "Unsupervised deep learning for optimizing wireless systems with instantaneous and statistic constraints," *submitted to IEEE Journal for possible publication*, 2020. [Online]. Available: https://arxiv.org/abs/2006.01641 (cited on page 12)

[86] C. Li, S. Yan, and N. Yang, "On channel reciprocity to activate uplink channel training for downlink wireless transmission in Tactile Internet applications," in *Proc. IEEE Int. Conf. Commun. (ICC) Workshop*, Kansas City, MO, May 2018, pp. 1–6. (cited on pages 13, 30, 31, 39, 95, and 99)

[87] C. Li, S. Yan, N. Yang, X. Zhou, and R. Chen, "One-way URLLC with truncated channel inversion power control," in *Proc. IEEE Global Commun. Conf. (Globecom) Workshop*, Waikoloa, HI, Dec. 2019, pp. 1–6. (cited on pages 14 and 100)

[88] C. Li, S. Yan, N. Yang, and X. Zhou, "Truncated channel inversion power control to enable one-way URLLC with imperfect channel reciprocity," *submitted to IEEE Trans. Commun.* (cited on page 14)

[89] C. Li, C. She, and N. Yang, "Unsupervised learning for secure short-packet transmission under statistical QoS constraints," in *Proc. IEEE Global Commun. Conf. (Globecom) Workshop*, Taipei, Taiwan (ROC), Dec. 2020, pp. 1–6. (cited on page 16)

[90] C. Li, C. She, N. Yang, and T. Q. S. Quek, "Secure transmission rate of short packets with queueing delay requirement," *IEEE Trans. Wireless Commun., accepted on 30 June 2021, Early Access.* (cited on pages 16 and 29)

[91] B. Nosrat-Makouei, J. G. Andrews, and R. W. Heath, "MIMO interference alignment over correlated channels with imperfect CSI," *IEEE Trans. Signal Process.*, vol. 59, no. 6, pp. 2783–2794, Jun. 2011. (cited on page 18)

[92] F. Kaltenberger, H. Jiang, M. Guillaud, and R. Knopp, "Relative channel reciprocity calibration in MIMO/TDD systems," in *Proc. Future Network Mobile Summit*, Jun. 2010, pp. 1–10. (cited on page 18)

[93] S. Yan, X. Zhou, N. Yang, T. D. Abhayapala, and A. L. Swindlehurst, "Channel training design in full-duplex wiretap channels to enhance physical layer security," in *Proc. IEEE Int. Conf. Commun. (ICC)*, May 2017, pp. 1–6. (cited on page 19)

[94] A. V. Oppenheim and G. C. Verghese, *Signals, systems and inference*. Upper Saddle River, NJ: Prentice Hallc, 2015. (cited on page 28)

[95] M. Kobayashi, N. Jindal, and G. Caire, "Training and feedback optimization for multiuser MIMO downlink," *IEEE Trans. Commun.*, vol. 59, no. 8, pp. 2228–2240, Aug. 2011. (cited on page 30)

[96] I. S. Gradshteyn and I. M. Ryzhik, *Table of integrals, series, and products*, 7th ed. San Diego, CA: Academic, 2007. (cited on pages 30, 44, 47, and 91)

[97] D. J. Love, R. W. Heath, and T. Strohmer, "Grassmannian beamforming for multiple-input multiple-output wireless systems," *IEEE Trans. Inf. Theory*, vol. 49, no. 10, pp. 2735–2747, Oct. 2003. (cited on page 32)

[98] B. Makki, T. Svensson, and M. Zorzi, "Finite block-length analysis of the incremental redundancy HARQ," *IEEE Wireless Commun. Lett.*, vol. 3, no. 5, pp. 529–532, Oct. 2014. (cited on page 42)

[99] ——, "Wireless energy and information transmission using feedback: Infinite and finite block-length analysis," *IEEE Trans. Commun.*, vol. 64, no. 12, pp. 5304–5318, Dec. 2016. (cited on page 42)

[100] D. Wu and R. Negi, "Effective capacity: A wireless link model for support of quality of service," *IEEE Trans. Wireless Commun.*, vol. 2, no. 4, pp. 630–643, Jul. 2003. (cited on pages 58, 59, and 60)

[101] M. Shehab, H. Alves, E. A. Jorswieck, E. Dosti, and M. Latva-aho, "Effective energy efficiency of ultra-reliable low latency communication," *accepted by IEEE Internet Things J.*, 2021. (cited on page 59)

[102] M. Amjad, L. Musavian, and S. Aïssa, "NOMA versus OMA in finite blocklength regime: Link-layer rate performance," *IEEE Trans. Veh. Technol.*, vol. 69, no. 12, pp. 16 253–16 257, Dec. 2020. (cited on page 59)

[103] J. Gregory and C. Lin, *Constrained optimization in the calculus of variations and optimal control theory*, 1st ed. Springer Publishing Company, Incorporated, 2007. (cited on pages 65 and 66)

[104] Y. Wang, X. Tang, and T. Wang, "A unified QoS and security provisioning framework for wiretap cognitive radio networks: A statistical queueing analysis approach," *IEEE Trans. Wireless Commun.*, vol. 18, no. 3, pp. 1548–1565, 2019. (cited on page 68)

[105] B. He and X. Zhou, "Secure on-off transmission design with channel estimation errors," *IEEE Trans. Inf. Forensics Security*, vol. 8, no. 12, pp. 1923–1936, Dec. 2013. (cited on page 72)

[106] S. M. Kay, *Fundamentals of statistical signal processing: Estimation theory*. Englewood Cliffs, NJ, USA: Prentice-Hall, 1993. (cited on page 72)

[107] C. Zhang, H. Zhang, J. Qiao, D. Yuan, and M. Zhang, "Deep transfer learning for intelligent cellular traffic prediction based on cross-domain big data," *IEEE J. Sel. Areas Commun.*, vol. 37, no. 6, pp. 1389–1401, Jun. 2019. (cited on page 78)

[108] Z. Gu, C. She, W. Hardjawana, S. Lumb, D. McKechnie, T. Essery, and B. Vucetic, "Knowledge-assisted deep reinforcement learning in 5G scheduler design: From theoretical framework to implementation," *IEEE J. Sel. Areas Commun.*, vol. 39, no. 7, pp. 2014–2028, Jul. 2021. (cited on page 78)

[109] P. K. Gopala, L. Lai, and H. El Gamal, "On the secrecy capacity of fading channels," *IEEE Trans. Inf. Theory*, vol. 54, no. 10, pp. 4687–4698, Oct. 2008. (cited on page 79)

[110] Y. Yang, Y. Li, W. Zhang, F. Qin, P. Zhu, and C. Wang, "Generative-adversarial-network-based wireless channel modeling: Challenges and opportunities," *IEEE Commun. Mag.*, vol. 57, no. 3, pp. 22–27, Mar. 2019. (cited on page 84)

[111] A. T. Z. Kasgari, W. Saad, M. Mozaffari, and H. V. Poor, "Experienced deep reinforcement learning with generative adversarial networks (GANs) for model-free ultra reliable low latency communication," *IEEE Trans. Commun.*, vol. 69, no. 2, pp. 884–899, Feb. 2021. (cited on page 84)

[112] H. Ye, L. Liang, G. Y. Li, and B. Juang, "Deep learning-based end-to-end wireless communication systems with conditional GANs as unknown channels," *IEEE Trans. Wireless Commun.*, vol. 19, no. 5, pp. 3133–3143, May 2020. (cited on page 84)

[113] E. Balevi, A. Doshi, A. Jalal, A. Dimakis, and J. G. Andrews, "High dimensional channel estimation using deep generative networks," *IEEE J. Sel. Areas Commun.*, vol. 39, no. 1, pp. 18–30, Jan. 2021. (cited on page 84)

[114] H. Sun, X. Chen, Q. Shi, M. Hong, X. Fu, and N. D. Sidiropoulos, "Learning to optimize: Training deep neural networks for interference management," *IEEE Trans. Signal Process.*, vol. 66, no. 20, pp. 5438–5453, Oct. 2018. (cited on page 87)

[115] W. Lee, M. Kim, and D. Cho, "Deep power control: Transmit power control scheme based on convolutional neural network," *IEEE Communications Letters*, vol. 22, no. 6, pp. 1276–1279, Jun. 2018. (cited on page 87)

[116] ——, "Transmit power control using deep neural network for underlay device-to-device communication," *IEEE Wireless Commun. Lett.*, vol. 8, no. 1, pp. 141–144, Feb. 2019. (cited on page 87)

[117] H. Lee, S. H. Lee, and T. Q. S. Quek, "Deep learning for distributed optimization: Applications to wireless resource management," *IEEE J. Sel. Areas Commun.*, vol. 37, no. 10, pp. 2251–2266, Oct. 2019. (cited on page 87)

[118] D. Liu, C. Sun, C. Yang, and L. Hanzo, "Optimizing wireless systems using unsupervised and reinforced-unsupervised deep learning," *IEEE Netw.*, pp. 1–8, Accepted to appear 2020. (cited on page 87)

[119] Y. Shen, Y. Shi, J. Zhang, and K. B. Letaief, "A graph neural network approach for scalable wireless power control," in *Proc. IEEE Global Commun. Conf. (Globecom) Workshop*, Dec. 2019, pp. 1–6. (cited on pages 88 and 89)

[120] ——, "LORM: Learning to optimize for resource management in wireless networks With few training samples," *IEEE Trans. Wireless Commun.*, vol. 19, no. 1, pp. 665–679, Jan. 2020. (cited on page 88)

[121] M. Eisen and A. Ribeiro, "Transferable policies for large scale wireless networks with graph neural networks," in *IEEE International Conference on Acoustics, Speech and Signal Processing (ICASSP)*, May 2020, pp. 5040–5044. (cited on page 89)

[122] ——, "Optimal wireless resource allocation with random edge graph neural networks," *IEEE Trans. Signal Process.*, vol. 68, pp. 2977–2991, Apr. 2020. (cited on page 89)

[123] Laplace's method - Wikipedia. [Online]. Available: https://en.wikipedia.org/wiki/Laplace%27s_method (cited on page 92)

[124] T. Yoo, N. Jindal, and A. Goldsmith, "Multi-antenna downlink channels with limited feedback and user selection," *IEEE J. Sel. Areas Commun.*, vol. 25, no. 7, pp. 1478–1491, Sept. 2007. (cited on page 95)